2015

Numerical Modeling and Analysis of Tidal Variance and Marsh Productivity in the Guana Tolomato Matanzas National Estuarine Research Reserve, Florida

Amanda S. Tritinger
University of North Florida, n00914123@unf.edu

NUMERICAL MODELING AND ANALYSIS OF TIDAL VARIANCE AND MARSH PRODUCTIVITY IN THE GUANA TOLOMATO MATANZAS NATIONAL ESTUARINE RESEARCH RESERVE, FLORIDA

by

Amanda Tritinger

B.S. University of Central Florida, 2013

A thesis submitted in partial fulfillment of the requirements
for the degree of Master of Science

The University of North Florida

College of Computing, Engineering, and Construction

April, 2015

Chairperson of the Supervisory Committee: **Professor Peter Bacopoulos**
Department of Civil Engineering

Members of the Supervisory Committee: **Professor Don Resio**
Department of Civil Engineering

Research Faculty, Research Director Nikki Dix
Department of Biology, GTMNERR

Thesis entitled “Numerical Modeling and Analysis of Tidal Variance and Marsh Productivity in the Guana Tolomato Matanzas National Estuarine Research Reserve, Florida” by Amanda Tritinger is approved:

_____ _____
Committee Chair: Peter Bacopoulos

_____ _____
Committee Member 1: Donald T. Resio

_____ _____
Committee Member 2: Nicole Dix

Accepted for the School of Engineering:

_____ _____
Department Chair: Murat Tiryakioglu

Accepted for the College of Computing, Engineering and Construction:

_____ _____
College Dean: Mark Tumeo

Accepted for the University:

_____ _____
Dr. John Kantner
Dean of the Graduate School

ABSTRACT

Long term sustainability in salt marsh and mangroves is dependent on dominant species, such as *Spartina alterniflora,* to capture organic and inorganic sediment. The research analyzes that sustainability. This work demonstrates the prediction of hydrodynamics and biomass density of salt marsh to provide useful information for the planning and mitigation of sea-level rise impacts on marsh sustainability in the Guana Tolomato Matanzas National Estuarine Research Reserve (GTMNERR), Florida. An advanced circulation code was applied to simulate hydrodynamics (i.e., shallow water equations) in the GTMNERR. The model used a set of parameters and conditions based on the GTMNERR domain to predict tides for present-day conditions, which was validated using tidal data from eight monitoring stations within the GTMNERR. The hydrodynamic model results (i.e., MLW and MHW) were then coupled with a marsh equilibrium model to assess year-to-year biomass density for saltmarsh cordgrass (*Spartina alterniflora*). Vegetative data were obtained from the staff of the GTMNERR and organized for future work towards validation of biomass density predictions.

Simulations were then performed with sea-level rise scenarios of 0.13 m, 0.22 m and 0.51 m, which are standardized cases of mild, moderate, and extreme rise for the northeast coast of Florida. The simulation results show nonlinear increase of tidal datums for given sea-level rise, thus leading to nonlinear change in biomass productivity. The modeling tool has engineering implications in the way of assisting the planning of dredging spoils to be laid over the marsh to sustain existing marsh against rising sea levels. The modeling tool further provides information about marsh migration due to sea-level rise, whereby coastal planners can use this information to designate and preserve existing uplands/wetlands that will house salt marsh in the future, as the marshes will migrate into such upland/wetlands areas.

ACKNOWLEDGMENTS

I'd like to thank the University of North Florida's (UNF) School of Engineering, College of Computing, Engineering and Construction (CCEC), and Taylor Engineering Research Institute (TERI). My genuine appreciation to professors Peter Bacopoulos and Don Resio, as well as research faculty, Nikki Dix for their aid in the development of this proposed thesis work. In addition, special thanks to Guana Tolomato Matanzas National Estuarine Research Reserve staff for sharing their work, experiences, and data collection. The marsh equilibrium model (MEM) and advice on its application was provided courteously by Dr. J.T. Morris. The National Oceanic and Atmospheric Administration provided information and data necessary for the development of this thesis, namely that provided through The Ecological Effects of Sea Level Rise Program (http://www.coastalscience.noaa.gov/projects/detail?key=162).

This research was funded in part under Award No. 2008-ST-061-ND0001 from the U.S. Department of Homeland Security (DHS) – Center for Natural Disaster and Coastal Resilience.

TABLE OF CONTENTS

TABLE OF FIGURES

LIST OF TABLES

LIST OF EQUATIONS

1. Introduction

The objective of this research was to develop a modeling tool to provide insight into the long term sustainability of mangrove and salt marsh systems in the Guana Tolomato Matanzas National Estuarine Research Reserve, after sea-level rise. This tool uses the relationship between biological components of the marsh and hydraulic conditions in the intertidal zone to predict possible migration of the dominant species in the salt marsh.

Coastal wetlands are a unique area and an extremely vulnerable habitat. They represent transitional areas between tidal flats and uplands and are exposed to the extremes (mean maxima and minima) of temperature, salinity concentrations, and water level elevation induced inundation caused by the tides. Salt marshes cover many extensive areas of estuaries and deltaic areas, where large bodies of water deposit sediment (silt and sand) into rivers and distributaries. They are an irreplaceable, unique ecosystem; one of the most productive ecosystems on earth (Farber et al., 2006). They are also being threatened worldwide by accelerated sea level rise.

Florida's coastal counties are home to the majority of Florida's population and economic livelihoods, and the steady rise in the density of both of these elements in coastal areas, with not much indication of decline. Florida's coastal wetlands protect these counties from considerable hydrologic hazards. If these wetlands are potentially inundated by sea level rise, they will not continue to protect these areas.

This study worked to examine the Guana Tolomato Matanzas National Estuarine Research Reserve (GTMNERR) on a high resolution spatial base. The goal was to create a model that is unlike other methods of analysis for the area and areas similar to it. Through data lumping and categorization, using less comprehensive and less involved variables, and a less detailed domain, a model is created that is less crude when it comes to processing power.

The hypothesis driving this work was that the high resolution, interactive tide marsh modeling methods used in this model can provide a more accurate and detailed prediction of biomass productivity for *Spartina alterniflora* in the GTMNERR. The low demand on computing power makes it more operational for coastal engineers. Further, due to the flexibility of possibly including rise in the model simulations, the tide-marsh model was able to perform the complex calculations for existing conditions and projections into the future.

Tidal hydrodynamics and marsh productivity were the physical and ecological processes explored in this study. The primary motivation behind this study was to better understand relatable transport processes in natural environments, such as the transport of pollutants or the forecasting of potentially hazardous storm events.

The Guana Tolomato Matanzas National Estuarine Research Reserve (GTMNERR) was chosen as the area of study due to its interesting and diverse ecosystem and its significant hydraulic structure. This w tidal hydrodynamics influence marsh ecology was examined, i.e., the productivity of *Spartina alterniflora* in the GTMNERR.

1.1 THE GUANA TOLOMATO MATANZAS NATIONAL ESTUARINE RESEARCH RESERVE (GTMNERR)

The GTMNERR is an enterprise between the US Department of Commerce, the National Oceanic and Atmospheric Administration (NOAA), and the Department of Environmental Protection (DEP). The GTMNERR was founded in 1999 and is one of 28 National Estuarine Research Reserves (NERR) started by NOAA.

The GTMNERR is located in north east Florida, south of the city of Jacksonville. It is divided into a northern section and a southern section (Figure 1). The city of St. Augustine is settled in between the two sections. The northern constituent is associated with the Tolomato and Guana River estuaries. The southern constituent is associated with Matanzas river estuary. The GTMNERR is joined to the Atlantic Ocean via the St. Augustine inlet and the Matanzas Inlet.

Approximately 64,487 acres of oyster bars, salt marsh and mangrove tidal wetlands, upland and offshore seas, and estuarine lagoons make up the GTMNERR. The reserve is also home to the northern furthermost mangrove habitation on the east coast of the United States (Zomlefer et al. 2006). Many animals seek sanctuary in the reserve as a critical feeding, nesting, and breeding ground.

The GTMNERR is made up of about one third upland habitat type (pines) within its drainage basin. Approximately 14% of the reserve is shrubs and brush lands, and 10% hardwood hammocks. Coastal salt marsh and open water habitat encompass nearly 15% of the watershed. Dominant species include Glasswort, saltwort, saltmarsh cordgrass (*Spartina alterniflora*), and black needle rush (Juncus roemerianus).

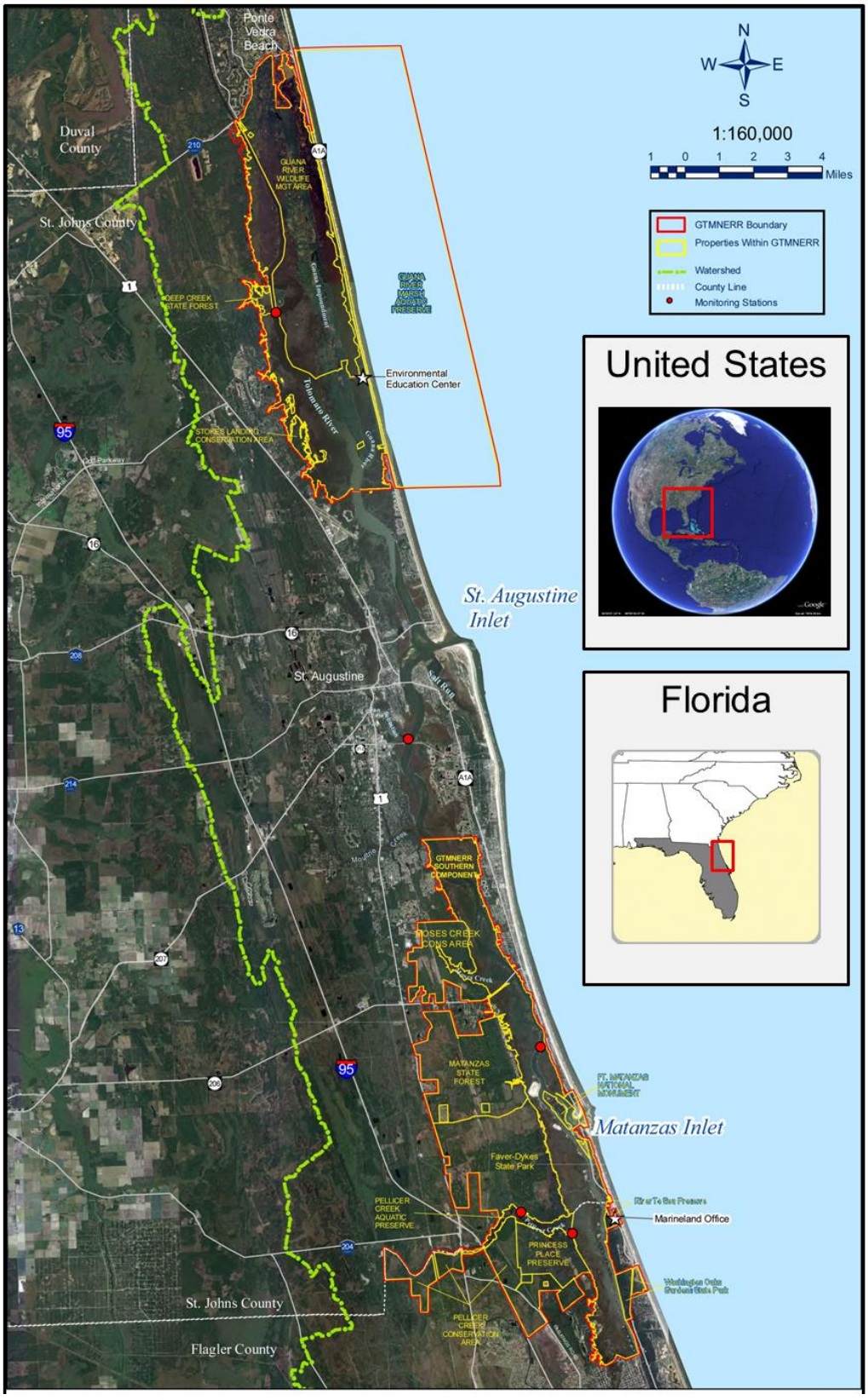

Figure 1. Geographic Map of GTMNERR- made up into a southern and northern component divided by the city of St. Augustine (DEP, 2015)

1.2 ENVIRONMENTAL LOCALE OF THE GTMNERR

The GTMNERR's topography has been shaped over the past 10,000 years. It is composed of estuarine lagoon bottoms, tidal flats, creeks, rivers, and dune ridges. The reserve ranges from an elevation of 12 meters above sea level at the northern end of the reserve and central regions of the Pellicer Creek Conservation Area, to sea level. It is located in the lower range of the Atlantic Coastal Plain.

The climate of this northeast region of Florida is of maritime influence, and primary moderated by the Gulf Stream. This causes the area to experience humid, subtropical marine climates with long, warm, humid summers accompanied by heavy rainfall, and mild, dry winters. On average the annual rainfall is around 55 inches. Half of which occurs in the months in between June and October.

The reserve is located in the Upper East Coast Drainage Basin. Approximately 467,000 acres drain into this watershed (Figure. 1) that the GTMNERR is a part of. The natural hydrodynamics of this drainage basin have been disrupted by human influence (i.e. dikes, inland wells, and the Guana Dam). The drainage basin is broken up into four sub sections, of which three drain to the GTMNERR. From north to south those drainage basins are the Tolomato River, the Matanzas River, and Pellicer Creek.; The last sub section is located south of the reserve's boundary line (Halifax River).

The Tolomato River has a drainage area of approximately 84 square miles. The basin is a part of the Intercostal Waterway (IWW). Due to its size and location, it is maintained as a public navigation channel and periodically dredged. The dredging process has straightened the path of the river out at some places. Consequently, spoil islands have been created from the upkeep of the channel, all of which are either fully or partially vegetated as of today.

The Matanzas River and Moses Creek are home to relatively undisturbed tidal marshes. The Moses Creek drains mostly flat woods and swamps from St. John's County. The creek eventually flows directly into the Matanzas River. The Pellicer Creek basin primarily drains small creeks and branches. The St. John's River Water Management District is responsible for this drainage system's watershed groundwater and surface water resources.

1.3 PHYSICAL PROCESSES OF THE GTMNERR

The St. Augustine and Matanzas Inlets connect the shallow estuary systems of the GTMNERR to the Atlantic Ocean. Collectively this system forms a barrier island estuarine system. Each inlet provides an oceanic exchange point for the estuarine ecosystem.

The St. Augustine Inlet connects the Matanzas and Tolomato rivers to the ocean. Originally a small naturally occurring inlet formed 120 meters south of where the inlet is currently located. In an effort to respond to public interests the channel was relocated in 1940 to its present-day position.

To maintain the inlet's location and navigability a jetty was constructed north of the inlet entrance. The jetty and the channel opening are sustained by the U.S. Army Corps of Engineers by updating the structure and dredging infrequently.

In 1993 Taylor Engineering of Jacksonville started an in depth study on the inlet. Morphologic, hydraulic, and coastal conditions in the inlet were identified in order to come up with a management plan. The study provided both a historical bathymetric analysis as well as a hydraulic model of the inlet.

In 2006 hydrology and current velocity were observed at a tidally driven coastline trifurcation, adjacent to the St. Augustine Inlet over nearly a semidiurnal period (Webb et al., 2007). The study showed that the mean inflow occurs through the central deep channel and mean outflow over the shoals. While Barrier Island estuarine systems like the one found in the GTMNERR are not rare along Florida's coast line, few have their hydrodynamic properties observed and documented to such an extent.

2. Literature Review

This research is predominantly concentrated on the tidal modeling and analysis, as well as the organic matter evolution simulations in the marshes of the Guana Tolomato Matanzas National Estuarine Research Reserve (GTMNERR). This literature review will provide background information necessary for a compressive understanding of the motivation behind this research. It will include a brief history on the origins and advancements in two dimensional and three dimensional circulation numerical tidal predicting models. A review of current working models in the area. This will be followed by an assessment of typical tide-marsh analyses. Then it will cover an understanding of biomass density and its relationship with accretion rates in marshes. Lastly the review will include a discussion on validation of the evolution modeling through vegetative data collection.

2.1 TWO DIMENSIONAL MODELING OF TIDES

The first attempts at better understanding tidal dynamics were accomplished through analytical studies of the linearization of the complete equations of motion (Lamb, 1932). As computers became more of a prominent tool however, this method was replaced with numerical models. These models used finite difference systems as a means to more accurately portray the tidal hydrodynamics (Leendertse, 1967).

In the 60s a series of studies were conducted at the University of Waterloo, Canada (Kowen, Unny, and Hill, 1969) where efforts were made to determine the flow characteristics of vegetated open channels. Roughness elements were glued to the bottom of a flume in the University's laboratory. Then flow over the simulated flexible vegetation was generated, controlled and monitored using a pilot tube technique that allowed them to record velocity distributions.

They concluded, as many often suggest, that use of a log law by which adjustments for the values of the roughness parameter and the origin intercept be made, be used to represent the vertical profile of mean velocities above the plants. This implies the assumption of the existence of an equilibrium layer above the plants, and that the production of turbulence is locally balanced by dissipation.

Li and Shen (1973) attempted to numerically predict sediment transport capacities in vegetated free surface flows based on a superposition procedure for the wakes produced behind isolated features. This technique was motivated by Petryk (1969). In this procedure they assumed local drag coefficients of 1.2, and produced values for mean drag coefficients of about 1.1 for staggered activities free of plant density. They used this method on the application of bed load, and then they likened the relative effect on sediment yields for diverse forms of tall vegetation.

Petryk and Bosmajian (1975) developed a quantitative process for predicting the manning's n coefficient as a measure of flow resistance as a function of flow depth and vegetation parameters. This method considered flow depths that were either less than or equal to the maximum height of tall vegetation. It's most practical application is in predicting the variation of the coefficient in correlation with change in depth.

Improved change to the traditional n-URh (where manning's n value is based on velocity, u and hydraulic radius, Rh) method was proposed by Kowen and Li (1980). This new proposal tapped into the use of biomechanical concepts and proposed the use of a field methodology for estimating flexural stiffness of natural vegetation. From this work the "board drop test" and a vegetation height method were developed.

A mathematical method for estimating the momentum and energy equations in multi-connected flows that plainly state the guidelines for the commutation of spatial averaging operators and spatial differentiation was developed by Raupach and Shaw (1982). Various momentum and energy dispersive terms that arise as a result of the three dimensional nature of the flow structure can be identified in the method, as well as the non-commutation of the operators mentioned.

After this mathematical method was created by Raupach and Shaw, Raupach et al. (1986) conducted a series of experiments that tried to illuminate the characteristics of the atmospheric flows over a vegetation canopy. To do so, a laboratory wind tunnel was used to created currents, and atmospheric flow over a simulated vegetation canopy (aluminum strips).

Velocity measurements were taken above and within the canopy. From these measurements they were able to estimate the various terms composing the turbulent kinetic energy balance within the canopy. These experiments made the importance of the turbulence term over the canopy an imperative player in open channel flow prediction.

The discretization of the temporal domain has always presented an obstacle for linear models due to local variance. In an attempt to fix this, time stepping schemes was replaced with domain-based schemes. This proved to implement governing equations of tidal circulation with high efficiency (Westerink, 1989). This allowed the model to examine non-linear tidal constituent relations at a highly precision. This was accomplished by solving harmonic solutions to the vertically integrated equations of tidal motion.

The propagation of water on land, and back off land was soon considered to have an effect on the overall model. For this a dissipative, finite element based procedure was developed to prevent instabilities from appearing due to the highly non-linear flow regime existing along the water to land boundary (Sidén and Lynch, 1988). The General Wave Continuity Equation (GWCE) is formulated to solve the integrated vertical equations of tidal motion.

For this study a finite element mesh is used to keep the land boundaries dry, salt marsh areas wet/dry, and draw a clear boundary line for the model. Research concerning manning's n roughness values for densely vegetated flood plains were performed by Arcement and Schneider (1989). They estimated n values for areas based on the factors that would cause roughness in channel flows and flood plains. The trees, vines, and brush surrounding the body of water mostly determined these values in wetland type areas.

A direct relationship between n values and the measured vegetation density of a given flood plain was determined. This work was then presented as a guide for selecting manning's roughness coefficients for natural channels and flood plains.

Drawing on the physical link between wake generation and the energy transfer from mean kinetic energy to turbulent kinetic energy at the scale of the plant stems and branches by aquatic plants, Nepf developed a model representative of vegetative drag and turbulence intensity. Field experiments using injecting dye at a continuous rate into a sampling port, and recording the flow through fluorometer. The end result was a plume concentration profile that agreed with the model for drag, turbulence and diffusion within the emergent vegetation.

A numerical model for the progression of the cross sectional view of channel flow was developed by D'Alpaos et al. (2006). The removal and addition of sediment to the channel, as well as the deposition of the marsh platform affect the flow of the tidal prism through the channel. While capturing this, the model also captures the transformation of additional vegetation to the marsh platform. It captures the resistance to flow as well as biomass addition/accretion caused by the vegetation.

The model captures the relationship between the hydroperiod and vegetation encroachment on the specified cross section of the channel. This research found that when marshes are dominated by *Spartina alterniflora*, a width to depth ratio of the channels negatively correlates with, or decreases with the increase of tidal flat evolution in the salt marsh.

Despite the GWCE formulation based solution techniques in idealized, lnear flow computations, field studies proved that other mechanisms may still exist that could better predict flow. Luettich et al. (1992) created ADCIRC (ADvanced CIRCulation), a finite element numerical model, backed by theory, methodology, and verification of the model. It was a two-dimensional, depth-integrated hydrodynamic model that took geometric boundary irregularities, small scale bathymetry differences, and agitations in elevation boundary conditions into account.

Bcaopoulos et al. (2008) presented development of this for use in the lower St. Johns River Basin in an effort to model flood assessments. Validation included hindcasting (use of data from Tropical Storm Fay) as well as water level data from five stations in the lower St. Johns River, accounting for the assessment of river flooding extent within the adjacent watershed basin. The results proved the need to capture and apply watershed runoff as an additional boundary condition in order to more accurately present storm surge.

Hagen et al. (2012) and Alizad et al. (2014) together presented the latest methodologies and technologies for tidal hydrodynamic-marsh productivity modeling of *Spartina alterniflora*. The purpose of this study is to translate these existing methodologies and technologies to the GTM-NERR as well as to introduce salinity into the overall physical-ecological dynamical balance of *Spartina alterniflora*. All of these inter-related physical and ecological processes would be influenced by rise (Hagen et al., 2012; Alizad et al., 2014), which was also explored in this study to provide an added dimension to the data-modeling tool.

2.2 EXISTING MODELS FOR THE GTMNERR

Throughout the life of the reserve, many modeling attempts to understand ecosystem health, flushing, water quality conditions, and water circulation in the domain have been made. From 1999 to 2001 the St. John's Water Management District (SJWMD) collected bathymetry data for these models. The SJRWMD collected bottom topography of the North Coast Basin by conducting surveys with bathymetric cuts predominantly spaced approximated 500 to 1000 foot intervals, and depth data at about 66 foot intervals along each track. The surveys produced both lateral and longitudinal depth cuts.

These data were then used by to create a two dimensional finite difference, curvilinear orthogonal numerical grid model for tidal water in the North Coastal Basin (McKee ink., 2002). The grid was used to determine water runoff into the intercostal water way, as well as the Matanzas and Tolomato estuary systems, as well as model non-point source pollution. Combining this model with GIS land use data, an extrapolation of possible outcomes can be made for possible present-day and future construction plans for the surrounding areas. This will then contribute to development of pollution load reduction goals and total maximum daily load values for the GTMNERR.

A study of a closure of a land barrier breach at the Matanzas Inlet was used to demonstrate the application of morphodynamic relations amongst prism, inlet throat area, and sand transport associated with ebb delta volume (Powell, 2006). These relations are beneficial for forecast of fluctuations in the throat area and the ebb delta volume when morphologic changes happen.

Tidal flats and marshes cover a large part of the GTMNERR. Around 15km^2 of this land cover is in tidal range. CH3D, a 3 dimensional hydrodynamic model was used to study this land cover's effect on the circulation in the estuaries (Tutak and Sheng, 2008). The model used non-flooding/drying and flooding/drying versions to quantify these effects. Simulations were generated representing flow at the Matanzas and St. Augustine inlets, and then compared to ADCP data collected in the area over a 12 hour period.

This study determined that including drying/flooding in a numerical model will improve the tidal simulations for stations located in regions with shallow channels or that are in proximity of large marsh coverage. Total flow rates through the channel were also improved when taking drying/flooding into account. The three dimensional model method can be used to offer guidance on the planning of sampling strategies for biogeochemical studies in the GTMNERR.

The proposed future work of the project was to improve the vegetation model used in CH3D. This would introduce friction caused by submerged and emerged vegetation. This would ultimately help predict the tidal marshes and flats' effect on salinity, water level, and currents during extreme events like hurricanes.

A model to better understand the ecological effects of sea-level rise in the Matanzas river basin has also been developed by Linhoss et al. (2015). This is the Sea Level Affecting Marshes Model (SLAMM). This model works by contouring the land surrounding the Matanzas River basin, in the GTMNERR into set land cover types, using a structure grid of 10m by 10m squares. The model applies present day sea levels, and then applies time steps towards a predicted sea level rise. The study is not as finite as the model in this research; however the results of both mimic each other.

This model works more with the relationship to wetland area and ecosystem services provided by various wetland types. It typically shows overly declining accretion rates in the seaward directions (Kirwan and Guntenspergen, 2009) and doesn't present an increase in accretion due to sediment supply. The model does not have the ability to accommodate simulating mechanistic processes for the entire domain either (i.e. it is locally focused), nor it is able to do so at the fine and flexible resolution that the ADCIRC and MEM loose coupling can provide.

2.3 TIDAL MARSH ANALYSIS

The majority of the water flux in any coastal body of water is due to the tides. According to research pulled together in Blanton et al (2004) "semidiurnal tides accounted for about 80% of inner and mid-shelf kinetic energy, while accounting for only about 30% of outer shelf energy." Tidal motion makes up the majority of energy in a water column, and it is also relatively predictable. The first models for measuring the tidal movement produced large discrepancies between the theoretical data and the actual data measured. As a result, many newer models are being created in an effort to better simulate the motion caused by tidal forces.

Tidal circulation can be grouped into two categories including a large number of individual tidal constituents. The two main categories of tides are "diurnal" and "semidiurnal." A diurnal tide, or a daily tide, is one that has a single high tide and a single low tide per tidal day. A semidiurnal tide, or a semi-daily tide, is a tide that has two high tides and two low tides per tidal day. Tidal energy can be broken down into an infinite amount of constituents, e.g., NOAA considers 37 of which are large enough to represent the full tide. This different tidal constituents and their changing relationship to Earth's water bodies causes the tide to be different in different locations throughout the day.

Of those 37 NOAA-defined tidal constituents there are eight major constituents; M2, S2, N2, K2, K1, O1, P1, and Q1. M2 is the principal lunar semidiurnal tide. It has the largest overall effect on the tide, and takes place every 12.4 hours. S2 is the principal solar semidiurnal tide and takes place every 12 hours. N2 is the larger lunar elliptic semidiurnal tide and takes place every 12.7 hours. K2 is the luni-solar semidiurnal tide and takes place every 11.97 hours. K1 is the lunar diurnal tide and takes place every 23.9 hours. O1 is the second lunar diurnal tide and takes place every 25.8 hours. P1 is the solar diurnal tide and takes place every 24 hours. Lastly, Q1 is the larger lunar elliptic diurnal tide and takes place every 26.9 hours. A tidal constituent is the push or pull created by some body of mass, for example the moon.

Each constituent has a different frequency and amplitude then the other constituents. When you put all of these constituents together, a varying collective overall tide is the result. This effect repeats itself approximately every 15 days. These constituents are important variables for many of the models used to calculate the power of the tides.

Tidal reactions happen at discrete frequencies determined by combinations of astronomical frequencies as well as frequencies (commonly known as shallow water tidal constituents) that result from nonlinear exchanges in the governing physics (Parker, 1991). The advantage of the analysis of tidal dynamics is the predictable aspect of the tides; that they are determined by the laws of physics.

Kreeke and Cotter (1974) examined the net discharge in lagoon-inlet systems, and created a model for it using the continuity and momentum of the flow. In the end, however, they found differences between the numerical and analytic solutions they created and the actual net discharge. Using their equations can provide physical insight into tidal activity; however there are addotopma; aspects to a lagoon that impact the movement of water.

In the lagoon other sources besides tides move water around and make it circulate throughout the domain, such as; local winds, bottom friction, freshwater input from rivers, input from precipitation, and output caused by evaporation. These are just a few of the variables that have an effect on a small body of water, there are many more to be accounted for when the study area is larger, for instance an ocean or sea.

The physics behind estuarine circulation are very complex. Estuarine systems rely heavily on the forcing of tidal driven currents, as well as variable bathymetry and bottom friction, energetic turbulence, and the potential for density gradients caused by the mixing of ocean and river waters. Despite this complexity, a key characteristic will always emerge, common to many systems when averaging circulation and stratification; exchange flow (MacCready and Geyer, 2010).

From traditional mid-twentieth century theories to present theories that use developments in parameterization of tidally average turbulent fluxes, the evolution of equilibrium flow can be traced with similar assumptions and solutions. In other words if you model the tidal forcing, and overall exchange of flow, a simplified estuarine system model can be sufficient. The tidal analysis and modeling carried out in this study is for barotropic (pressure-driven) hydrodynamics, while baroclinic (density-driven) hydrodynamics are ignored.

The evolution of a salt marsh is determined from its vertical accretion rates in correspondence with the tidal hydroperiod (duration and range of tidal inundation, as measured by MHW and MLW). Accretion results from organic sediment influx (sediment trapping) and the production of organic matter (primary production). A correlation between marsh accretion and biomass productivity related to tidal hydroperiod, as defined by MHW and MLW, has also been identified from fieldwork analysis using marsh organ and biomass sampling (Morris, 2002).

Therefore, if biomass production in coastal wetland areas is modeled, and its change due to rise, we could effectively quantify the adverse effect of sea-level rise. Equation 20 and 21 of this paper come from this work and represents the Marsh Equilibrium Model (MEM) developed by Morris et al. based on long term measurements of sediment build up and marsh biomass production.

Given a set of physical parameters, and the bathymetry of an area, tidal dynamics can be modeled from the area to provide water surface levels using a 2 dimensional hydrodynamics model. Water surface levels have been found to correlate directly with biomass density of the dominant species in tidal marshes (Morris, 2002; Hagen, et al., 2012; Alizad et al., 2015). This study used two-dimensional fields of mean low water (MLW) and mean high water (MHW) that were calculated from the ADCIRC hydrodynamic model.

Hagen et al. 2012 coupled the 2D ADvanced CIRCulation model with the zero dimensional parametric biomass equation from Morris et al. 2002. This extended the zero-dimensional (i.e., point-location) biomass curve to a (two-dimensional) marsh landscape for simulation of rise effects on salt marsh accretion. The work in this thesis adapted the previous work by Hagen et al. to cover the GTMNERR domain, and show the ability to move this practice to multiple estuaries.

It should be noted that this thesis work takes a single step from present-day conditions to 50 years out for sea-level rise scenarios of 0.13, 0.22 and 0.51 m, whereas the next logical step in this research will be to take an incremental step size to go from present day to 50 years out (e.g., see iterative scheme by Alizad et al., 2015).

3. Motivation

The primary motivation behind this study was to better understand relatable hydrodynamic and ecological processes in natural environments, with particular focus on how tidal hydrodynamics influence marsh ecology, i.e., the productivity of *Spartina alterniflora* in the GTMNERR. In order to develop a comprehensive model that could applicably predict hydrodynamics and ecology in the GTMNERR, it was important to first review the historical practices in this field of modeling.

Applying this model to the Guana Tolomato Matanzas National Estuarine Research Reserve (GTMNERR) provides a useful tool for affectively predicting the effects of storm surge, and sea level rise (SLR) in the area. The model could also be used for a variety of other practices. It could help out with selecting the most dynamically friendly area for a restoration project, or it could help plan for possible dredging projects in the area. Due to the model's foundation in physics, tweaks can be made to it (i.e. depth changes, flow changes, etc.) according most possible projects and physical changes.

Another motivation for applying the ADCIRC model to the area are the NOAA gauges currently located in the GTMNERR. The area has several gauges along the Reserve that are consistently collecting real time water level data. Most ADCIRC models are validated by comparing water levels in the model to that of observed water levels collected by gauges similar to the ones in the GTMNERR.

The collection of 8 tidal gauges that provided validation data to this model were established in the late 1970s. They have been collecting data since their implementation. Primarily the water level data collected by these sensors every 6 minutes was evaluated. Due to the wealth of time and variability of the data collected by these NOAA gauges, the model simulation period was be based on vegetation collection times.

Validation of biomass density prediction using ADCIRC is also more likely to be validated in the GTMNERR than in other areas due to the collection of vegetation data through the reserve. Currently the NERR collect data like canopy height, dominant species, and percent cover data that they have made available for this study. These data can be used and manipulated to help find a relationship to the biomass density predictions in the ADCIRC model.

The GTMNERR has been collecting this vegetation data (including 3x3 foot plot pictures, species population counts, and canopy cover) consistently in six locations since 2012. Collection dates can be seen in figure 2.

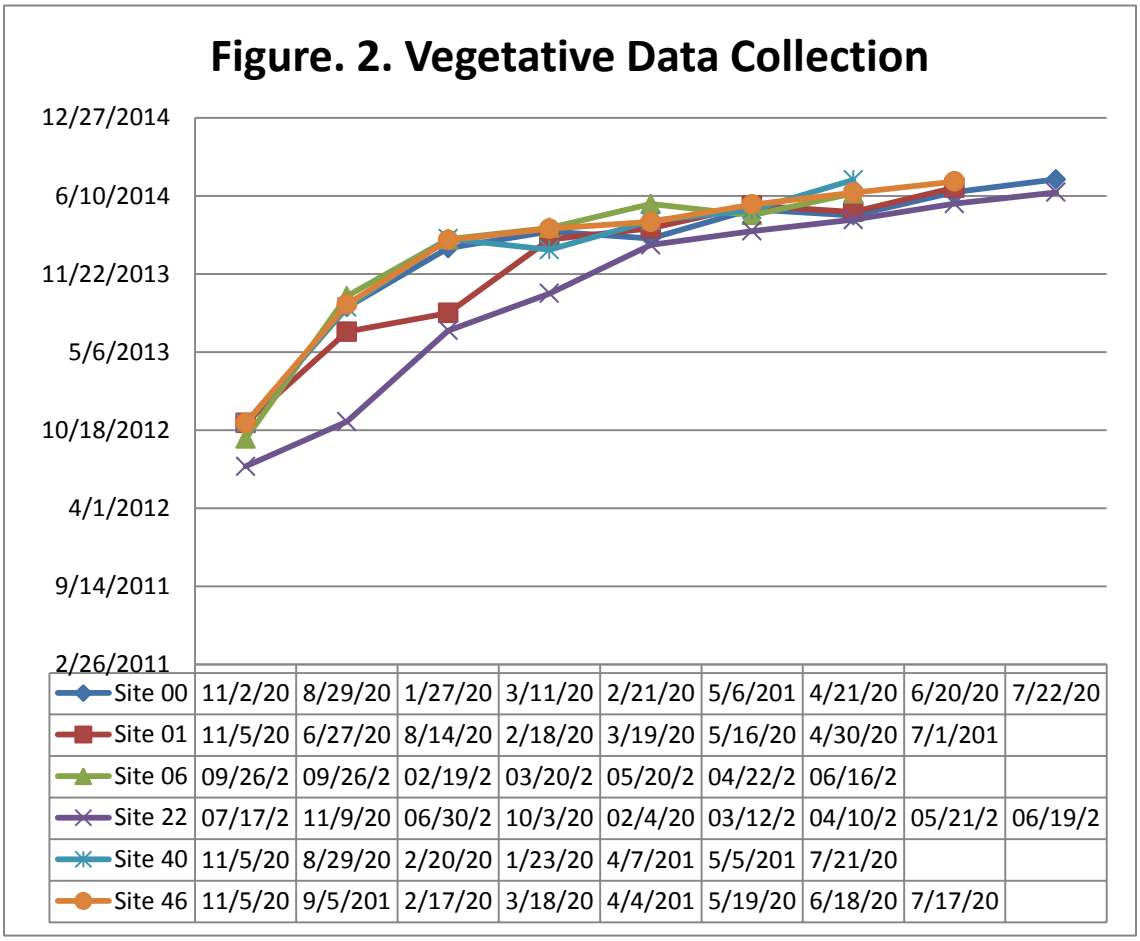

Site 00	11/2/20	8/29/20	1/27/20	3/11/20	2/21/20	5/6/201	4/21/20	6/20/20	7/22/20
Site 01	11/5/20	6/27/20	8/14/20	2/18/20	3/19/20	5/16/20	4/30/20	7/1/201	
Site 06	09/26/2	09/26/2	02/19/2	03/20/2	05/20/2	04/22/2	06/16/2		
Site 22	07/17/2	11/9/20	06/30/2	10/3/20	02/4/20	03/12/2	04/10/2	05/21/2	06/19/2
Site 40	11/5/20	8/29/20	2/20/20	1/23/20	4/7/201	5/5/201	7/21/20		
Site 46	11/5/20	9/5/201	2/17/20	3/18/20	4/4/201	5/19/20	6/18/20	7/17/20	

Figure 2. Vegetative Data Collection.

No ADCIRC model was currently in existence for the GTMNERR that has been validated in this way previous to this study. In addition, no model for the prediction of biomass density existed for the area. The ADCIRC model was adapted in this study in order to accomplish this.

This untapped and unexplored wealth of vegetative data collection is unparalleled compared to the once-a-year collection typical of most NERRs and is ideal for biomass density validation for the proposed ADCIRC model of the GTMNERR because it gives vast insight into what is actually happening on the ground in the GTMNERR to compare to model outputs. This model will provide a tool to the GTMNERR for the prediction of future accretion development in the estuary and general evolution of the salt marshes. Acquiring such a tool would be influential in defending the reserve against devastation caused by storms, development, and sea level rise.

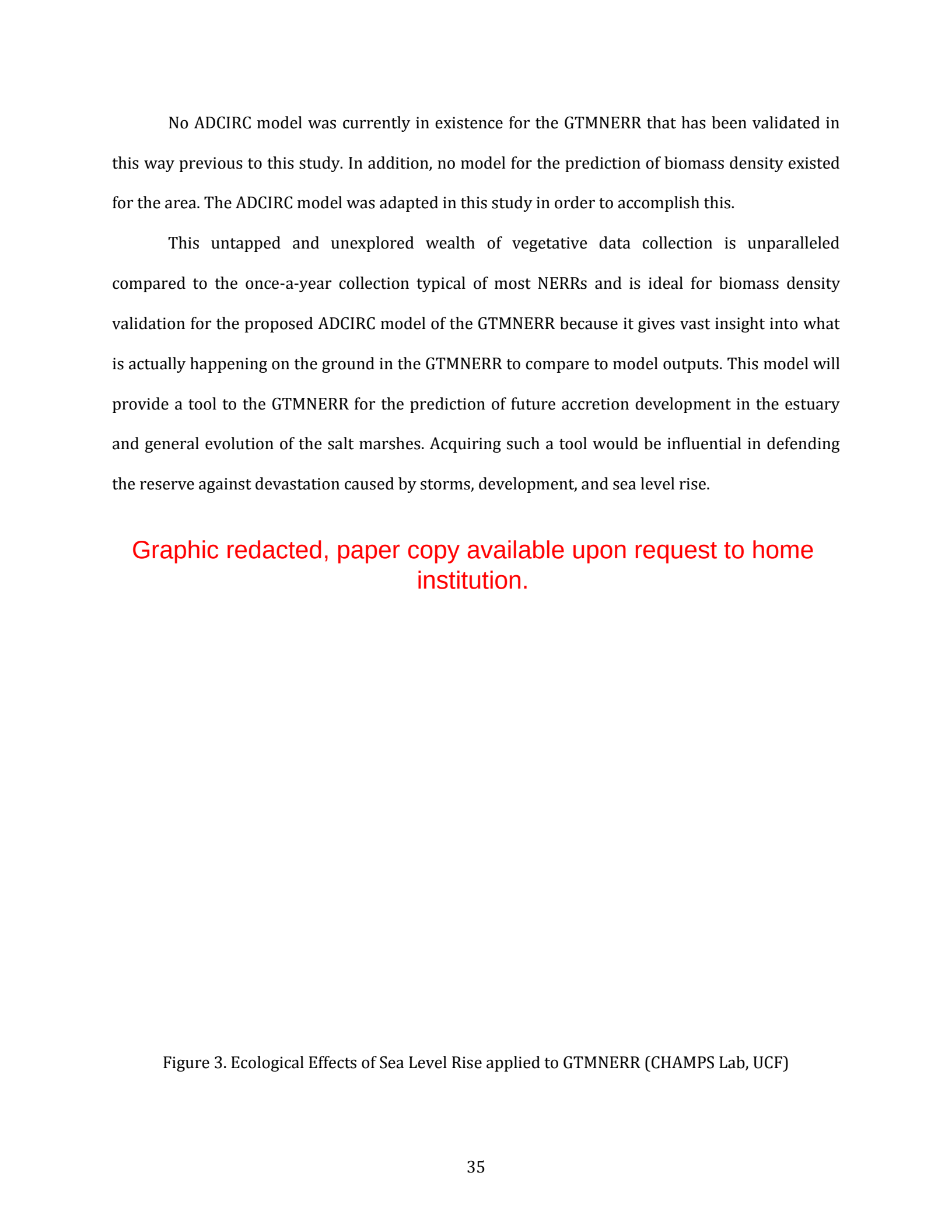

Figure 3. Ecological Effects of Sea Level Rise applied to GTMNERR (CHAMPS Lab, UCF)

Figure 3 represents the connectional relationship between the observational data, global climate change scenarios, and field and lab experiments to the ultimate prediction of the implications of sea level rise on places like the GTMNERR. The flow chart has been adapted from NOAA's Ecological Effects of Sea Level Rise Program (NOAA-EESLR project). This program has been working at creating a flow between data, models, results, assessments, and management tools. It effectively represents the motivation behind this research, as well. Ideally the work done using observations and field data in the GTMNERR leads to a coupled model, and better results. They were then be assessed and used for assistance in engineering management practices in the GTMNERR.

4. Model Concepts

The Advanced Circulation (ADCIRC) model provides a tool for efficient computation of the prediction of hydrodynamic circulation along coastlines, estuaries, and shelfs. Behind the mode is a universally integrated system of equations and procedures. Hydrodynamic, bathymetric, and sediment transport models were taken into account when designing ADCIRC (Luettich et al., 1992).

The continuous-Galerkin, shallow-water equations model (CG-SWEM) of Kubatko et al. (2006) was used for the numerical calculation of tidal hydrodynamics (shallow-water equations). Simulated hydrodynamic variables contain water surface elevations (units = m) and depth-integrated velocities (units = m/s). The numerical solution procedures of CG-SWEM use a continuous Galerkin-based handling of the governing equations which include the shallow water equations.

4.1 BASIC THEORY AND METHODOLOGY OF ADCIRC

ADCIRC uses a Boussinesq approximation simplification of the turbulent incompressible Reynolds equation as well as the hydrostatic pressure approximation to form a numerical model of the coastal/shelf circulation. These equations, though they are three dimensional equations, are only accurate in the horizontal direction due to the simplification process. The equations are, using the right handed Cartesian coordinate system, as follows;

equation 1 ... $$\frac{\partial u}{\partial x}+\frac{\partial v}{\partial y}+\frac{\partial w}{\partial z}=0$$

equation 2 ... $$\frac{\partial u}{\partial t}+u\frac{\partial u}{\partial x}+v\frac{\partial u}{\partial y}+w\frac{\partial u}{\partial z}-fv=-\frac{\partial}{\partial x}\left[\frac{p}{\rho_\circ}-r\right]+\frac{1}{\rho_\circ}\left[\frac{\partial \tau_{xx}}{\partial x}+\frac{\partial \tau_{yx}}{\partial y}+\frac{\partial \tau_{zx}}{\partial z}\right]$$

equation 3 ... $$\frac{\partial v}{\partial t}+u\frac{\partial v}{\partial x}+v\frac{\partial v}{\partial y}+w\frac{\partial v}{\partial z}+fu=-\frac{\partial}{\partial y}\left[\frac{p}{\rho_\circ}-r\right]+\frac{1}{\rho_\circ}\left[\frac{\partial \tau_{xy}}{\partial x}+\frac{\partial \tau_{yy}}{\partial y}+\frac{\partial \tau_{zy}}{\partial z}\right]$$

equation 4 … $\frac{\partial \rho}{\partial z} = -\rho g$

Where f is the Coriolis parameter, g is the acceleration of gravity, r is the tide generating potential, v is the molecular viscosity, p(x,y,z,t) are time averaged pressure, ρ(x,y,z,t) are time averaged density of water, $\rho_\circ$ is the reference density of water, t is time, and T is the integration time scale for separating turbulent and time averaged quantities.

τ_{xx}(x,y,z,t), τ_{yx}(x,y,z,t), τ_{zx}(x,y,z,t), τ_{xy}(x,y,z,t), τ_{yy}(x,y,z,t), and τ_{zy}(x,y,z,t) are the respective derived time averaged velocities in the x, y, and z directions minus the respective departures of the instantaneous turbulent velocities from the time averaged velocities integrated over the time scale for separating turbulent and time averaged quantities subtracted by the combined viscous and turbulent Reynolds stress factors in each direction.

Pressure can be eliminated as a dependent variable from equations 2 and 3 using the vertical momentum equation. This following will result (where equation 2 and 3 are replaced by equation 5 and 6 respectively);

equation 5 … $\frac{\partial u}{\partial t} + u\frac{\partial u}{\partial x} + v\frac{\partial u}{\partial y} + w\frac{\partial u}{\partial z} - fv = -\frac{\partial}{\partial x}\left[\frac{p}{\rho_\circ} + g\mathrm{Z} - r\right] + \frac{\partial}{\partial z}\left(\frac{\tau_{zx}}{\rho_\circ}\right) - b_x + m_x$

equation 6 … $\frac{\partial v}{\partial t} + u\frac{\partial v}{\partial x} + v\frac{\partial v}{\partial y} + w\frac{\partial v}{\partial z} + fu = -\frac{\partial}{\partial y}\left[\frac{p}{\rho_\circ} + g\mathrm{Z} - r\right] + \frac{\partial}{\partial z}\left(\frac{\tau_{zy}}{\rho_\circ}\right) - b_y + m_y$

Where b_x is equal to acceleration of gravity for the given water density reference differentiated across the x axis multiplied by the integration in the difference in density from the depth to the free surface elevation relative to the geoid subtracted by baroclinic x forcing. Whereby is equal to acceleration of gravity for the given water density reference differentiated across the y axis multiplied by the integration in the difference in density from the depth to the free surface elevation relative to the geoid subtracted by baroclinic y forcing. M_x is the total stress given the reference water density minus horizontal momentum diffusion in the x direction. M_y is the total stress given the reference water density minus horizontal momentum diffusion in the y direction.

The solution to these equations is the boundary equations given by equations 7, 8, 9, and 10;

$$\boldsymbol{equation\ 7} \ldots \ w = \frac{\partial \zeta}{\partial t} + u\frac{\partial \zeta}{\partial x} + v\frac{\partial \zeta}{\partial y}$$

$$\boldsymbol{equation\ 8} \ldots \ \tau_{zx} = \tau_{sx}, \tau_{zy} = \tau_{sy}$$

Where $\tau_{sx}(x,y,t)$ and $\tau_{sy}(x,y,t)$ are the wind stresses applied at the water surface.

$$\boldsymbol{equation\ 9} \ldots \ w = -[\frac{\partial h}{\partial t} + u\frac{\partial h}{\partial x} + v\frac{\partial h}{\partial y}]$$

$$\boldsymbol{equation\ 10} \ldots \ u = 0, v = 0 \ at \ z = -h + z_0$$

Equation 7 is the boundary condition at the free surface. Equation 9 is the boundary equation at the bottom. In the model, land surface boundary equations will be specified for normal flux. Normally this will be considered 0 for river boundaries or solid boundaries. At open boundaries, like ocean or along river exits, the free surface equation will be specified. Typically a radiation boundary condition will be used to allow water to propagate out or enter into the domain. These are the governing equations of ADCIRC.

4.2 TWO DIMENSIONAL DEPTH INTEGRATION ADCIRC OPTION (ADCIRC-2DDI)

This study used the ADCIRC model to primarily focus on the influence of tide driven hydrodynamics in the GTMNERR. Using the vertically integrated equations of mass and momentum conservation the ADCIRC two dimensional depths integrated (ADCIRC-2DDI) model performed tidal simulations. Shallow water wave equations were used (Kolar et al., 1994), and the hybrid bottom friction formula. Lateral diffusion and dispersion effects are employed, and baroclinic terms are neglected in order to avoid time costliness (within acceptable accuracy).

These base line formulas lead to the following set of balance laws. They are presented in non-conservative, primitive, form and expressed in a spherical coordinate system;

$$\textbf{equation 11} \ldots \frac{\partial \zeta}{\partial t} + \frac{1}{R \cos \phi}\left[\frac{\partial UH}{\partial \lambda} + \frac{\partial (VH \cos \phi)}{\partial \phi}\right] = 0$$

$$\textbf{equation 12} \ldots \frac{\partial U}{\partial t} + \frac{1}{R \cos \phi} U \frac{\partial U}{\partial \lambda} + \frac{1}{R} V \frac{\partial U}{\partial \phi} - \left(\frac{\tan \phi}{R} U + f\right) V$$

$$= -\frac{1}{R \cos \phi} \frac{\partial}{\partial \lambda}\left[\frac{P_s}{\rho_0} + g(\zeta - \alpha\eta)\right] + \frac{1}{H} M_\lambda + \frac{\tau_{s\lambda}}{\rho_0 H} - \tau_* U$$

$$\textbf{equation 13} \ldots \frac{\partial V}{\partial t} + \frac{1}{R \cos \phi} U \frac{\partial V}{\partial \lambda} + \frac{1}{R} V \frac{\partial V}{\partial \phi} - \left(\frac{\tan \phi}{R} U + f\right) U$$

$$= -\frac{1}{R} \frac{\partial}{\partial \phi}\left[\frac{P_s}{\rho_0} + g(\zeta - \alpha\eta)\right] + \frac{1}{H} M_\phi + \frac{\tau_{s\phi}}{\rho_0 H} - \tau_* V$$

$$\textbf{equation 14} \ldots M_{\lambda,\phi} = \frac{E_{h_2}}{R^2}\left[\frac{1}{\cos^2 \phi} \frac{\partial^2 (U,V) H}{\partial \lambda^2} + \frac{\partial^2 (U,V) H}{\partial \phi^2}\right]$$

Where t is time, λ is degrees longitude (east of Greenwhich positive), ϕ is degrees latitude (north of equator positive), U is the depth integrated velocity in the longitudinal direction, V is the depth integrated velocity in the latitudinal direction, H is the height (total) of the water column, h is the bathymetric depth relative to Mean Sea Level (MSL), ζ is the free surface elevation relative to MSL, f is the Coriolis parameter, p_s is the atmospheric pressure at the free surface, E_{h2} is the horizontal eddy viscosity, $\tau_{s\lambda}$ is the applied free surface stress in the longitudinal direction, $\tau_{s\varphi}$ is the applied free surface stress in the latitudinal direction, τ_* quadratic bottom stress, η is the Newtonian equilibrium tide potential, and R is the radius of the earth.

Vertical integration across surface elevation by the momentum conservation equations (Blumberg and Mellor, 1987) is represented in the longitudinal direction by equation 12, and the latitudinal direction by equation 13. ADCIRC-2DDI takes equations 12-14 and projects them from a spherical form into a rectilinear form using a Carte Parallelogrammatique projection (Pearson, 1990) in order to smooth out finite element based solutions for the equations.

After this projection, spatial dependence of shallow water equations are resolved using the finite element method. This takes the equations from their primitive form and converts them into the generalized wave continuity equation (GWCE) formulation (Sidén and Lynch, 1988). ADCIRC implements the discretized form of the GWCE along with the non-conservative form of the conservation of momentum equations. Both of which are discretized for time.

After manipulation and depth forcing a high efficiency formulation is developed. Due to this formulation's high amplitude and phase propagation characteristics it is highly accurate. The conservation of momentum equations' matrix is dependent on time. The grouping of these formulas and procedures are what make ADCIRC-2DDI so effective.

As for bottom the accounting of bottom friction in the system, this is heavily depth dependent. This can be seen in the bottom friction formula;

$$\boldsymbol{equation\ 15} \ldots \tau_* = \frac{C_f\sqrt{U^2 + V^2}}{H}$$

The bottom friction factor, C_f, can be computed the following three ways;

$$\boldsymbol{equation\ 16} \ldots C_f = \frac{f_{dw}}{8}$$

$$\boldsymbol{equation\ 17} \ldots C_f = \frac{g}{C_C^2}$$

$$\boldsymbol{equation\ 18} \ldots C_f = \frac{n_m^2 g}{h^{1/3}}$$

Where f_{Dw} is the Darcy Weisbach friction factor, C_C is the Chezy friction coefficient, and n_m is Manning's friction factor. The ADCIRC model used will use the following formula;

$$\boldsymbol{equation\ 19} \ldots C_f = C_{fmin}[1 + \left(\frac{H_{break}}{H}\right)]^{\frac{\gamma}{\theta}}$$

Where C_{fmin} is the minimum bottom friction factor that is approached in deep waters, and H_{break} is the height at which break depth occurs, θ represents how rapidly the bottom friction factors reaches its upper and lower limits, and ϒ represents how quickly the C_f increases as depth increases. For this study 10 m, 10, and 1/3 were the values given for H_{break}, θ, and ϒ, respectively.

The tested combined formulas behind the ADCIRC-2DDI model are what make it such a powerfully accurate prediction model.

5. Methods

In order to replicate the tidal flows (two dimensional) the following procedures were taken. The West North Atlantic Tidal model (WNAT) domain was utilized to create open ocean forcings being forced at full tide into the system. The GTMNERR domain was defined. A set of parameters were defined for the area, and ADCIRC was run. Post run calculations were then done to analyze biomass density evolution curves. The following is a brief explanation into each step taken in this study. This is the set up for a grounded understanding in the results of this study.

5.1 FOUNDATION OF MODEL EFFORTS

Model bathymetry was obtained from John et al. (2003) to provide bathymetric description for the inshore domain including St. Augustine Inlet, Matanzas Inlet and the Atlantic Intracoastal Waterway. Model bathymetry for the offshore and deep-water domain (Figure 4) is provided by the WNAT model of Hagen et al. (2006). Meshing of the inshore domain is guided by a 50-m element-size criterion; however, shorelines of high curvature and narrowly sized channels are defined using elements sized as low as 25 m. The localized mesh that is developed for the GTMNERR is merged into the large-scale domain of Hagen et al. (2006).

The preliminary mesh for the GTMNERR large-scale domain contains 148459 nodes and 287176 elements. Figure 5 shows the bathymetry of the WANT model, displayed in meters below Mean Sea Level (MSL). To give perspective the continental shelf break is boxed in this Figure, this is at a depth of 183 m below MSL. The bathymetry ranges from zero to around 8000 meters in sections of the deep area of the basin. The element size gets to around 25m around the creeks.

Figure 4. The Large-Scale Finite Element Mesh (Hagen, 2006)

Figure 5. Bathymetry of WNAT Model Domain (in meters below MSL) (Bacopoulos, 2005)

The WNAT model encompasses the Gulf of Mexico, the northern portion of the Atlantic Ocean, and the Caribbean Sea all west of the 60° west meridian. It is bounded by south, north, and west by South America, North America, and Central America, respectively. Overall the model's domain covers approximately 8.4 million km^2.

Figure 4 shows the finite element mesh created using a LTEA (Hagen et al., 1998) based technique. The mesh is made up of nodal points with x,y, and z values representing latitude, longitude, and depth. Each node is connected to three other nodes by a line, of which interpolation between the two points takes place when modeling flow over the line. The LTEA technique places more nodes in the areas where there is more intricate bathymetry details (typically the more shallow areas).

This is apparent when comparing Figures 4 and 5. In Figure 5 the areas represented by dark blue are less than 100 meters deep, and in Figure 4 these areas have more nodes (or points). For example, when looking at the continental shelf region, it should be noted there is an increase in grid resolution, yet in the Atlantic Ocean, there are far fewer nodes. This helps capture the rapid changes in water flow over quickly changing bathymetry in the shallow region, while save computing time over the ocean and sea domains.

Next, it was time to create the GTMNERR domain. It was necessary to include a large portion of the deep ocean basin. This is called the large domain approach (Westerink et al., 1995). This allows for the open ocean boundary conditions of the GTMNERR domain to be enforced as well as the nonlinear response to tides to occur in the shallow waters, as this is typically where the tides will affect the hydrodynamics more due to the bottom interaction. It was important when selecteing this large computational domain to know that it encompasses a large expanse of subterranean ocean as well as the coastline that will be connecting the ocean to the domain area of interest. This coast line is where the large domain will overlap with the region of interest domain, allowing for simple boundary condition calculations.

This large domain approach also allowed for more simple boundary conditions to be set up in the model. This results in the astronomical forcing to be applied by the coupling of the global ocean model, so that the effect of harmonic behavior of tides in the deep ocean regions is accurately predicted. Using this method creates the benefit of nonlinear processes in the deep ocean to be non-significant to the model. Due to the benefits of this method the WNAT model is ideal for providing domain that sits far into the depths of the ocean.

Now that a large domain has been secured, it was time to move on to the GTMNERR finite element meshing. Using the before mentioned bathymetry (John et al., 2003) as well as survey data provided by NOAA and surveys done by the Army Corps, the area was be discretized to include its coastline and bathymetric data. This is created by automatic mesh generation, a process provided by the program Surface-water Modeling System (SMS) (Zundel, 2006).

These data used to generate the mesh was developed using a digital elevation model (DEM) that was made using LiDar data as well as coastline shape files. The mesh generation by SMS is similar to the WNAT model; however the level of discretization was higher due to the more finite details of the GTMNERR bathymetry. Figure 6 shows the GTMNERR mesh generated; it has 148459 computational nodes and 287176 triangular elements.

Figure 7 demonstrates the nodal density of the mesh in meters. This is the concentration of nodes necessary to accurately resolve the shoreline and bathymetric features of the Guana Tolomato Matanzas National Estuary Reserve. This bathymetry and topography is shown in Figure 8. When comparing figure 7 to 8 it is noted that the more shallow areas tend to have a more dense concentration of nodes and elements. This is due to the complexity of the GTMNERR's streams and rivers.

In other words, as the bathymetry changes more rapidly from meter to meter along the ocean floor, more nodes were needed to represent this change in depth. Likewise, where the mesh covers the ocean the amount of nodes needed to computationally represent the bathymetry is becomes much less as the depths of the domain become greater. These nodes each hold spatial data for their area and help ADCIRC to compute the basic physics of the model by filling that data into the equations mentioned earlier.

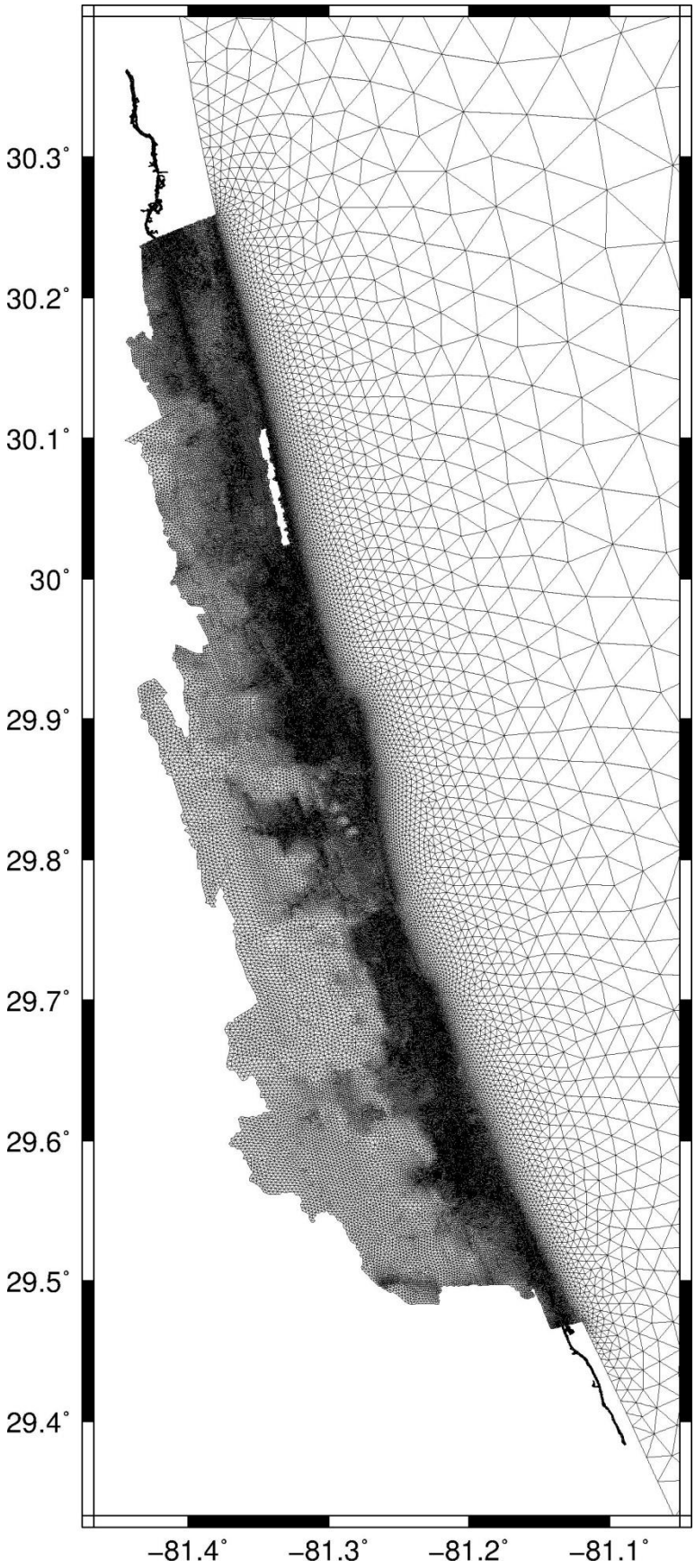

Figure 6. GTMNERR Finite Element Mesh used for Model Simulations

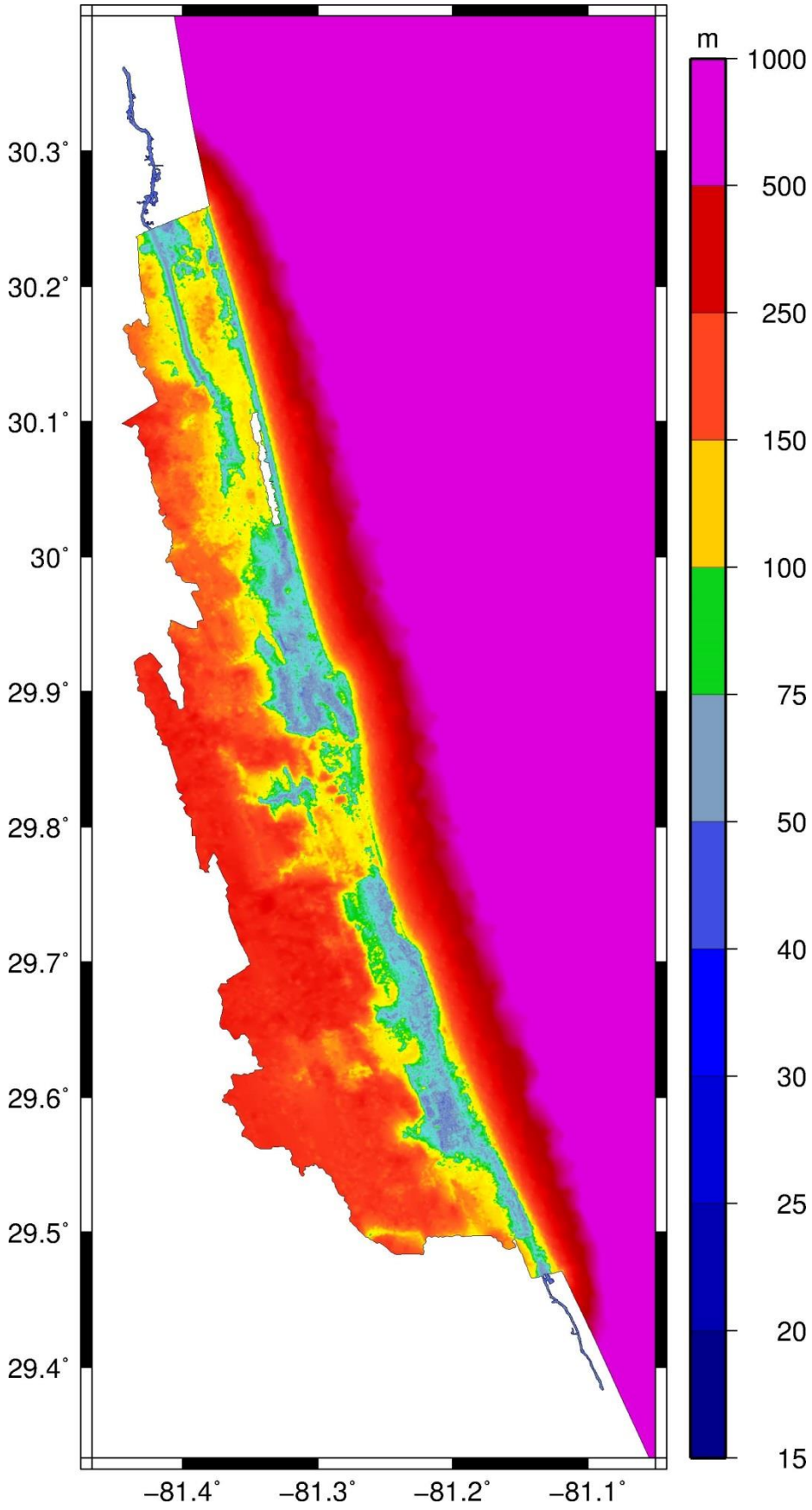

Figure 7. GTMNERR Finite Element Mesh Size and Distribution

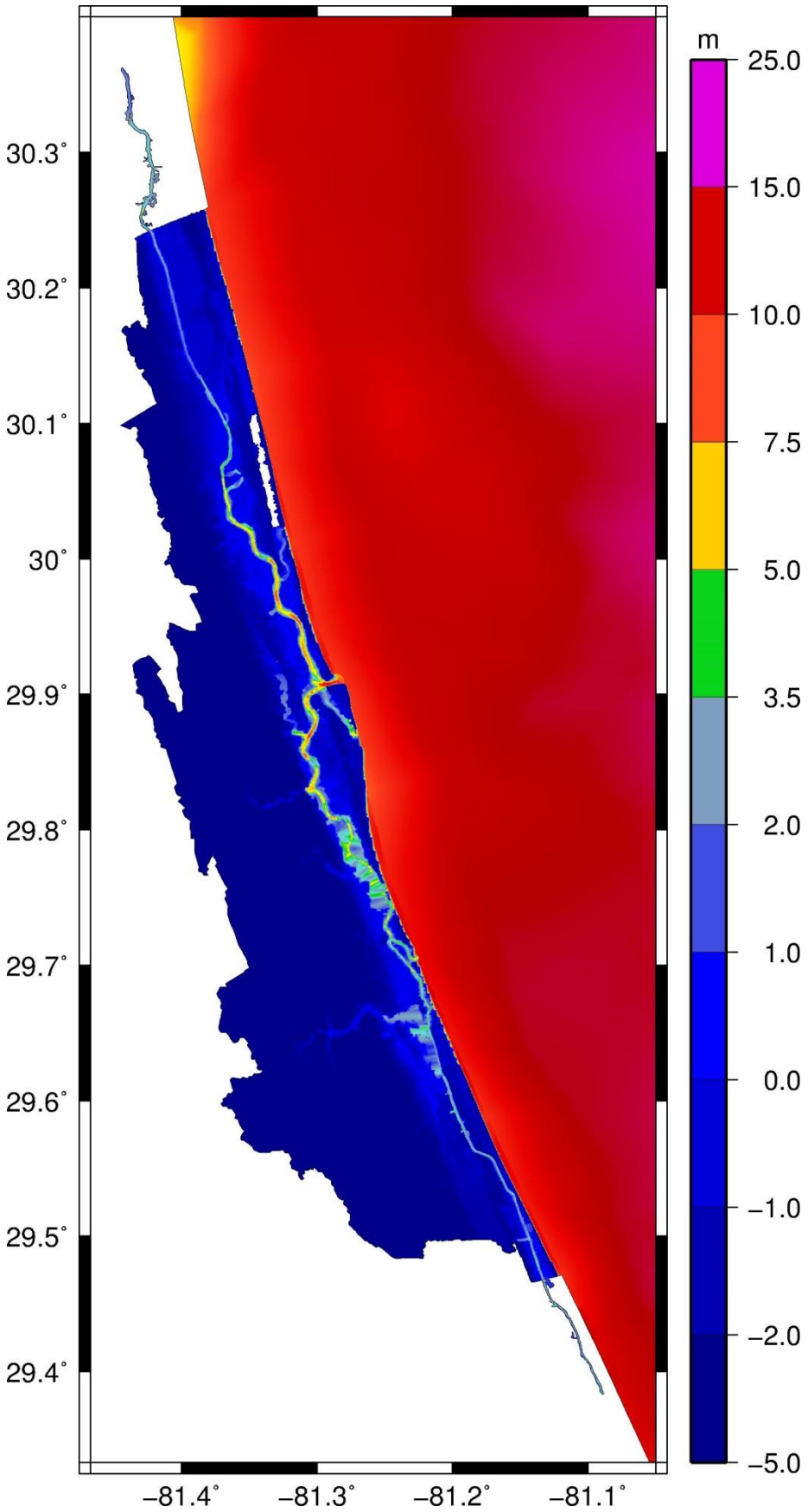

Figure 8. GTMNERR Model Representation of Bathymetry and Topography

5.2 MODELING PARAMETERS AND BOUNDARY CONDITIONS

After the WNAT model domain and the GTMNERR model domains were created, the ADCIRC preparation began. The following parameterizations and boundary conditions listed all remain constant over the period of time chosen to run the simulation. The model was prepped, so that tidal conditions began with a cold start (i.e. conditions begin at zero and ramp up). The tidal constituents chosen to have acting forcing on the model are K1, O1, M2, S2, N2, K2, and Q1. Table 1 shows the amplitude and period of these constituents. These eight tidal forcings were applied as boundary elevations at the deep-water, open-ocean boundary of the WNAT and as tidal potentials over the interior of the computational domain (Figure 5).

TABLE 1. PRINCIPAL TIDAL CONSTITUENTS (APEL, 1987)

Graphic redacted, paper copy available upon request to home institution.

The specific parameters were set up for the preliminary run in the fort.15 file. In this file certain options were turned on or off with a 0 or 1, respectively. Also listed are run time, time step, starting time, duration of ramp function, H_0, time weighting factors, friction factors, acceleration of gravity, and the center of the projection were clarified. The tidal constituents to be considered (Table 1) were also clarified. The coordinates of each tidal gauge were provided, where ADCIRC will use this fort.15 file to output the desired water surface elevations for this model.

After setting all conditions for present day conditions (sea level rise = 0m), the model is run. Time-series water levels were resynthesized and summed up to represent water surface elevations at each time step. The time step is 360 seconds, or 6 minutes. Output is in the form of Fortran files of point and vector values at each node. The values were calculated at every node (globally) and at the eight specific gauge locations (for which each time step is written out). These files were then manipulated and analyzed.

Three more runs were made after this, adjusting for sea level rise. The initial conditions, including bathymetry values, remain the same as the previous run. One nodal attribute is added, however. The fort.13, or nodal attributes file, held the information on sea level rise scenarios. For no sea level rise this value is zero, for mild it is 0.13, for moderate it is 0.22, and for extreme the value is 0.51. Figure 9 shows the top of this file for the first and second SLR runs (i.e. the SLR=0m and SLR=0.13). Note the correspondence of the changed sea_surface_height_above_geoid value between the no SLR and mild SLR scenarios. Values for the sea level rise scenarios (mild, moderate, and extreme) were selected based on predictions by Parris et al. (2012), shown in Figure 10.

ADCIRC Model 148459 3 sea_surface_height_above_geoid m 1 0.00 primitive_weighting_in_continuity_equation 1 1 0.030000 mannings_n_at_sea_floor m 1 0.0200000000 sea_surface_height_above_geoid 0	ADCIRC Model 148459 3 sea_surface_height_above_geoid m 1 0.13 primitive_weighting_in_continuity_equation 1 1 0.030000 mannings_n_at_sea_floor m 1 0.0200000000 sea_surface_height_above_geoid 0

Figure 9. Top of Nodal Attribute File (fort.13) for 0.0m and 0.13m SLR Scenarios

Graphic redacted, paper copy available upon request to home institution.

Figure 10. shows predictions of sea level rise from Parris et al. (2012).

5.3 THEORY ON BIOMASS DENSITY CALCULATIONS

Biomass density (i.e., productivity) of the marshes in the GTMNERR is evaluated using the following method. Figure 11 effectively demonstrates marsh vertical accretion with respect to a set of datums. It shows the location of the marsh platform (or elevation) and its vertical accretion in relationship to where the sea level is at Mean High Water (MHW) and Mean Low Water (MLW). Mean Sea Level (MSL) is the arithmetic mean of water levels over the record, MLW is the average of low water of each tidal cycle over the record, and MHW is the average of high water of each tidal cycle over the record

Utilizing the output from the ADCIRC-2DDI model, water levels for selected areas was recorded. The areas chosen were based on where the observational data were collected. For each set point the MHW, MLW, and elevation of that point were noted for further calculation. Six locations were chosen due to their identification as the six locations of which vegetation data was collected. These data were collected (MHW, MLW, and elevation) and then were utilized to find the biomass density in the target specie of the study; *Spartina alterniflora* grass.

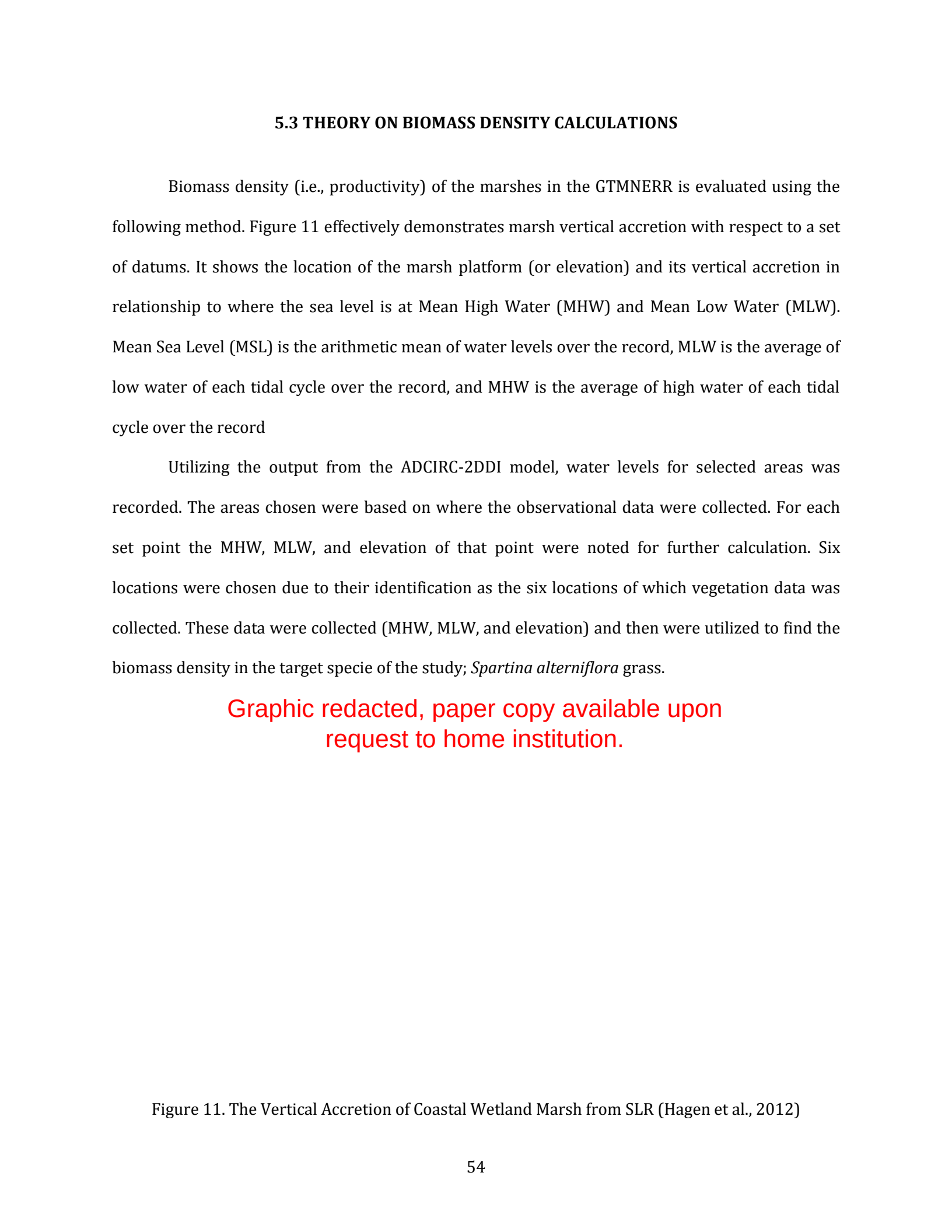

Figure 11. The Vertical Accretion of Coastal Wetland Marsh from SLR (Hagen et al., 2012)

Biomass density, species specific, is best described as the accumulation of organic matter per area. The GTMNERR's dominant species is *Spartina alterniflora*. Morris et al. (2002) did a study in Goat Island on the inter-relationships between *Spartina alterniflora* and their collection of organic and inorganic sediment. This was done using SETs and recording the accretion level of monitored plots. Also monitored, was the growth of the *Spartina alterniflora* in the area.

At each visit the sediment elevation was recording using the pins in the SET tests, and the accretion rats were calculated given the change in vertical rise from a set horizontal point in the marsh platform. The heights of selected *Spartina alterniflora* were recorded, as well as the growth of any other *Spartina alterniflora* in the given monitored plots. These data were recorded and reviewed with respect to monitored tidal datums in the area and the relative depth of the marsh platform. The outcome was equation 20 and 21. Biomass density is a function of relative marsh surface elevation. This is shown in equation 20.

equation 20 … $B = aD + bD^2 + c$

Where B is biomass density measured in grams/meters2, a, b, and c are coefficients that determine the upper and lower depth limits, and magnitude of B, and D = relative depth. Relative depth can be measured by the above mentioned datums; this is shown in equation 21.

The values of a, b, and c will differ regionally as a function of tidal range, salinity, climate, and dominant species.

equation 21 … $D = \dfrac{(MHW - E)}{(MHW - MLW)}$

Where E is relative marsh surface elevation in meters. For the before mentioned *Spartina alterniflora* (Dame et al., 2000) the values for a, b, and c are 1000, -3718, and 1021 respectively (Hagen and Morris, 2012). All meter values are in NAVD 88 units, and coefficients are based on the findings of the study that took place in North Carolina. This may introduce error (i.e. NC vs. FL values), and could be worth further investigation, perhaps in the form of future validation work.

equation 22 … $\frac{dB}{dD} = 2\text{bD} + \text{a}$

In order to analyze the hydro-marsh model results, the derivative of the biomass equation must be solved for non-dimensional depth. This is shown in equation 22. The accretion rate for the salt marsh platforms is dependent on organic and inorganic sediment build up (Morris et al., 2002). In order to keep from becoming completely submerged, these two sediment types are each necessary to maintain marsh productivity against increasing sea levels (Nyman et al., 2006). Morris et al. 2002 developed a linear function for the rate of total accretion (seen in equation 23).

equation 23 … $\frac{dY}{dt} = (q + kB)D \; for \; D > 0$

Where q represents the inorganic sediment, and k is the organic sediment. These values varies based on estuary system (Morris et al. 2002). The marsh elevation platform change is shown in equation 24;

equation 24 … $Y(t + \Delta t) = Y(t) + dY$

Where the marsh platform has a change of dY meters every del(t) years.

Figure 12 demonstrates the dynamic coupling between the ADCIRC and Marsh Equilibrium Model (MEM) models. Black boxes show parameters that are not changed, and gold boxes are the parameters that are being changed through the simulation. The overall outline of the model coupling is of the hydrodynamic modeling feeding into the Marsh Equilibrium Model (MEM) until the desired output is accomplished. It should be noted that this thesis work takes a single step from present-day conditions to 50 years out for sea-level rise scenarios of 0.13, 0.22 and 0.51 m, whereas the next logical step in this research was to take an incremental step size to go from present day to 50 years out (e.g., see iterative scheme by Alizad et al., 2015).

Using equation 25, the biomass curves presented in this research could be used to produce the ideal amount of artificial accretion an engineer would have to distribute to an area. This is an example of an engineering solution for possible erosion (Hagen et. al,2012). This accretion would be added at time equal to zero in the MEM model. This is proposed work.

equation 25 … $\Delta z_n = SLR(\frac{B_{max} - B_n}{B_{max}})$

Where Δz_n is local thickness of engineered accretion (m), SLR is the applied sea level rise (m), B_n is the local biomass density, and B_{max} is the maximum possible biomass density (g/m^2).

Graphic redacted, paper copy available upon request to home institution.

Figure 12. Marsh Equilibrium Model Flowchart (adapted from Hydro Marsh Model Flow Chart by (Alizad et al., 2015)

After hydrodynamics were modeled using the shallow equations models in ADCIRC-2DDI the results were stored. Using a Python v2.7 a "Tidal Datums" code (Hagen et al. 2012) was used to separate out the MHW and MLW and create two raster files for each. These files represent the average MHW and MLW at set points. Using the Inverse Distance Weighted (IDW) method at a setting of 16, these values were interpolated from creeks and rivers onto the salt marsh land.

These values were then applied to the MEM for the calculation of biomass density over the marsh landscape. The MEM has been demonstrated as being capable of accurately predicting the response to sea level rise in salt marshes (Morris et al. 2002).

Surface-Water Modeling System (SMS) was used to make this calculation everywhere throughout the GTMNERR domain. After the ADCIRC run for zero sea level was done computing, the outputs were collected and Tidal Datums code was executed. This generated a Fortran file for MHW and MLW averages throughout the GTMNERR. These files were each input into SMS. The intermittently wet and dry areas as well as the fully dry areas were cut away. Values remaining were the MHW and MLW for only the fully wet area. These values were interpolated over the dry parts of the mesh. The IDW method was used, pulling from the sixteen closest nodes.

The data calculator was then used in SMS to solve first for D (equation 21) using MLW, MHW, and Elevation, then for B (equation 20) using D, a, b and c,for the entire ADCIRC GTMNERR mesh. The biomass density was then categorized and organized. Biomass productivity in the marsh less than 370 g/m^2 were categorized as low, between 370 and 750 g/m^2 were categorized as medium, and more than 750 g/m^2 are considered high productivity (Alizad et al., 2015).

6. Observation Data

The physical and ecological processes explored in this study were tidal hydrodynamics and marsh productivity. The study examines how tidal hydrodynamics influence marsh ecology, i.e., the productivity of *Spartina alterniflora* in the GTMNERR.

Tidal gauges throughout the GTMNERR and vegetation data sources were sought out to fill in the rest of the data picture of tidal hydrodynamics and marsh productivity for the GTMNERR. The field data collection, the additional data sources, and the numerical modeling were fused together to provide a validated data-modeling tool for tide and marsh-productivity simulations of *Spartina alterniflora* in the GTMNERR.

6.1 NOAA TIDE GAUGES

Eight water elevation gauges in the GTMNERR validated the ADCIRC model. Figure 13 shows a geographic map of the GTMNERR. The stars indicate the eight tide gaging stations with tidal predictions (1—Pablo Creek; 2—Tolomato River; 3—Vilano Bridge; 4—St. Augustine; 5—Anastasia Island; 6—Fort Matanzas; 7—Matanzas River Headwaters; 8—St. Augustine Beach) including the one gaging station at St. Augustine Beach that also contains historical water level data (red-filled star). The background map is sourced from the Friends of the GTM Reserve (2014). Table 2 provides the exact locations of the eight tide gaging stations.

Observed water surface elevations for a set time period were collected from these stations. The geographic spread, ranging from the north tip (star 1) to the south tip (star 8) of the GTMNERR provide for a good amount of validation data. The locations of the gauges range in land cover variance as well (from beaches, to the head of creeks, to river heads). The spectrum of location represented differences in tidal current, and the variety land cover helped capture variance in stress due to bottom and boundary cover differences.

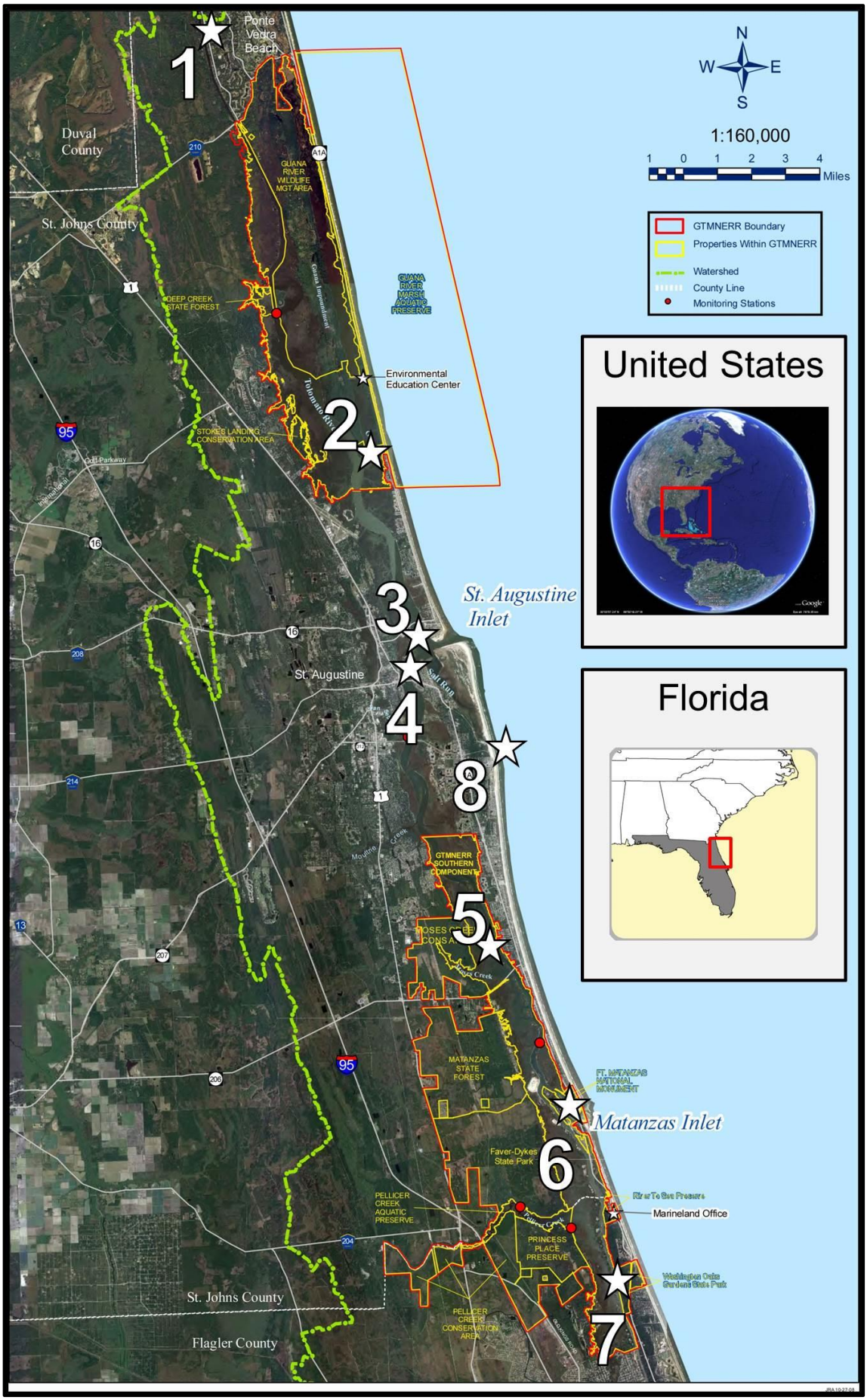

Figure 13. Location of NOAA Tidal gauges

Tides and water levels			
Station	°N	°W	Detail
Pablo Creek	30.3230	81.4380	NOAA tidal constituents
Tolomato River	29.9900	81.3200	NOAA tidal constituents
Vilano Bridge	29.9100	81.3000	NOAA tidal constituents
St. Augustine	29.8920	81.3100	NOAA tidal constituents
Anastasia Island	29.7930	81.2720	NOAA tidal constituents
Fort Matanzas	29.7150	81.2380	NOAA tidal constituents
Matanzas River Headwaters	29.6300	81.2100	NOAA tidal constituents
St. Augustine Beach	29.8567	81.2633	NOAA tidal constituents and verified water levels

Table 2. Data Sources used in Water Elevation Prediction Model Validation for GTMNERR

From the eight different tidal gauges, of varying locations and cover water surface elevations were collected. A time period was selected based on overlapping availability of water surface elevation data for all eight gauges. The overlap is 9/21/1999 – 10/21/1999. Figures 14 through 21 show the 30 days of the water surface elevations that were collected from NOAA tidal gauge observations. They were compared to the results from the ADCIRC model.

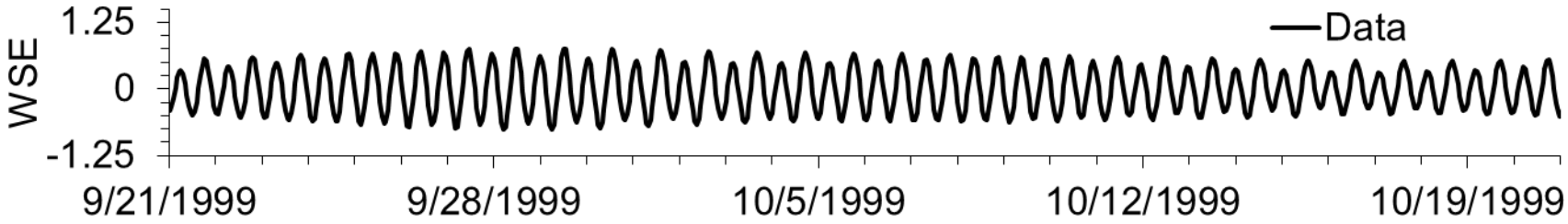

Figure 14. Sta. 1: Observed Water Levels at Pablo Creek, FL NOAA Gauge Station

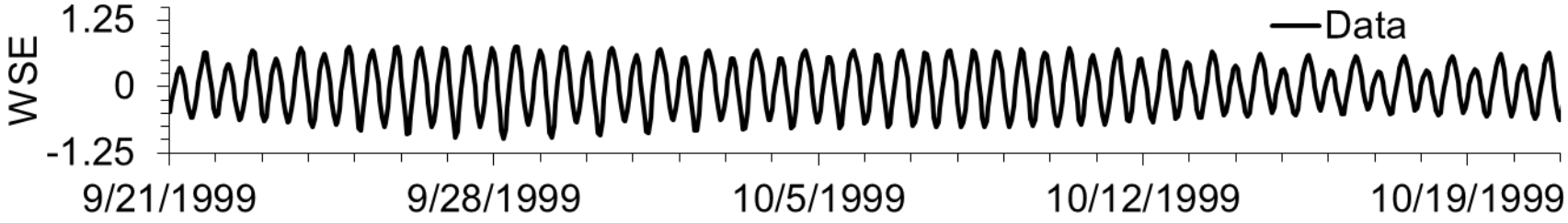

Figure 15. Sta. 2: Observed Water Levels at Tolomato River, FL NOAA Gauge Station

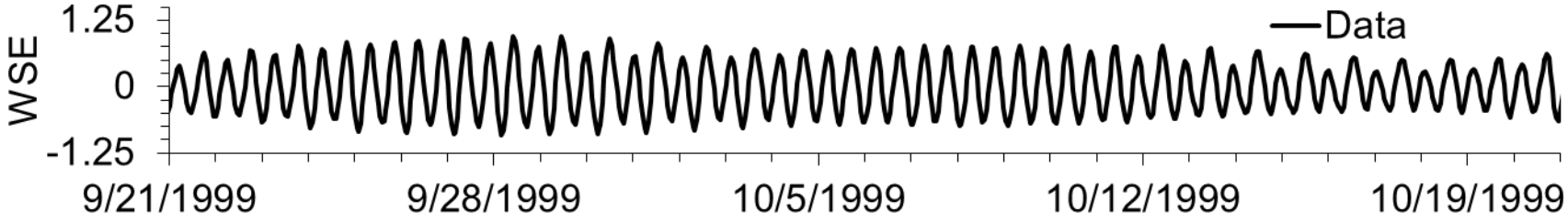

Figure 16. Sta. 3: Observed Water Levels at Vilano Bridge, FL NOAA Gauge Station

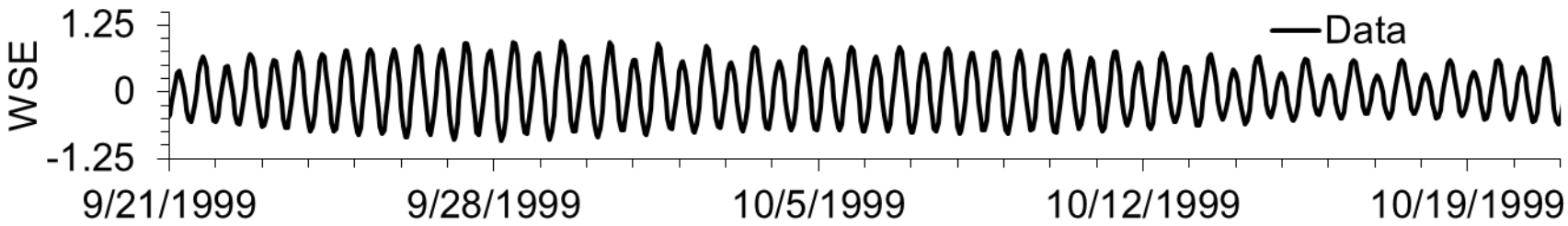

Figure 17. Sta. 4: Observed Water Levels at St. Augustine, FL NOAA Gauge Station

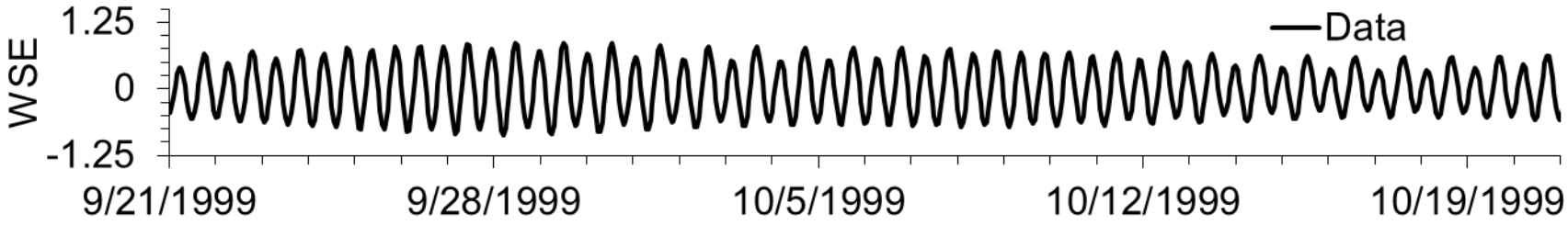

Figure 18. Sta. 5: Observed Water Levels at Anastasia Island, FL NOAA Gauge Station

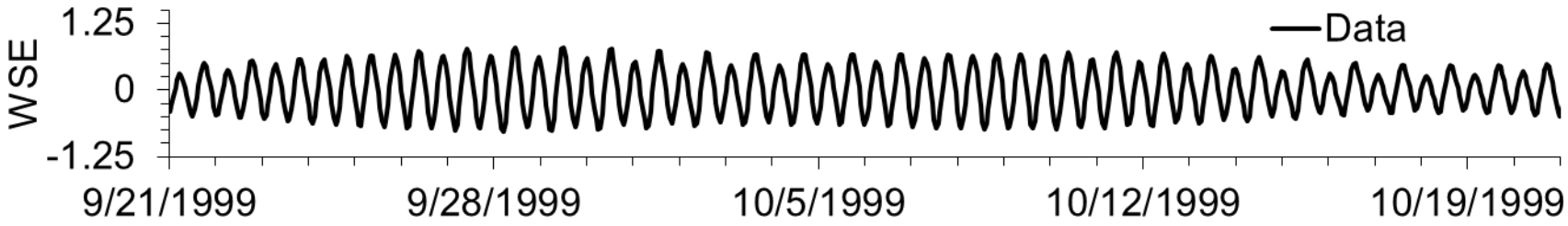

Figure 19. Observed Water Levels at Fort Matanzas, FL NOAA Gauge Station

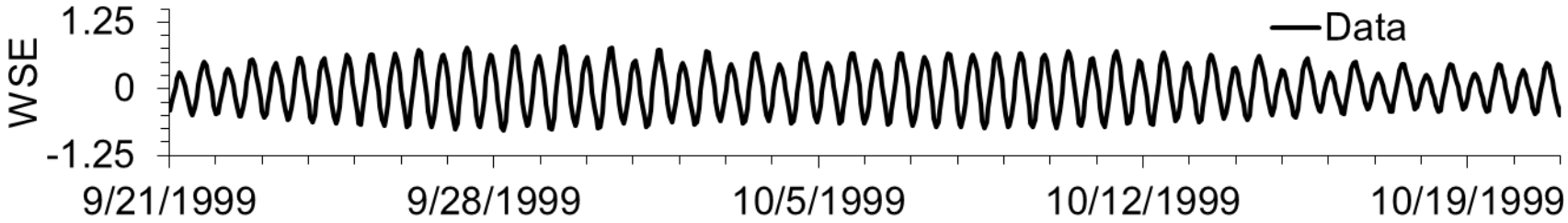

Figure 20. Observed Water Levels at Matanzas River Headwaters, FL NOAA Gauge Station

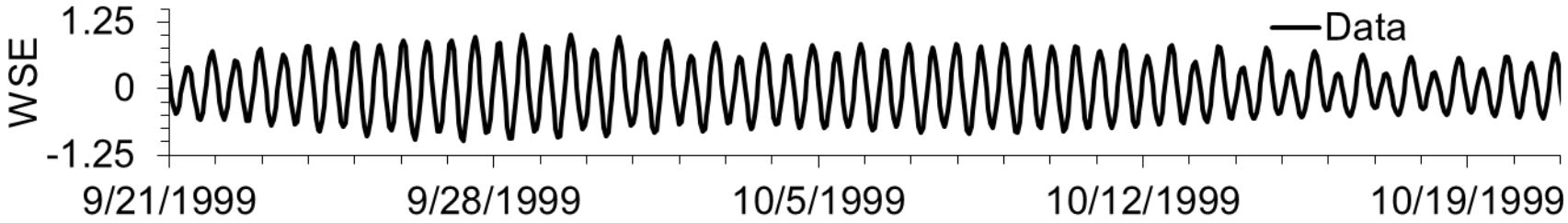

Figure 21. Observed Water Levels at St. Augustine Beach, FL NOAA Gauge Station

6.2 VEGETATION PLOTS

For biomass density support the NERR's Emergent Vegetation data were utilized. For the GTMNERR six separate locations were used for this data collection program. Figure 22 shows the locations of the six emergent vegetation-monitoring sites. Table 3 shows the name and location of each site, and its five plots. Moses Creek (06) and Pellicer Creek (46) are sites where transects extend to the terrestrial transition zone.

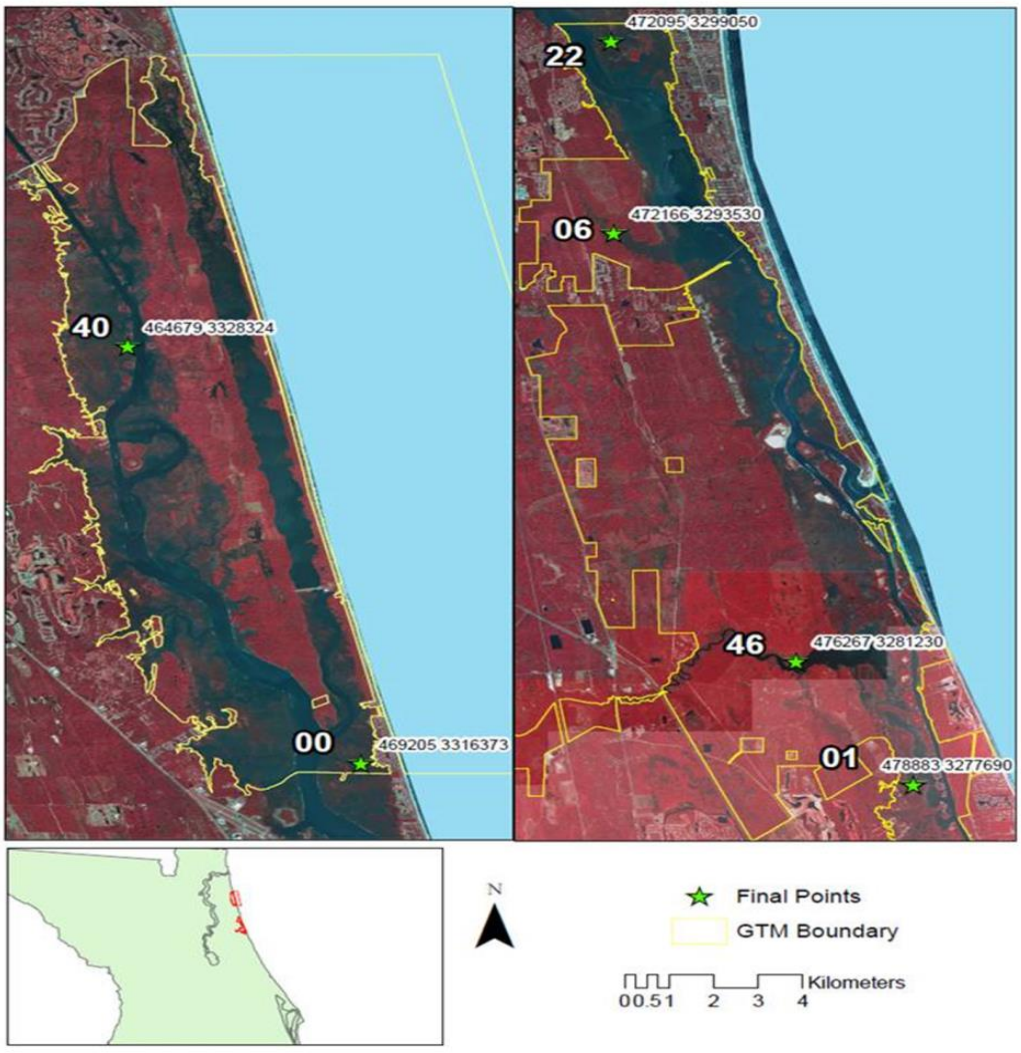

Figure 22. Geographic Map of GTM-NERR with Location of Emergent Vegetation Data Plots (Friends of the GTM Reserve)

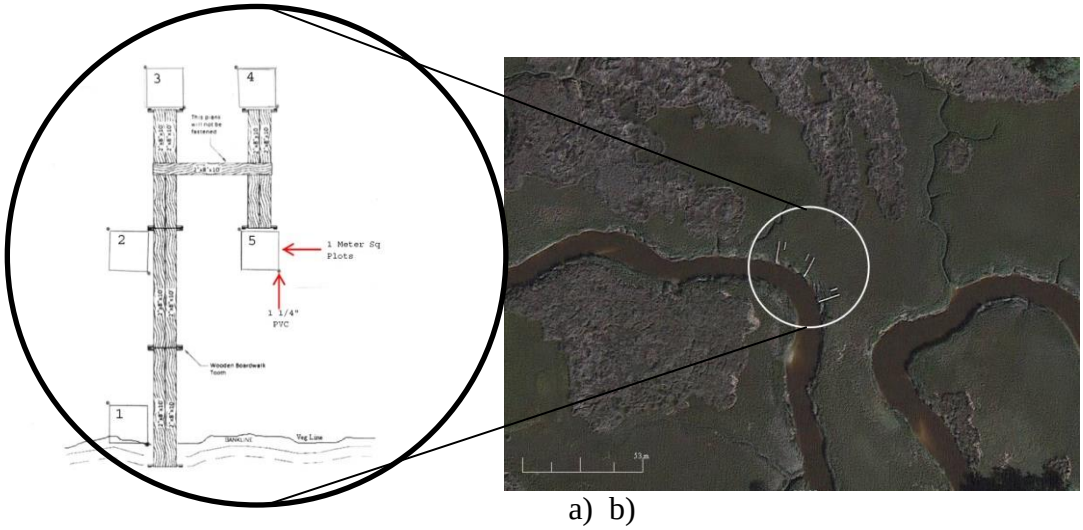

a) b)

Figure 23. Schematic of Emergent Vegetation Platform at Moses Creek (06) (GTMNERR)

The Emergent Vegetation data collection program focusses on collecting all observational data helpful in better understanding the current state of intertidal vegetation in the GTMNERR. Each site is located in an area that may be inundated by tidal water, yet accessible during low tide. Every site has five separate 1 m^2 plots that is monitored throughout the year.

TABLE 3. GTMNERR EMERGENT VEGETATION IDENTIFICATION.

Site	Transect	Plot	Distance to Shore (m)	Latitude	Longitude
Moses Creek (06)	A	1	0	29.771394	-81.287933
		2	6	29.771442	-81.287901
		3	10	29.771462	-81.287880
		4	10	29.771488	-81.287909
		5	6	29.771460	-81.287932
	B	1	0	29.771471	-81.288064
		2	6	29.771521	-81.288050
		3	10	29.771546	-81.288042
		4	10	29.771545	-81.288004
		5	6	29.771512	-81.288018
	C	1	0	29.771295	-81.287893
		2	6	29.771303	-81.287828
		3	10	29.771309	-81.287797
		4	10	29.771339	-81.287800
		5	6	29.771332	-81.287840
Pellicer Creek (46)	A	1	0	29.660466	-81.245138
		2	6	29.660507	-81.245178
		3	10	29.660526	-81.245203
		4	10	29.660512	-81.245226

		5	6	29.660485	-81.245200
	B	1	0	29.660592	-81.244983
		2	6	29.660619	-81.245034
		3	10	29.660630	-81.245071
		4	10	29.660610	-81.245087
		5	6	29.660591	-81.245050
	C	1	0	29.660700	-81.244880
		2	6	29.660729	-81.244927
		3	10	29.660750	-81.244952
		4	10	29.660730	-81.244981
		5	6	29.660705	-81.244949
Hat Island (00)	A	1	0	29.978087	-81.319459
		2	6	29.978039	-81.319473
		3	10	29.978010	-81.319484
		4	10	29.978014	-81.319513
		5	6	29.978044	-81.319508
	B	1	0	29.978042	-81.319306
		2	6	29.977992	-81.319327
		3	10	29.977963	-81.319342
Hat Island (cont)	B (cont)	4	10	29.977971	-81.319371
		5	6	29.978002	-81.319359
	C	1	0	29.978166	-81.319317
		2	6	29.978217	-81.319294
		3	10	29.978249	-81.319287
		4	10	29.978258	-81.319314
		5	6	29.978223	-81.319330
Washington Oaks (01)	A	1	0	29.629071	-81.218338
		2	6	29.629027	-81.218307
		3	10	29.628998	-81.218293
		4	10	29.628983	-81.218318
		5	6	29.629012	-81.218337
	B	1	0	29.629021	-81.218481
		2	6	29.628969	-81.218473
		3	10	29.628938	-81.218474
		4	10	29.628935	-81.218503
		5	6	29.628967	-81.218506
	C	1	0	29.629005	-81.218658
		2	6	29.628952	-81.218664
		3	10	29.628924	-81.218673
		4	10	29.628925	-81.218702
		5	6	29.628960	-81.218698
Moultrie Creek (22)	A	1	0	29.821484	-81.288791
		2	6	29.821437	-81.288815

		3	10	29.821416	-81.288838
		4	10	29.821427	-81.288849
		5	6	29.821457	-81.288849
	B	1	0	29.821542	-81.289043
		2	6	29.821491	-81.289057
		3	10	29.821456	-81.289061
		4	10	29.821450	-81.289035
		5	6	29.821481	-81.289024
	C	1	0	29.821828	-81.289068
		2	6	29.821875	-81.289057
		3	10	29.821908	-81.289045
		4	10	29.821902	-81.289017
		5	6	29.821867	-81.289022
Pine Island (40)	A	1	0	30.085513	-81.366661
		2	6	30.085536	-81.366605
		3	10	30.085545	-81.366564
		4	10	30.085519	-81.366557
		5	6	30.085507	-81.366597
	B	1	0	30.085399	-81.366582
		2	6	30.085414	-81.366526
		3	10	30.085417	-81.366488
Pine Island (cont)	B (cont)	4	10	30.085393	-81.366478
		5	6	30.085384	-81.366516
	C	1	0	30.085585	-81.367012
		2	6	30.085571	-81.367078
		3	10	30.085558	-81.367112
		4	10	30.085533	-81.367107
		5	6	30.085543	-81.367063

Vegetative data collection consisted of canopy height (maximum and average), percent coverage, and dominant species. These observations were all noted, and then a camera was used to snap a top view photo. All of these data were collected then input into a shared file. The locations and identification of each site are listed in Table 3. Each location (00, 01, 06, 22, 40, and 46) has three sites. Each site has 5 plots. The detailed location of each separate plot is shown in Table 3. The division, or hierarchy, of the plots is demonstrated in Figure 24.

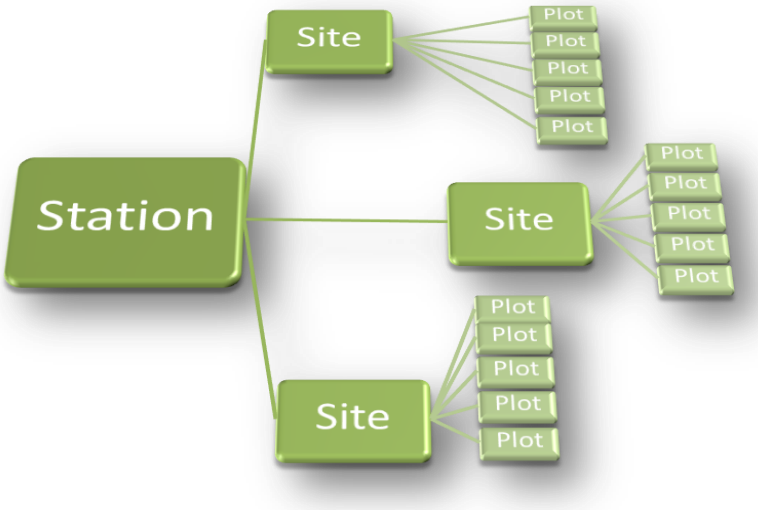

Figure 24. Hierarchy of GTMNERR Emergent Vegetation Sites

Typically the National Estuarine Research Reserves require emergent vegetation data to be collected at the peak of biomass production of the dominant species for the salt marsh once per year. The GTMNERR however, has collected data almost once a month in 2014 to determine when peak growing season is. This means that this specific study has a wealth of data from which to choose from on a yearlong time. Table 4 shows vegetation data time line availability from which a run time can be chosen. It can also be noted, that from their research, the *Spartina alterniflora's* peak biomass production is from April to May.

Time Line	Jan 1-15	Jan 16 - end	Feb 1 -15	Feb 16 -end	Mar 1-15	Mar 16 - end	Apr 1 -15	Apr 16 -end	May 1-15	May 16 - end	June 1 -15	June 16 -end	July 1-15	July 16 - end	Aug 1 -15	Aug 16 - end	Sep 1 -15	Sep 16 - end	Oct 1-15	Oct 16 - end	Nov 1 -15	Nov 16 -end	Dec 1 -15	Dec 16 -end
Data																								
2014 Veg Data		1-23,27	2-4	2-17to21	3-11,12	3-18,19,20	4-4,7,10	4-21,22,30	5-5,6	5-16,19,20,21		6-16,18,19,20	7-1	7-17,18,21,22										
2013 Veg Data												6-27,30			8-14	8-29	9-5	9-26	10-3					
2012 Veg Data														7-17				9-26,28				11-2,5,7,9		

TABLE 4. EMERGENT VEGETATION DATA COLLECTION PERIODS

Findings from the emergent vegetation program state that the GTMNERR is an ecotone of two different emergent vegetation habitats; salt marsh and mangroves (typically black). The dominant marsh species within the GTMNERR is *Spartina alterniflora*.

Other dominant species are Batis maritime, Sarcocornia ambigua, Juncus roemerianus, Distichlis spicata, and Avicennia germinans. The findings suggest that Spartina alterniflora, which is the case study species used in the calculations of this study dominates all but the two most southern Emergent Vegetation site.

Figures 26 through 30 show the percent coverage of *Spartina alterniflora* per emergent vegetation stations in the GTMNERR in 2014. This is important because biomass coefficients are based on this species. For most of the sites *Spartina alterniflora* is the dominant species, however this is not the case for a select few. The dominant species for these plots is listed at the top of the graph. If no dominant species is listed, typically the rest of the plot is mostly unvegetated.

Figure 25 shows the average height of *Spartina alterniflora* for each emergent vegetation station. This information combined with a proposed future work study could help validate biomass density predictions. Ideally, clippings of *Spartina alterniflora* could be collected form each site and their heights recorded. These clippings would then be dried and weighed. The weight of each would provide grams per height ratio. Then, Figure 25 would be used to determine average height at each site. Applying this ratio would provide an average weight in grams (i.e. height * grams/height ratio = grams). The percent cover seen in Figures 26 through 29 would then multiply this ratio. Each plot is 1 meter by 1 meter. So this would provide the researcher with a grams/m^2 value to compare to predicted biomass productivity.

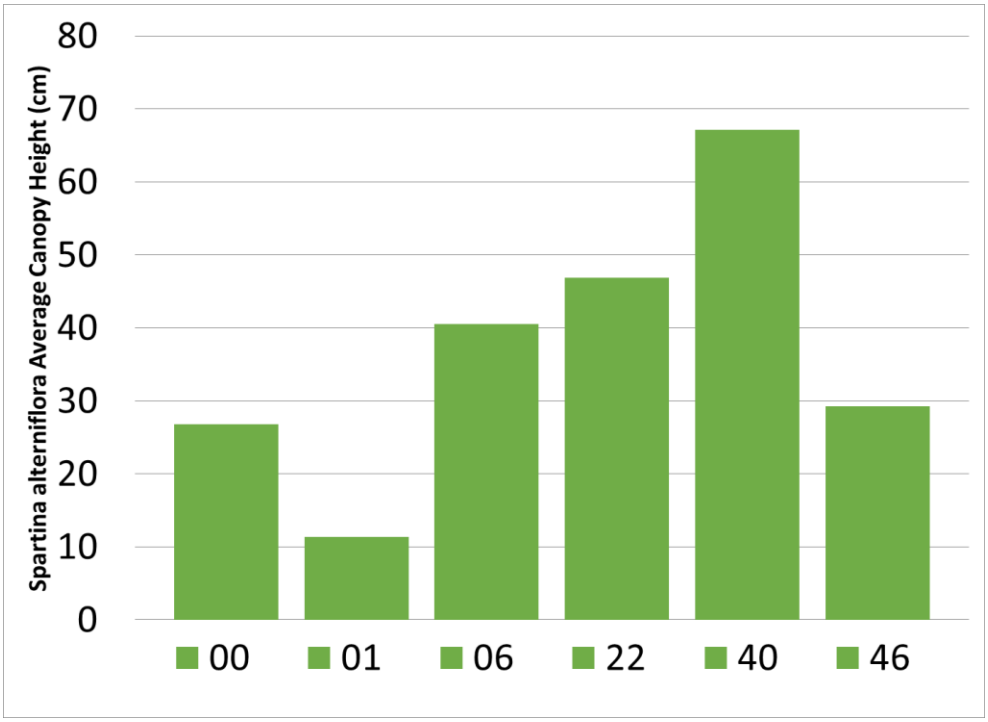

Figure 25. Average *Spartina alterniflora* Height per Emergent Vegetation Station

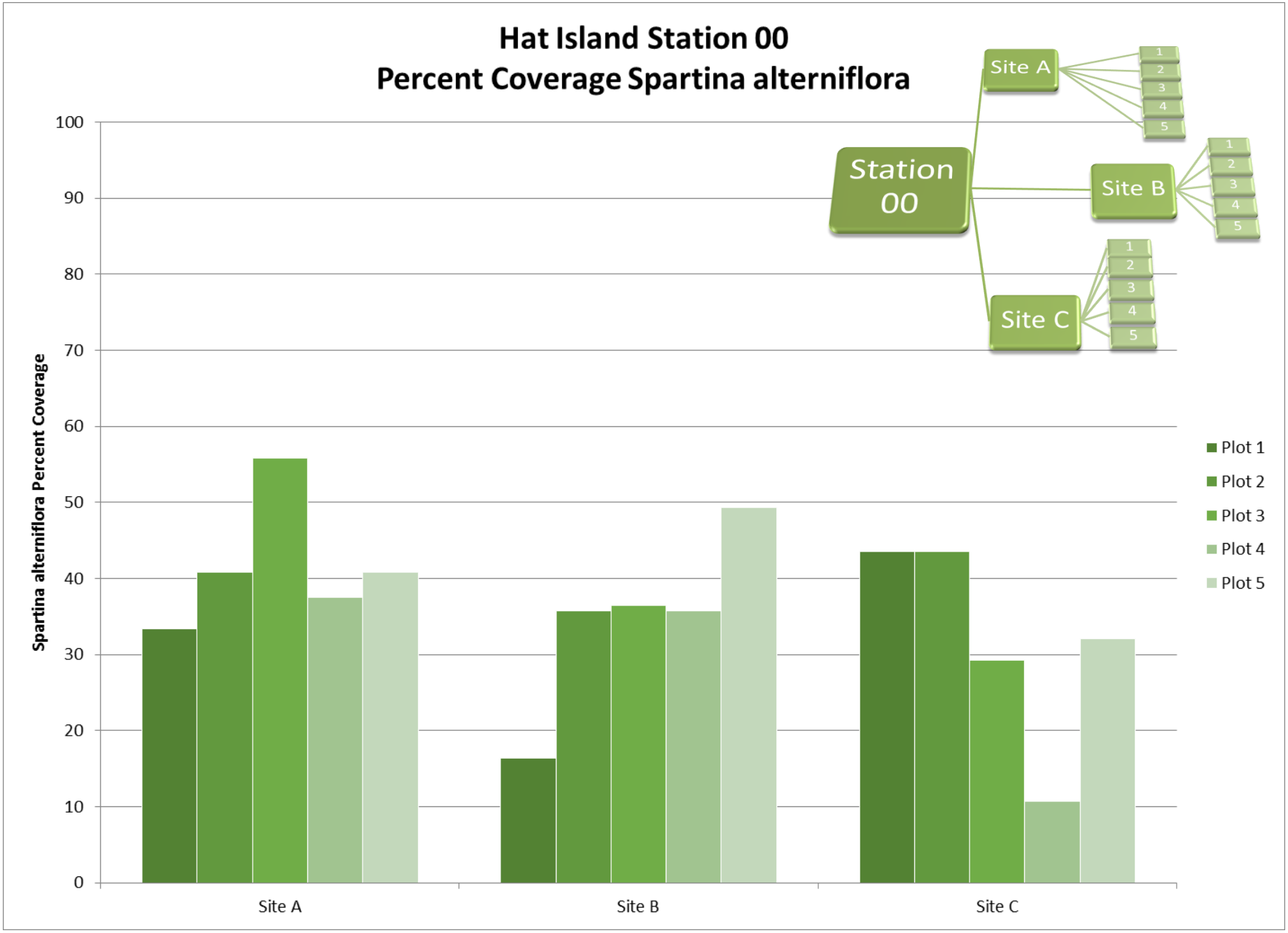

Figure 26. Percent Coverage of *Spartina alterniflora* at Hat Island, FL

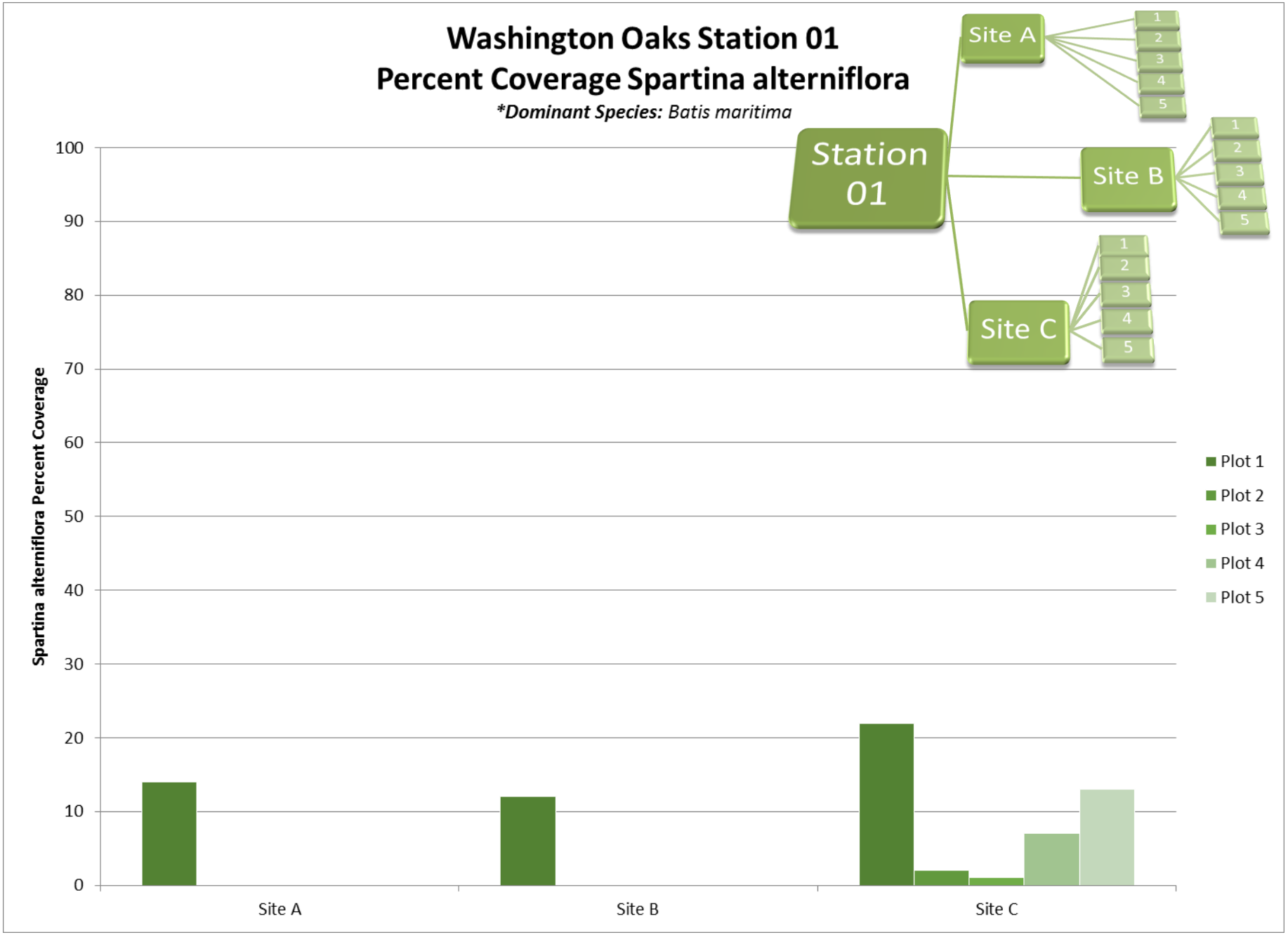

Figure 27. Percent Coverage of *Spartina alterniflora* at Washington Oaks, FL

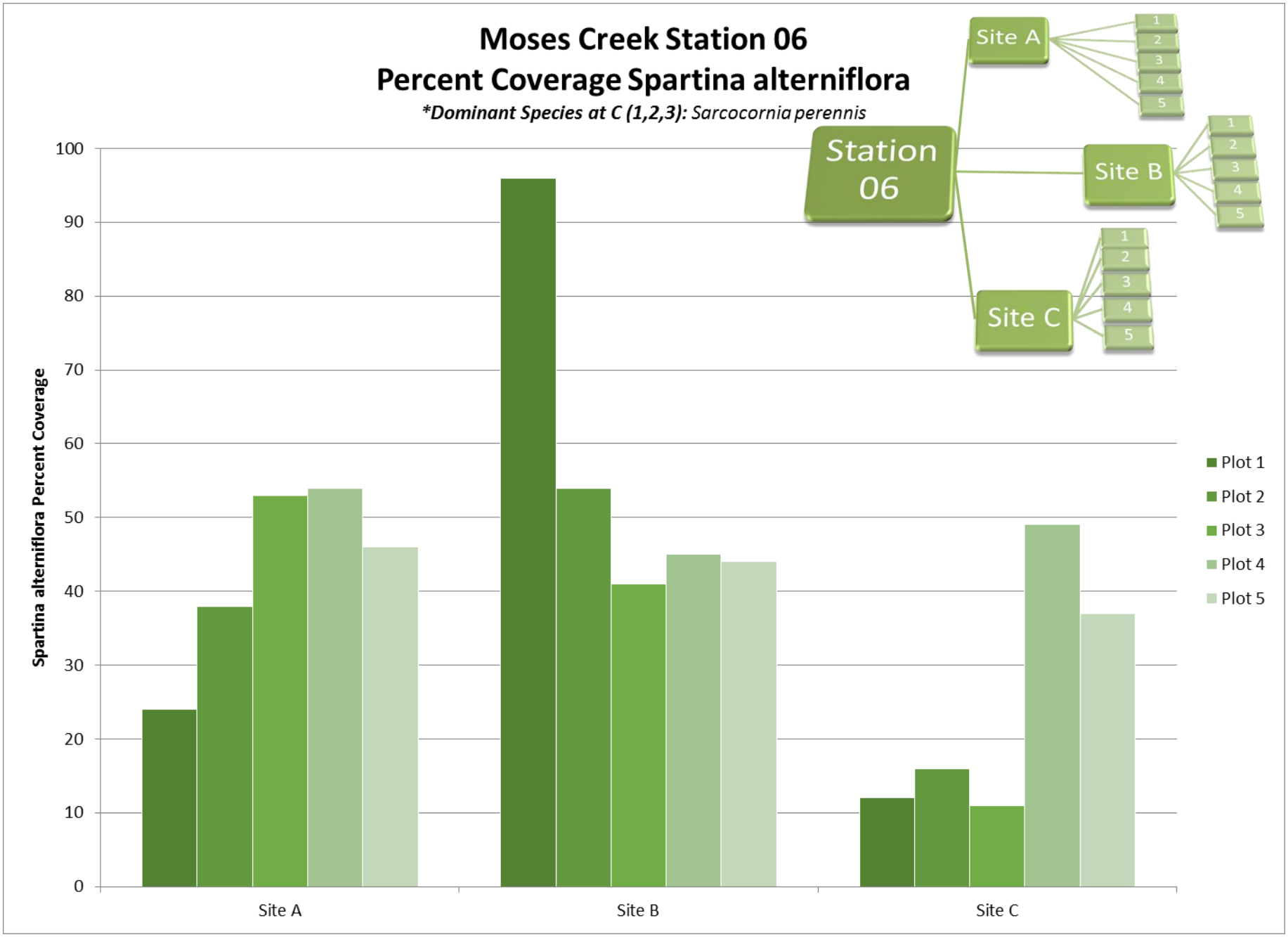

Figure 28. Percent Coverage of *Spartina alterniflora* at Moses Creek, FL

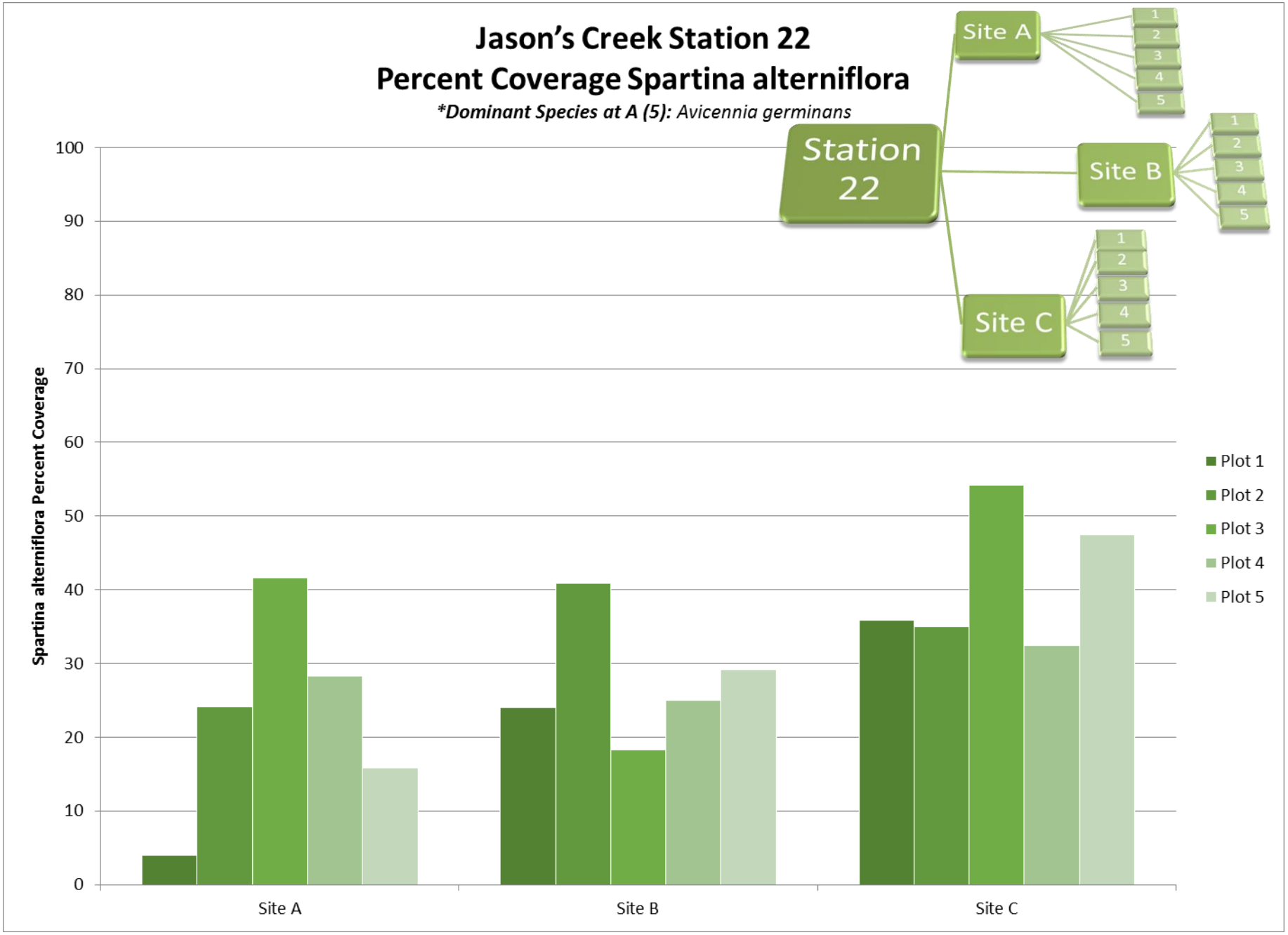

Figure 29. Percent Coverage of *Spartina alterniflora* at Jason's Creek, FL

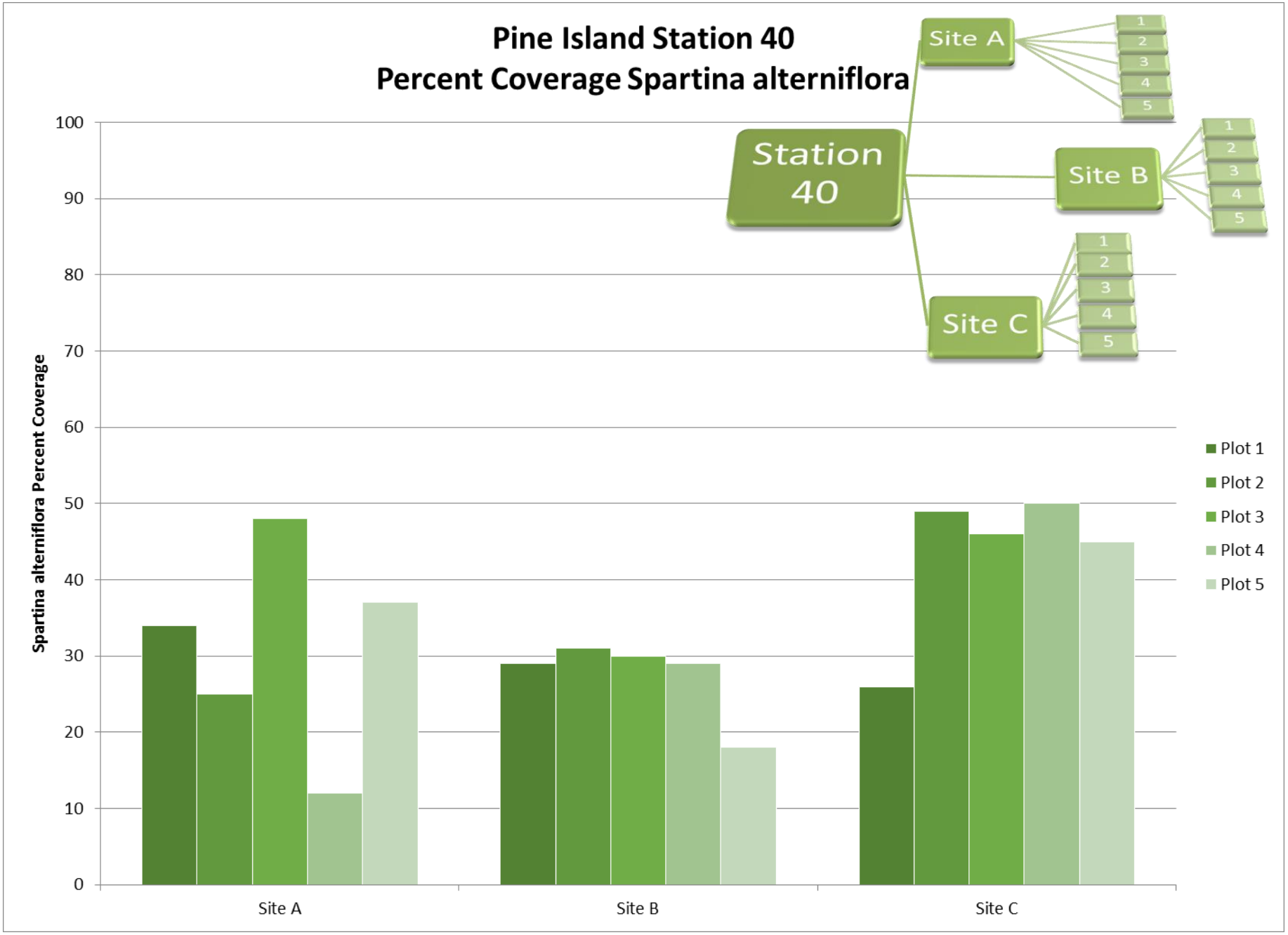

Figure 30. Percent Coverage of *Spartina alterniflora* at Pine Island, FL

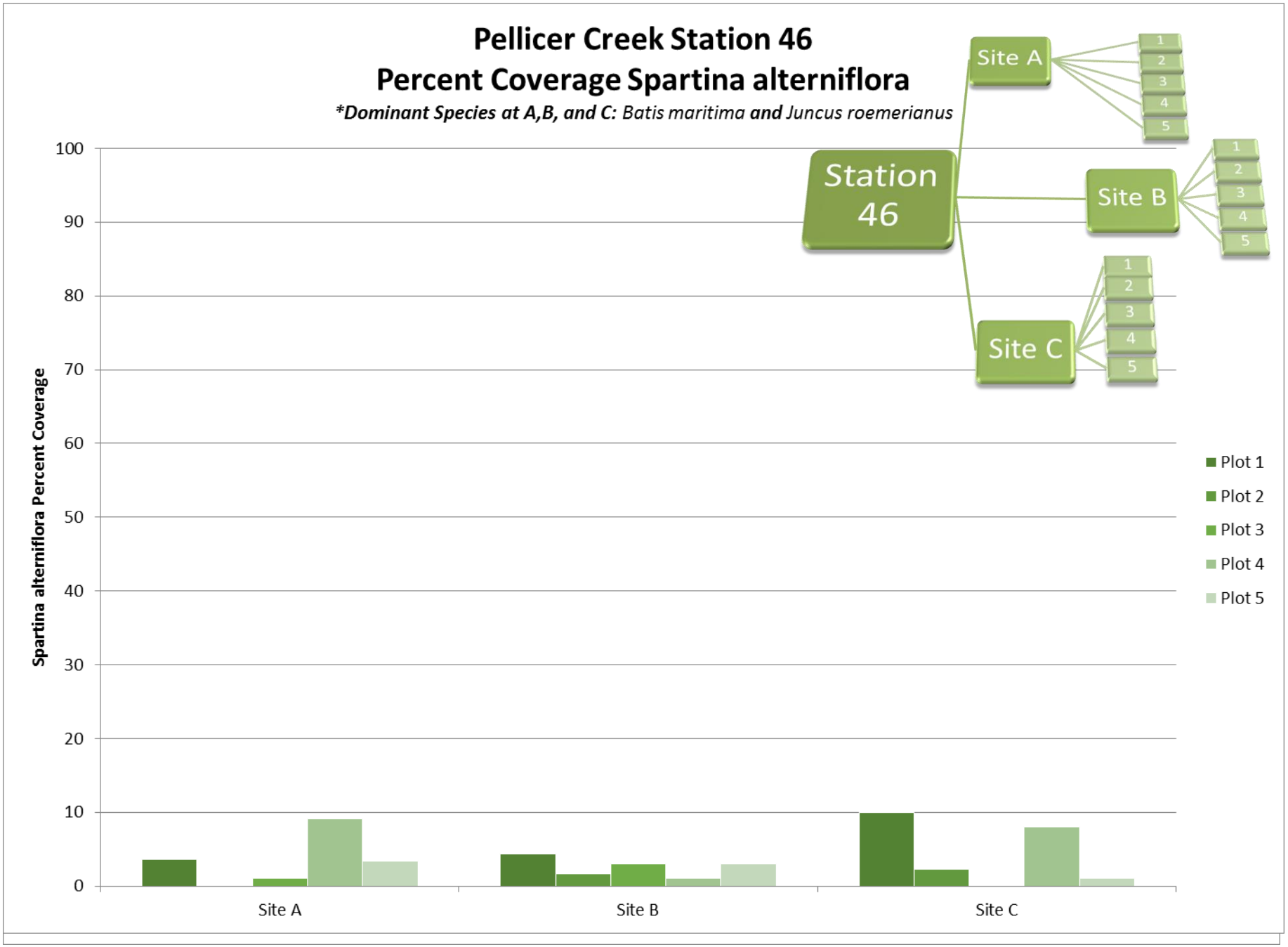

Figure 31. Percent Coverage of Spartina alterniflora at Pellicer Creek, FL

7. Model Results

The research produced a current and tidal driven hydraulic model. The model was validated using the eight tidal gauges that were collecting water level data in the Guana, Tolomato, and Matanzas Rivers. Biomass density was calculated by the model for the six emergent vegetation locations as well as for every node in the entire domain. These data were then compared to the data collected from the emergent vegetation program by the GTMNERR staff in 2014.

7.1 WATER SURFACE ELEVATION DATA

Preliminary runs were made. Small parameter adjustments were then applied. A final model was then applied in an attempt to reproduce the two dimensional tidal flows within the Guana Tolomato Matanzas National Estuarine Research Reserve. The run was made for 30 days. ADCIRC-2DDI-CD effectively modeled the tidal driven hydrodynamics for the 30 day time period with time steps of 360 seconds. At each time step the physical parameters, boundary equations, and basic equations were applied to each node and interpolated over every triangular element.

After computing the hydrodynamics for each node and saving the results, Matlab was used to pull out 30 day plots at each NOAA gauge (coordinates given in Table 2). A 30 day period was chosen to represent the full 14 day cycle (plus a 12 hour period on each side). The water surface elevation at each of the 8 tidal gauge locations was then plotted over the observed data by the gauge. Figures 32 – 39 show the water surface elevations at each gauge location.

It should be noted that the first few days are considered a “ramp up” period, as ADCIRC was started with a cold start. This period is the time it takes for the model to align with consistent oscillation. This run had a cold start when the run was made, this means starting conditions for the model were zero, meanwhile for the true observational data this is not so.

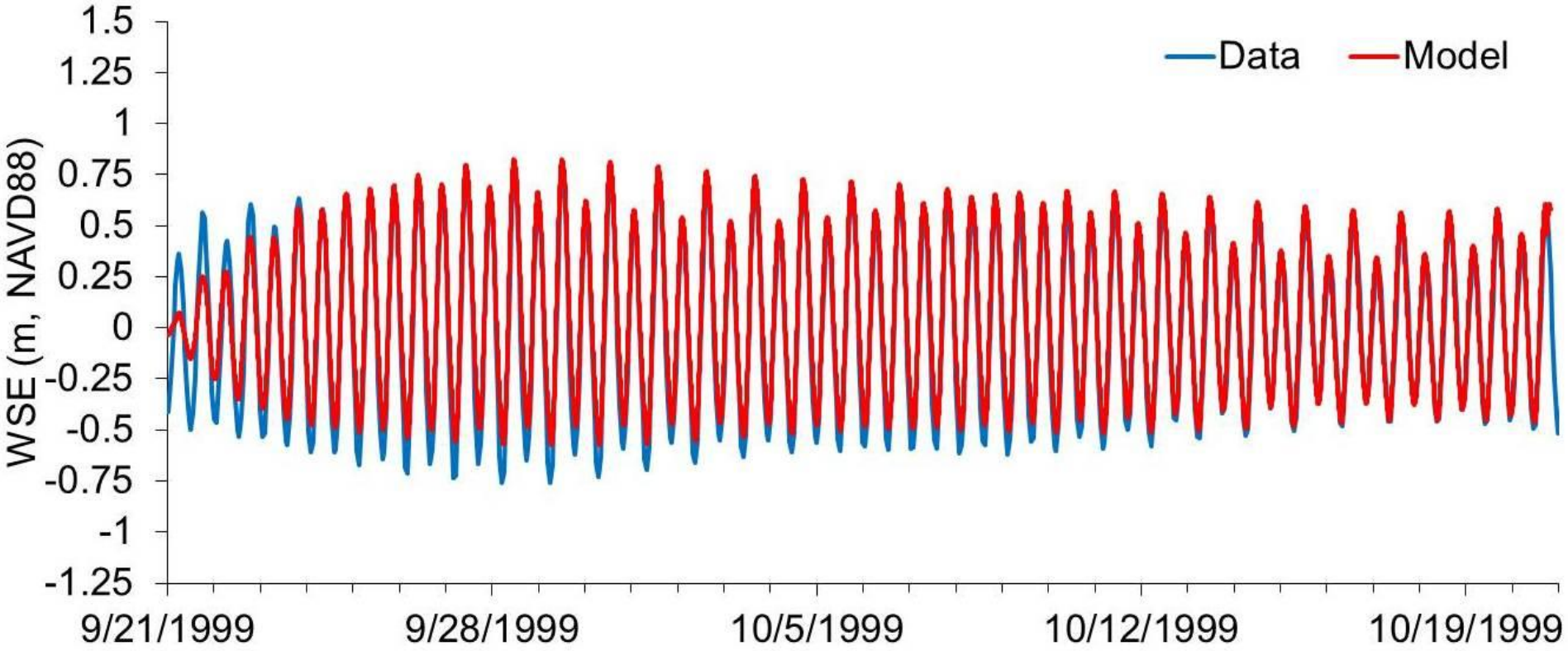

Figure 32. Sta. 1: Pablo Creek, FL Data vs. Model Water Surface Elevation

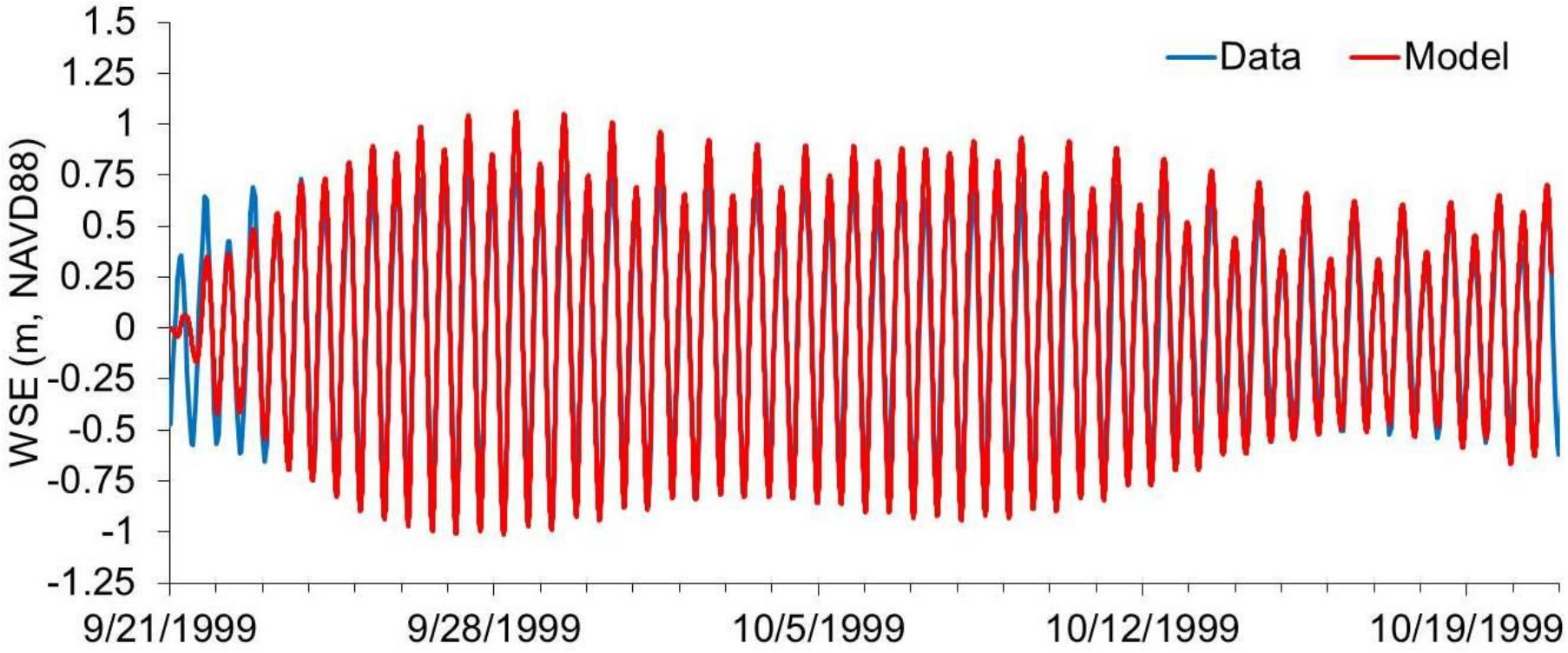

Figure 33. Sta. 2: Tolomato River, FL Data vs. Model Water Surface Elevation

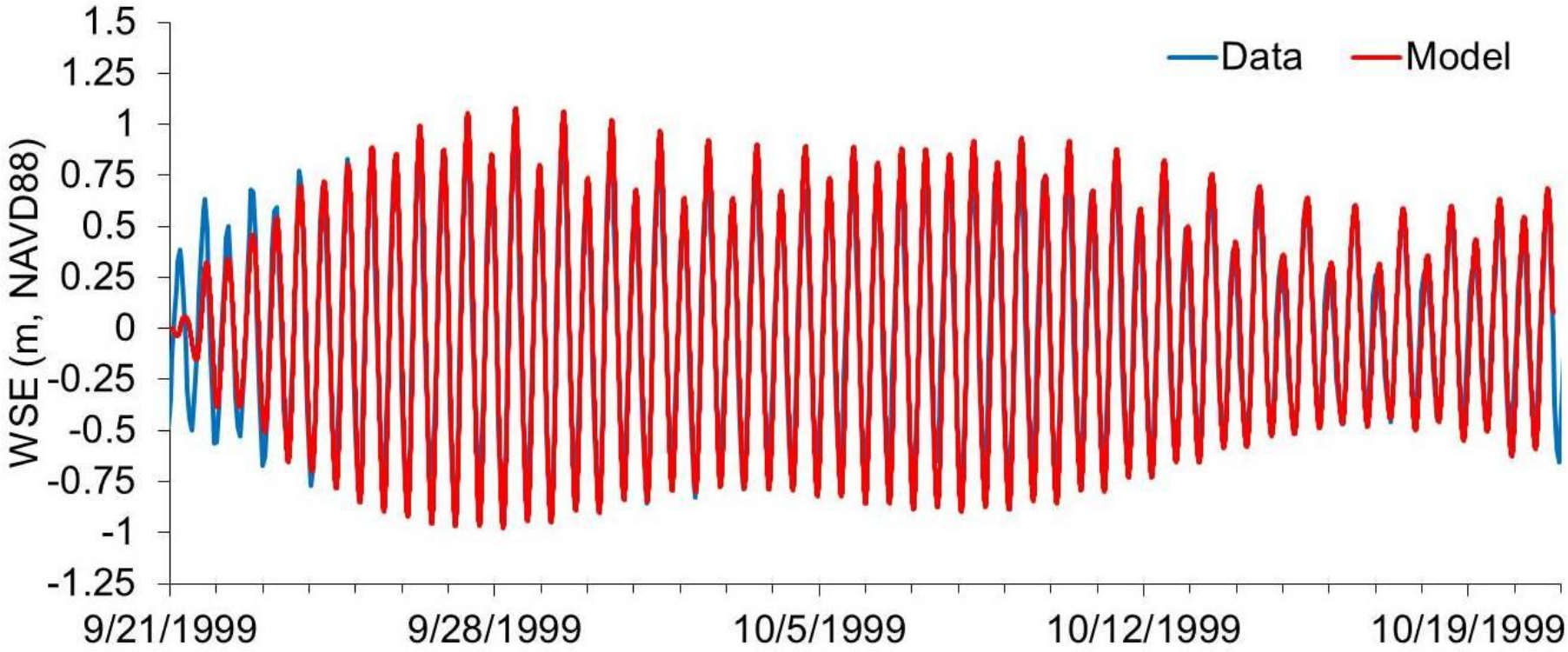

Figure 34. Sta. 3: Vilano Bridge, FL Data vs. Model Water Surface Elevation

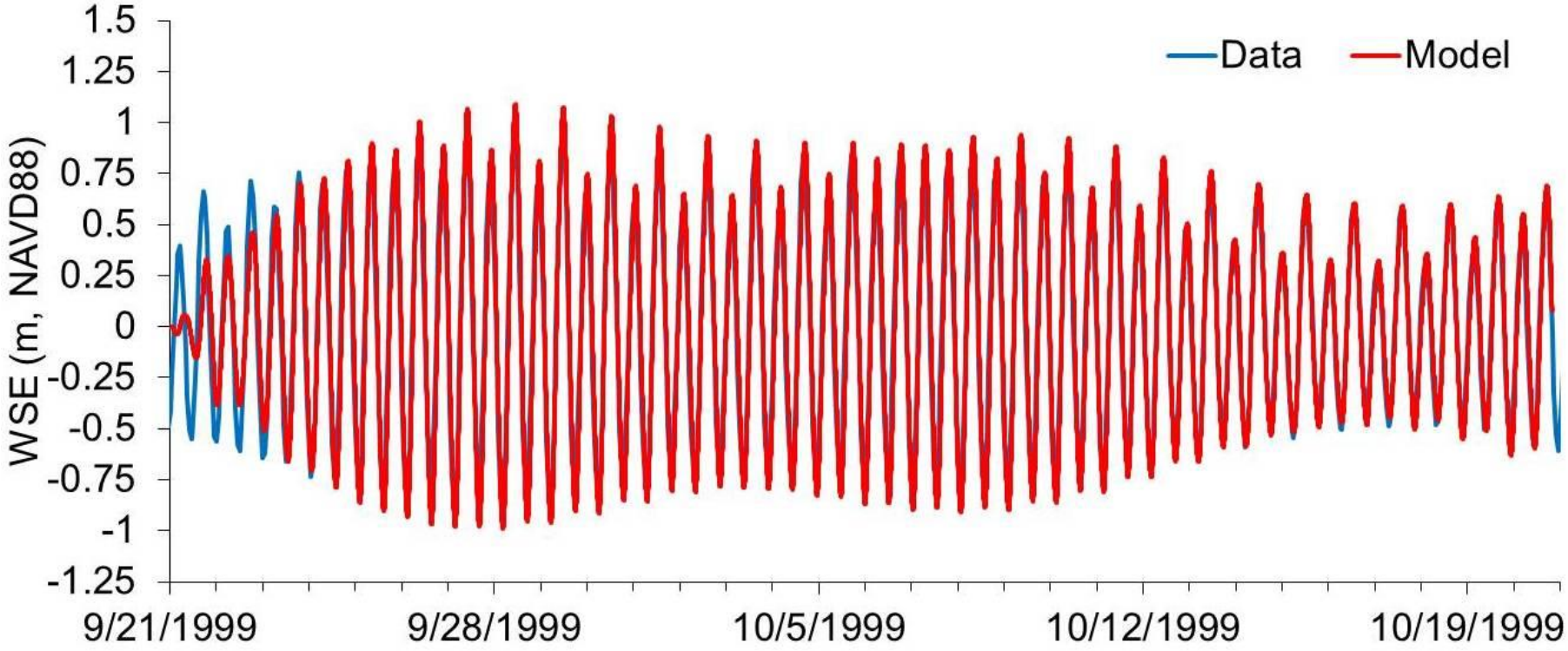

Figure 35. Sta. 4: St. Augustine, FL Data vs. Model Water Surface Elevation

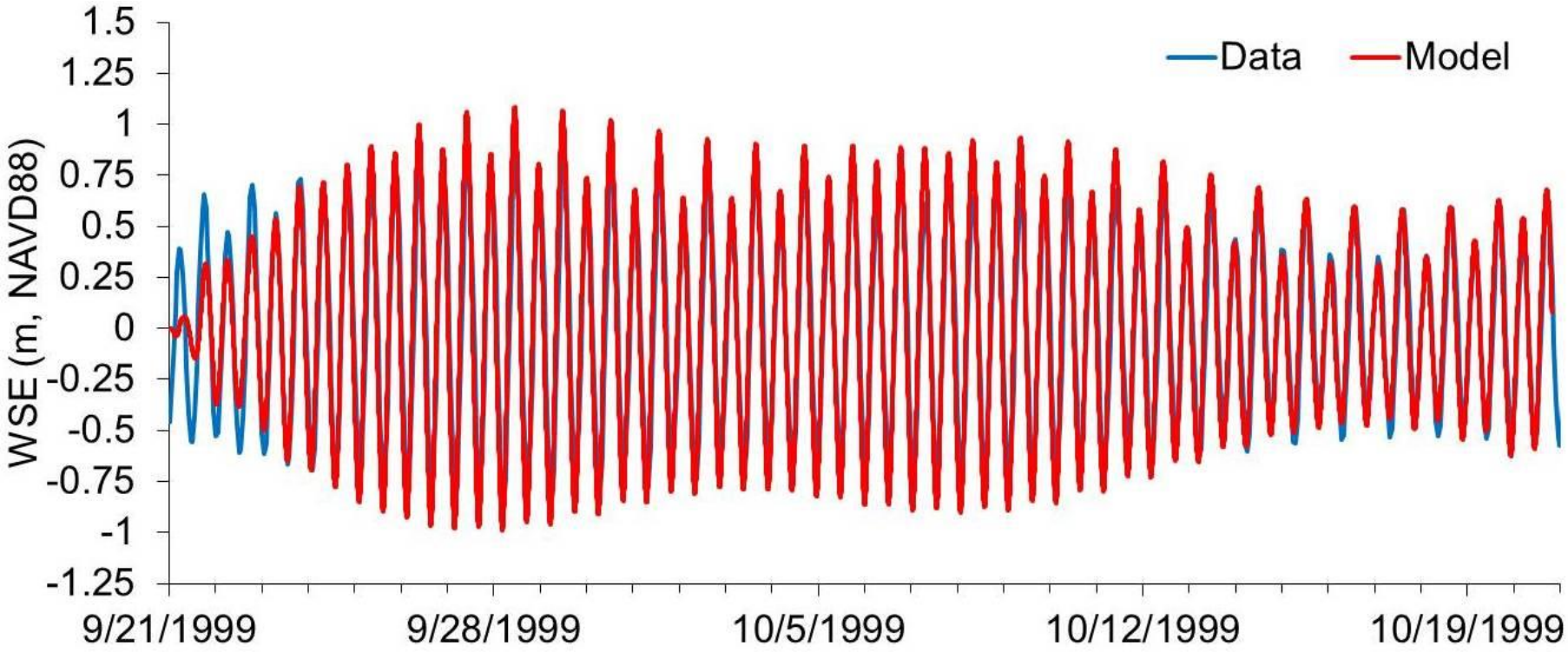

Figure 36. Sta. 5: Anastasia Island, FL Data vs. Model Water Surface Elevation

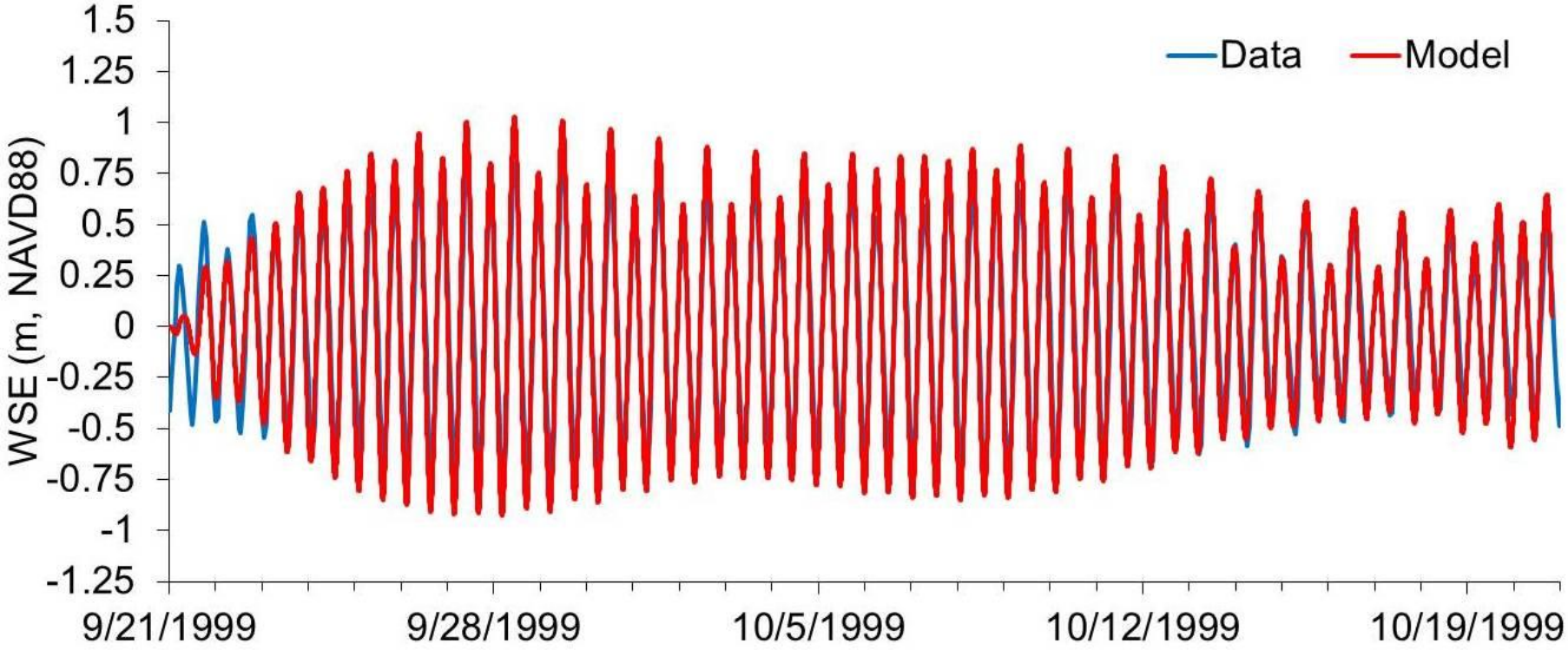

Figure 37. Sta. 6: Fort Matanzas, FL Data vs. Model Water Surface Elevation

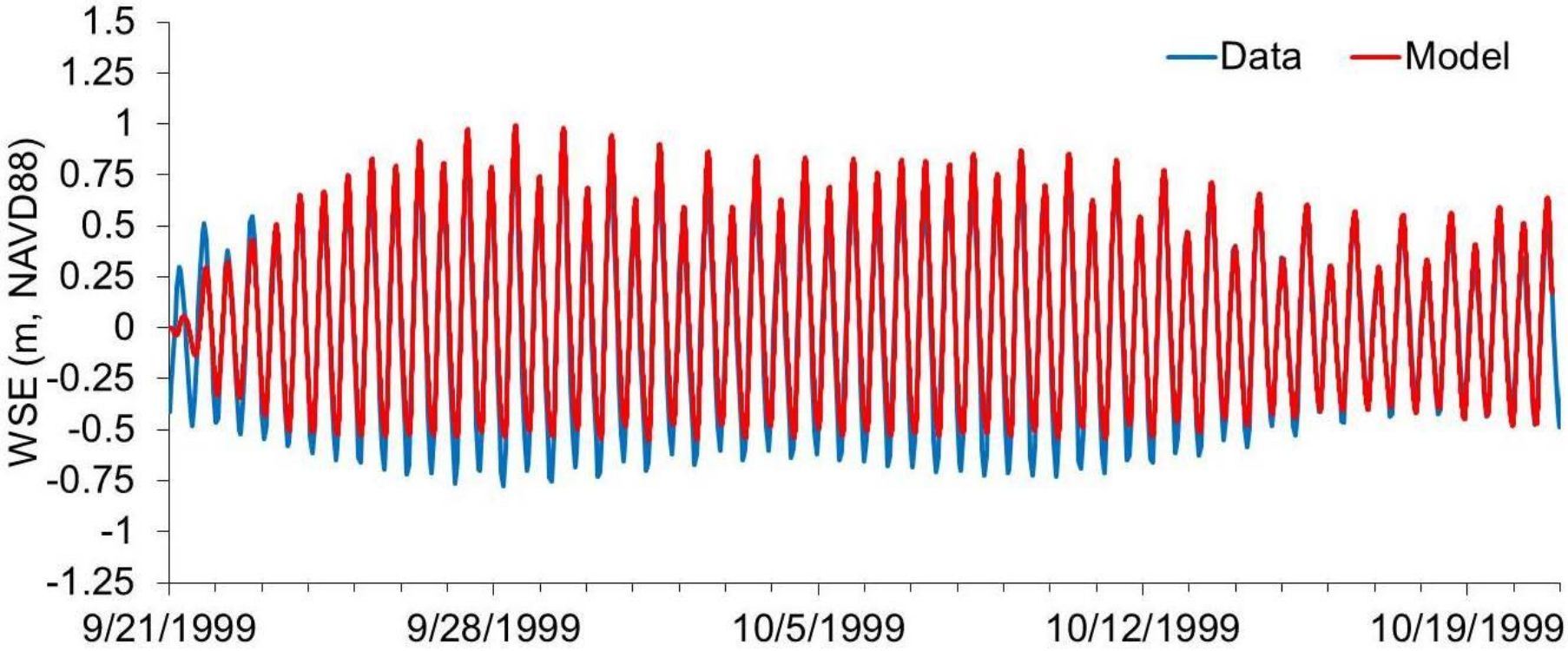

Figure 38. Sta. 7: Matanzas River Headwaters, FL Data vs. Model Water Surface Elevation

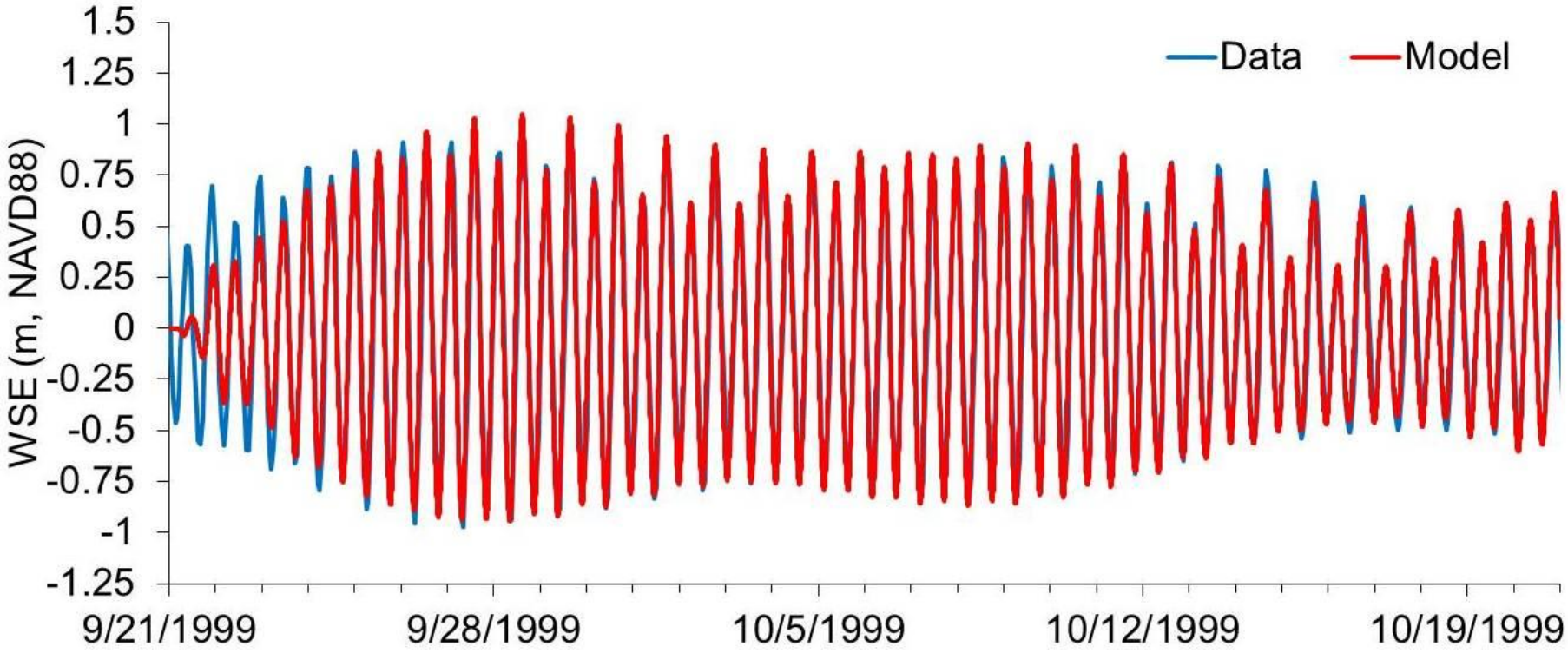

Figure 39. Sta. 8: St. Augustine Beach, FL Data vs. Model Water Surface Elevation

Figures 31 through 38 are tidal resynthesizes of the eight NOAA gage locations. They show a comparison of observational data from September and October 1999 (collected from NOAA) to the model's simulation of water surface elevation at those station locations. For all 8 stations period seems to be accurately predicted. Table 5 shows the confidence in the model to observation comparison for each station; where equations 25 and 26 were used to determine values of RMSE and R^2.

Statistics On Run 1 Vs. Observational Data									
	sta. 1	sta. 2	sta. 3	sta. 4	sta. 5	sta. 6	sta. 7	sta. 8	**Ave ± Std**
RMSE=	0.275	0.052	0.140	0.125	0.124	0.134	0.216	0.141	**0.15±.06**
R^2=	0.930	0.939	0.878	0.880	0.936	0.950	0.852	0.953	**0.91±.04**

TABLE 5. ROOT MEAN SQUARE ERROR AND R2 MODEL TO OBSERVATION COMPARISON

equation 26 … $RMSE = \sqrt{\frac{\sum(Obs_i - Model\ Run\ 1_i)}{N}}$

equation 27 … R^2

$$= \left(\frac{N \sum Obs_i Model\ Run\ 1_i - (\sum Obs_i)(\sum Model\ Run\ 1_i}{\sqrt{N(\sum {Obs_i}^2) - (\sum Obs_i)^2}\sqrt{N(\sum {Model\ Run\ 1_i}^2) - (\sum Model\ Run\ 1_i)^2}} \right)^2$$

R^2 represents the goodness of fit between historical and model elevations. The i value is the index of time, and N is the number of times. Using a method (similar to that used in Hagen et al., 2005) of comparing qualitative to quantitative results as good or not. Though the errors were less in the larger domain, estuaries tend to be more difficult in modeling. These results can be considered pretty good.

7.2 MHW AND MLW DATA

Now that water surface elevations have been evaluated, MHW and MLW must be as well. As was shown in equation 21, the biomass formula depends on MHW and MLW. Recall, the equation for D (relative depth) is dependent on MHW, MLW, and elevation. While elevation is determined from the bathymetry in the model, MHW and MLW are predicted by the simulation. This is why it is important to pull them out from the run as well.

Figure 40 represents the look of MLW (in blue) and MHW (in red) for the GTMNERR domain. The MLW and MHW in this snapshot range from .7 m above sea level to .7 below. Figure 41 shows the accuracy of the MHW and MLW predicted by the model versus observations for the eight tidal gauging stations. All predictions are similar to observations with exception of the Pablo Creek Station 1 MLW model prediction, this discrepancy can be the result of improper bathymetric definition. This could be cause for further work refining the smaller tributaries within the mesh representing the GTMNERR. Given the specific use of biomass density, this particular prediction of Pablo Creek MLW is not an issue due to its location being so far away from any of the six vegetation plots.

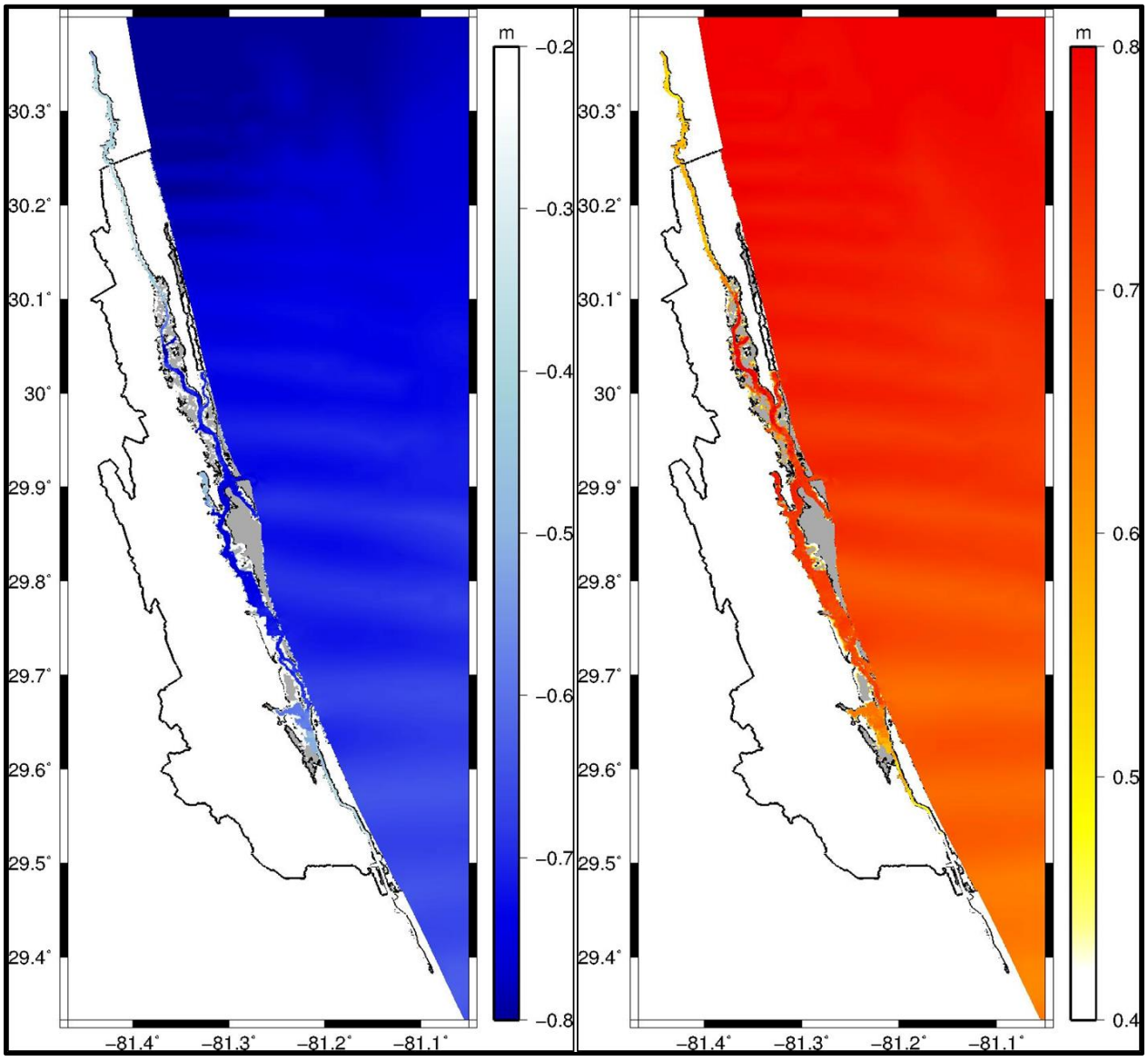

Figure 40. GTMNERR Water Surface Elevation Limits (MHW, MLW)

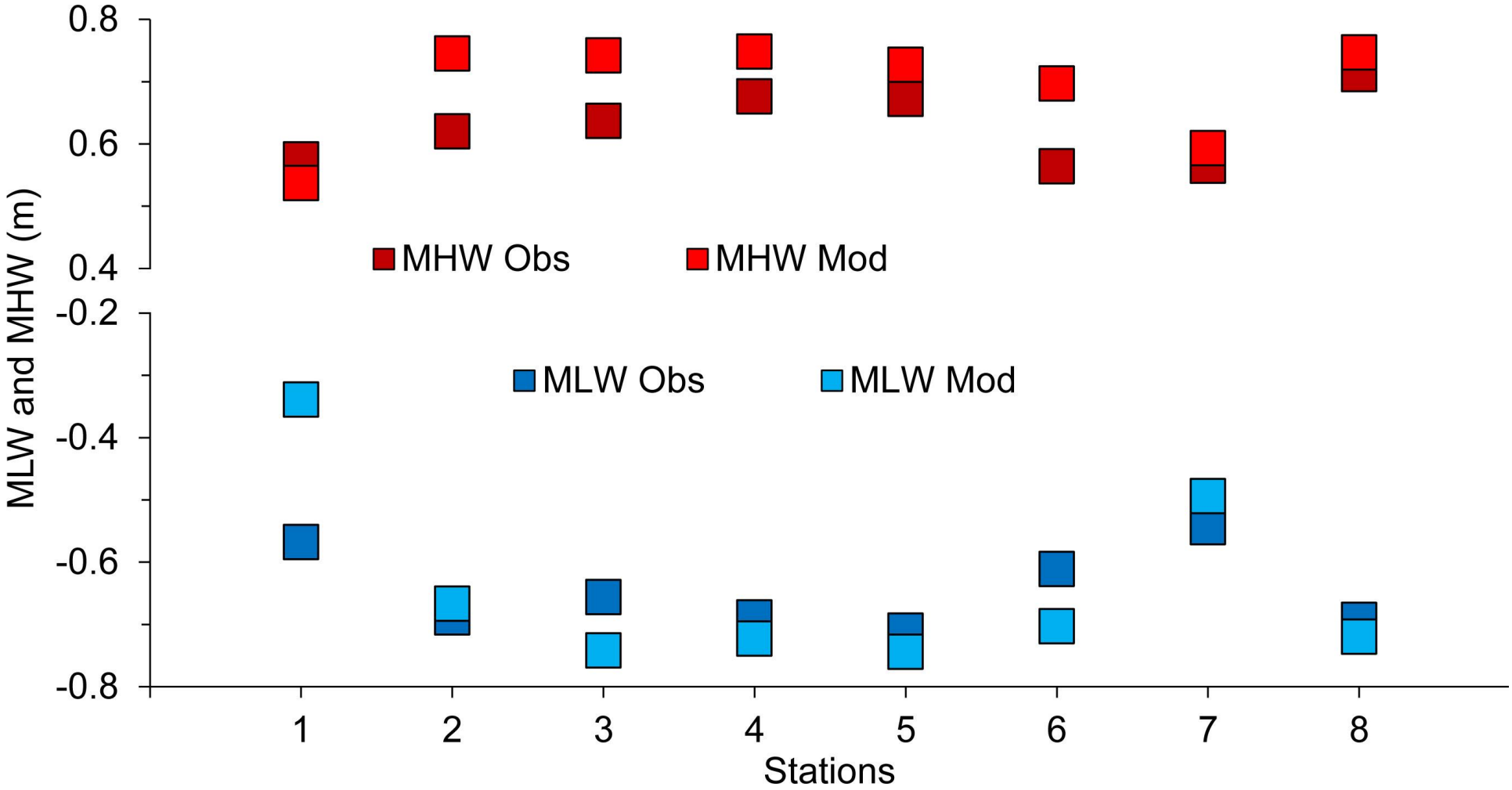

Figure 41. GTMNERR MHW and MLW Observed vs. Model for Eight Tidal gauges

	Observation Data		*Model Run Produced Data*	
Station	*MLW (m)*	*MHW (m)*	*MLW (m)*	*MHW (m)*
1	-0.57	0.58	-0.50	0.61
2	-0.69	0.62	-0.75	0.83
3	-0.66	0.64	-0.77	0.79
4	-0.69	0.68	-0.75	0.76
5	-0.71	0.67	-0.73	0.74
6	-0.61	0.56	-0.72	0.72
7	-0.54	0.57	-0.50	0.69
8	-0.69	0.71	-0.75	0.74
AVG ± SD. (m)(NAVD88)	-0.65± 0.06	0.63± 0.05	-0.68 ± 0.11	0.74 ± 0.06

TABLE 6. MHW AND MLW FOR MODEL RUN VS. OBSERVATIONS

Table 6 and Figure 41 show the average MHW and MLW at the eight given stations during the observation time period compared to the present day simulation run. The MHW and MLW were averaged for the entire run using the Python code; "Tidal Datums" (Hagen et al. 2012). After the code was compiled and run for the outputs of the first run modeled using ADCIRC, FORTRAN files containing these data were created. These data were viewed in SMS, and the values at each latitude and longitude location for the eight gauges was collected.

Table 6 and Figure 41 show the average observed MLW and MHW in the GTMNERR is -0.65± 0.06 m (NAVD88) and 0.63±0.05 m (NAVD88) for each gauge location (where population considered was the eight gauges). Figure 39 represents this given the snapshots of MLW and MHW being about -0.7 m to 0.7 m throughout the entire area. On average the model calculated MLW and MHW values of -0.68 ± 0.11 m (NAVD88) and 0.74 ± 0.06 m (NAVD88) respectively for the eight stations.

Consistently we are seeing MHW being over-predicted more often than MLW. This could be due to three possible factors; lack of definition along creeks and rivers, misrepresentation of elevation of the tidal gauge, or inaccuracy of LiDar data. More likely this is because the LiDar is picking up the tops of the salt marsh grasses instead of the salt marsh platform when it is collecting the set of data that will produce the digital elevation model. This does not allow the overland flooding to occur when it should, and thusly the MHW values are predicted as higher than actual. Real Time Kinetic (RTK) survey data would be able to solve this or the issue of the misrepresentation of the tidal gauge elevation.

This statistical analysis demonstrates how MLW and MHW are spatially variable. This better exemplifies why one single station worth of MHW and MLW values do not fully describe the biomass productivity for the entire GTMNERR. MHW and MLW are spatially dependent, as supported by the statistics generated here. If only one point were used, error would be introduced into the calculations due to the changes in WSE per location.

7.3 BIOMASS DENSITY DATA

The MHW and MLW, now validated at the eight tidal gauges, are used to estimate biomass density. The values of MLW and MHW had to be extrapolated onto the marsh to avoid use of false values due to “dry” areas. SMS was used to pull MHW and MLW data onto the mesh. Nodes in dry areas were deleted, and remaining nodes were converted to a scatter set. The scatter set was then interpolated back onto the original mesh (Longitude, Latitude, and Z elevation) using the inverse distance weighted (IDW) method. The IDW used the nearest 16 points as a reference, weighting those closest greater than those farthest away.

After interpolation, MHW and MLW were recorded at each of the six vegetation plots. The topography was also pulled for every plot location. From Equation 20 and 21 the values were calculated from the edge of the marsh inward. Figures 42 through 47 show the results of these calculations. The six locations for these biomass curves were selected based on the areas that the vegetation data were collected from by the GTMNERR.

Figures 42 through 47 show the biomass density in grams per meter squared per year for varying values of relative depth as the topography of the marsh platform changes relative to sea state conditions. The figures also reference each vegetation plot's MLW, MHW, local topography, and average biomass. They show the biomass density for the reference plot as the elevation changes.

This effectively shows the threshold of biomass density production. When B is less than zero it does not show up on the plot, because no production is occurring at these elevations. This helps scientists to better understand where the production in the salt marshes is occurring. The curve represents the B values for differing values of relative depth as elevation of the marsh platform to mean sea level changes.

The gray dot shows the local biomass exactly at exact location of the selected plot. local topography, MLW, and MHW are shown as the green, blue, and red dots (respectively). This shows the values taken from the hydrodynamics model used to solve for local biomass productivity. The curve represents biomass productivity using the same exact values, but with a changing local topography.

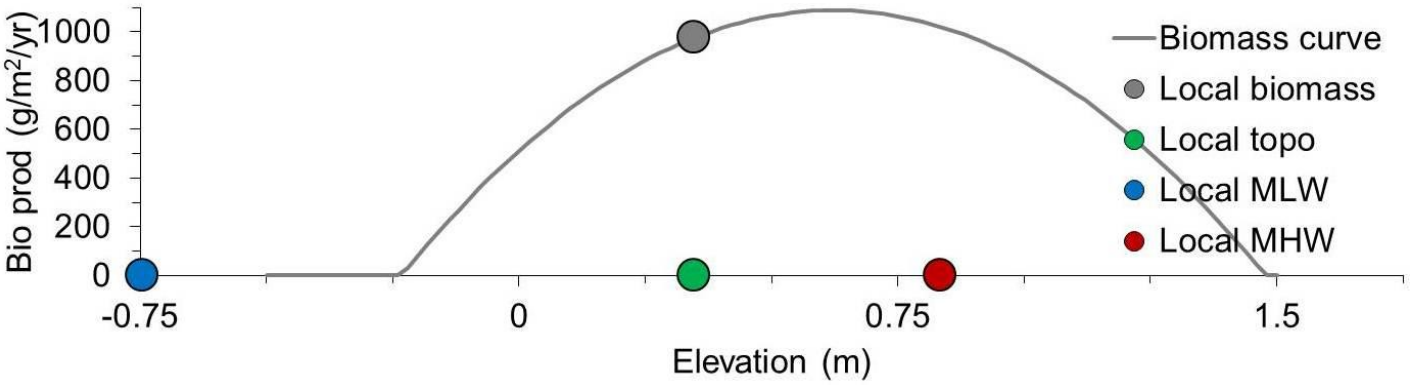

Figure 42. Biomass Curve and Local Predictions for Pine Island (Plot 40)

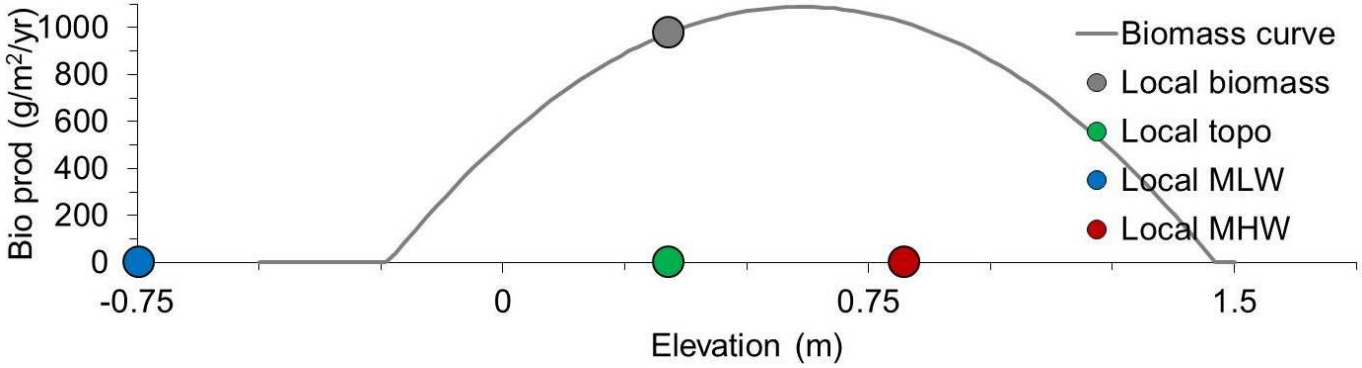

Figure 43. Biomass Curve and Local Predictions for Hat Island (Plot 00)

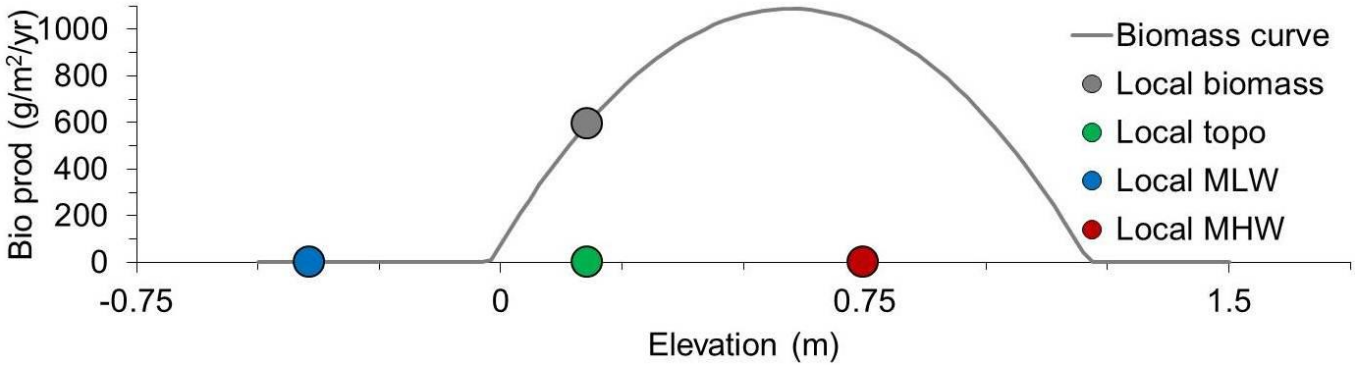

Figure 44. Biomass Curve and Local Predictions for Jason's Creek (Plot 22)

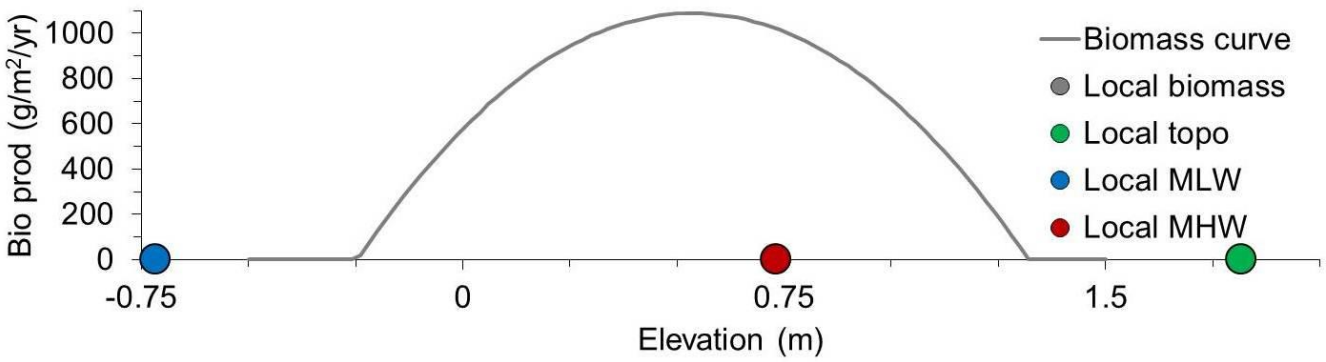

Figure 45. Biomass Curve and Local Predictions for Moses Creek (Plot 06)

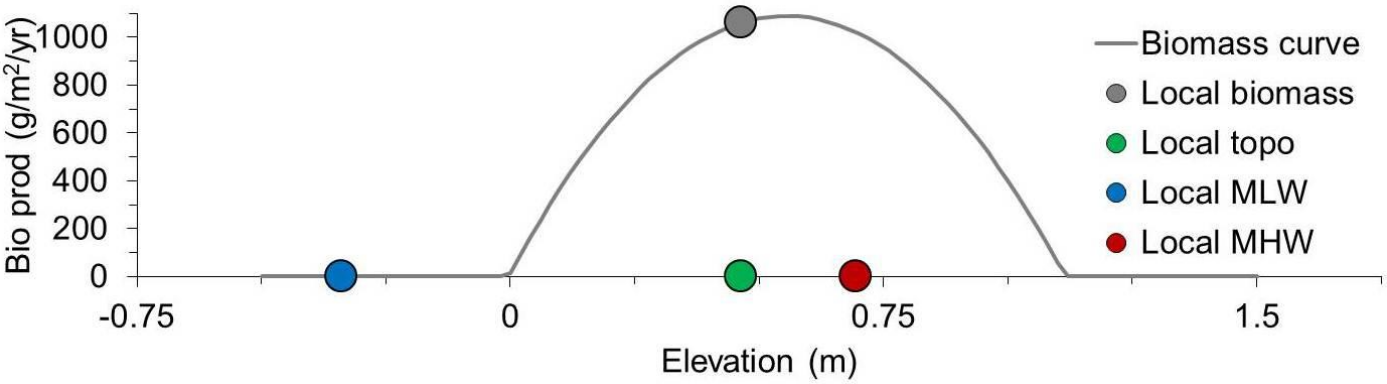

Figure 46. Biomass Curve and Local Predictions for Pellicer Creek (Plot 46)

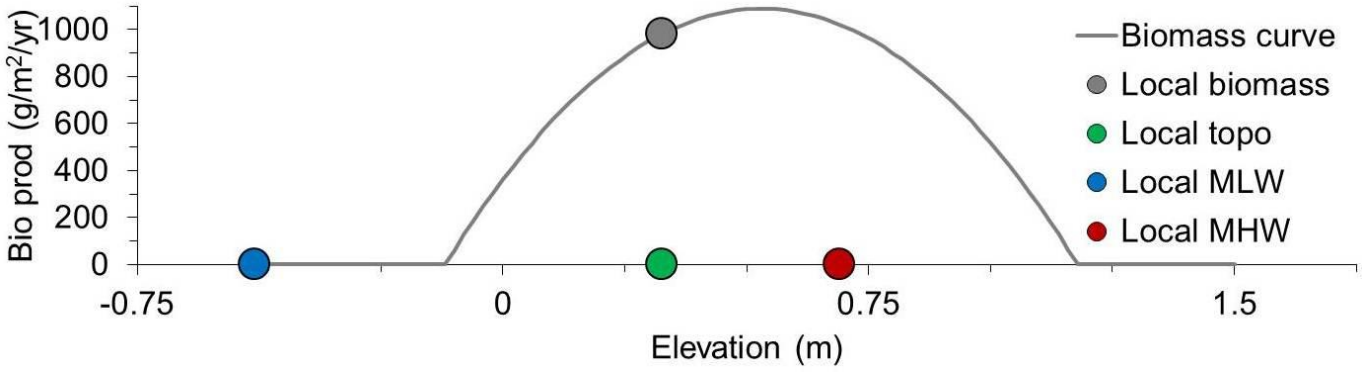

Figure 47. Biomass Curve and Local Predictions for Washington Oaks (Plot 01)

Figures 42 through 47 represent biomass curves for each of the six vegetation plots. The curves show the biomass productivity in g/m^2 per year as the elevation changes. The green dot shows the local topography being considered. The blue and red dots show the MLW and MHW (respectively) for the vegetation plot. The curve shows the change in biomass productivity for the year as the elevation changes. This could be used to understand biomass productivity as you move inward from the water line or the change in biomass productivity as the elevation of the marsh increases or decreases.

The biomass productivity is very low at Jason's Creek (Figure 44). This is mostly due to the fact that this location is relatively high in elevation. The biomass productivity at Mosess Creek (Figure 45) is negative and therefore not on the curve at all. This is due to the fact that the location this information was chosen from is below 0 or is now below surface water elevation. This could also be due to the error introduced by using an incorrect topography value.

These figures show what power a tool like this would provide the GTMNERR staff. For example, if they were working on choosing a location to do a restoration project, or were deciding where the salt marshes were more susceptible to being lost to SLR they could run this model and create similar plots for their own locations of concern. This would be chosen based on which biomass production curves have a steeper slope. A steeper slope means the biomass production is more likely to decline quicker due to a change in sea state.

The vegetation data collected in 2014 helps play a role in analyzing these curves. The locations where the curve tends to be more oblong shaped, are also the locations that have less *Spartina alterniflora* cover according to the data collection. The Washington Oaks site as well as the Pellicer Creek location each show that *Spartina alterniflora* are not actually the dominant species in these areas. The biomass density equation is based on the collection of data from the study done on this dominant species alone; therefore these biomass curves are most likely inaccurate.

8. Analysis

The validation of the ADCIRC-2DDI model was successful. The water surface elevation at the eight gauge stations lined up, as did the MHW and MLW values. Therefore the biomass curve input values are reliable. It is important to note the assumptions made in this model that made the production more efficient for the level of accuracy. For example, baroclinic effects were ignored and one manning's n value was applied to the entire model. This value was chosen due to the accuracy of a similar model done north of this area using the same value (Bacopoulos et. al, 2013). Had the results of this model been less accurate, changes these assumptions would be considered.

8.1 BIOMASS DENSITY CURVE RELIABILITY

The equation used to determine biomass density (Equation 20) is reliant on the coefficients a, b, and c. These values were determined in the study mentioned previously (Morris et al., 2012) of the biomass of *Spartina alterniflora* in the marsh organ. This study focused specifically on *Spartina alterniflora* alone, therefore the area of consideration for these curves most have this marsh grass as its dominant species.

From the collected vegetation data provided by the GTMNERR, for at least the past three years, every vegetation plot had *Spartina alterniflora* as its dominant species except the two most southern vegetation plots. Plots 46 and 01 mostly have Batis maritime and Juncus roemerianus as their dominant species, though *Spartina alterniflora* is often present. This begs the question of reliability of the curves for these two plots.

The greatest reliability issue with the biomass curve perdition is the input of local topography for the salt marsh. The bathymetry used in the ADCIRC model is developed using Light Detection and Ranging (LIDAR) data. The LIDAR incorporates high resolution three dimensional data into a high quality Digital Elevation Model (DEM) that can be used in ADCIRC.

The method presents the question of whether the LIDAR is picking up the edge of the salt marsh or the top of the marsh grasses when it is collecting its elevation data. This obviously creates an issue of possible error in the biomass curves. This issue is discussed in Bilskie et al., 2013. Medeiros et al., 2015 goes into further detail on how to adjust for this error.

For and the calculated biomass production of the GTMNERR at present day conditions, a conservative value of 6 cm (Hladik and Alber, 2012) error was chosen as representation for possible vertical error in the GTMNERR. This was based on Table 7 values. Given the average height of the *Spartina alterniflora* in the GTMNERR, they are classified as small in this work; yet also range up to an average of the high 67 cm at one location. Thus the value of 6 cm was chosen as error and is represented as E.

Cover class	RTK elevation (m)	RTK elevation difference (m)	Domain DEM Error (m) (unmodified)	Test Site DEM Error (m) (unmodified)	Test Site DEM Error (m) (modified)	RTK grouping
Tall S. alterniflora	0.36	–	0.25	0.27	0.05	a
Medium S. alterniflora	0.77	0.42	0.11	0.09	− 0.03	b
Short S. alterniflora	0.87	0.09	0.05	0.03	− 0.03	c
Intertidal mud	0.89	0.03	0.04	–	–	cd
S. virginica	0.95	0.05	0.04	0.04	− 0.01	de
D. spicata	0.96	0.01	0.08	0.05	− 0.02	de
B. maritima	0.99	0.04	0.04	0.04	< 0.01	de
Salt pan	1.01	0.02	0.03	0.01	− 0.03	e
J. roemerianus	1.02	< 0.01	0.17	0.1	− 0.06	e
B. frutescens	1.23	0.21	0.12	0.12	− 0.01	f

TABLE 7. LIDAR-DERIVED DEM ACCURACIES FOR SALT MARSH (HLADIK AND ALBER, 2012)

Two more runs were made where E (error) was both added to and subtracted from the bathymetry in the GTMNERR mesh. The results from these runs were then put to use in Figures 48 through 53 show the likely error caused by erroneous Lidar elevations. This would give a planner a better understanding of the confidence interval of this tool, and how conservative they need to be.

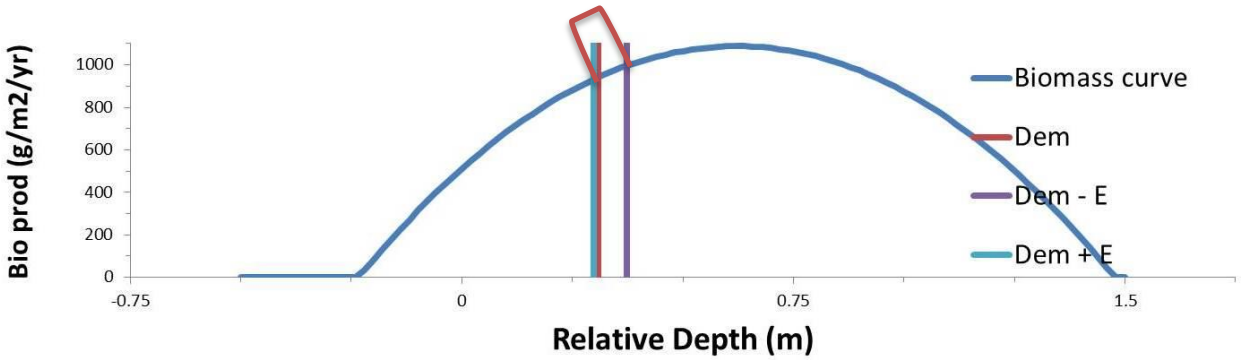

Figure 48. Biomass Curve and Local Predictions for Pine Island (Plot 40) with Error

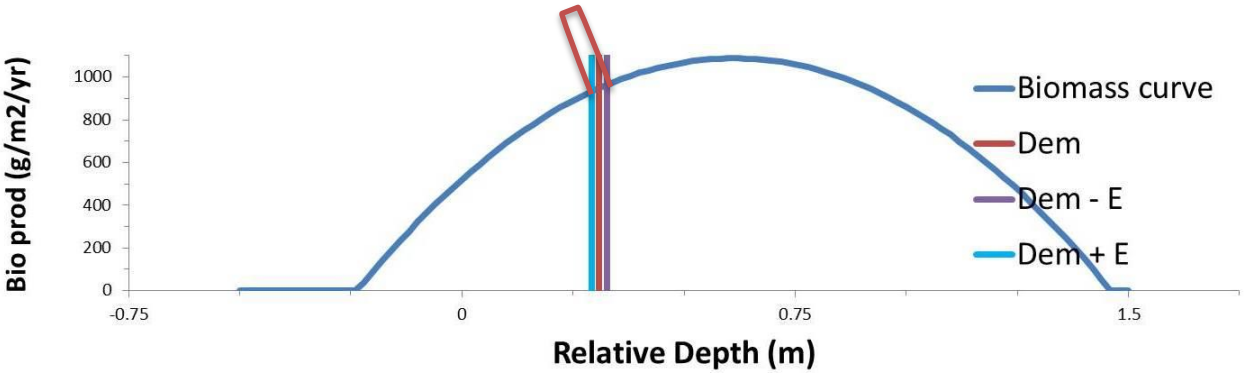

Figure 49. Biomass Curve and Local Predictions for Hat Island (Plot 00) with Error

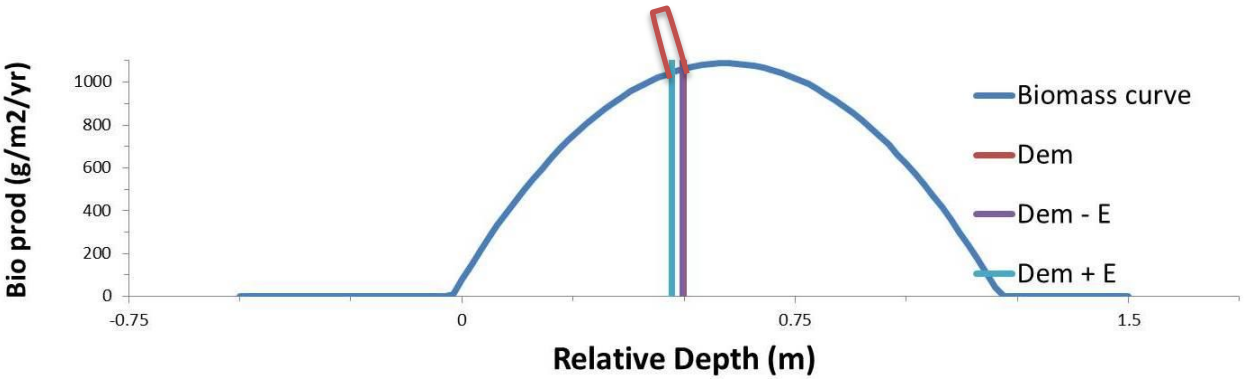

Figure 50 Biomass Curve and Local Predictions for Jason's Creek (Plot 22) with Error

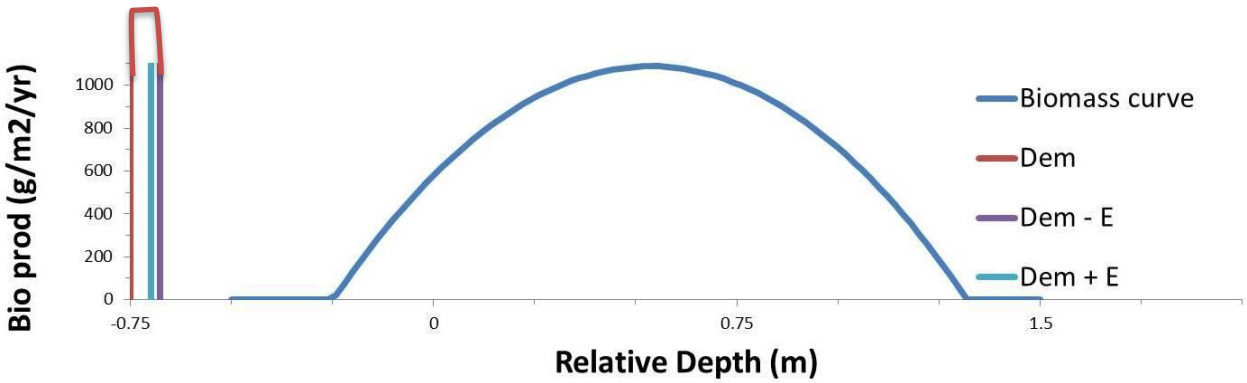

Figure 51. Biomass Curve and Local Predictions for Moses Creek (Plot 06) with Error

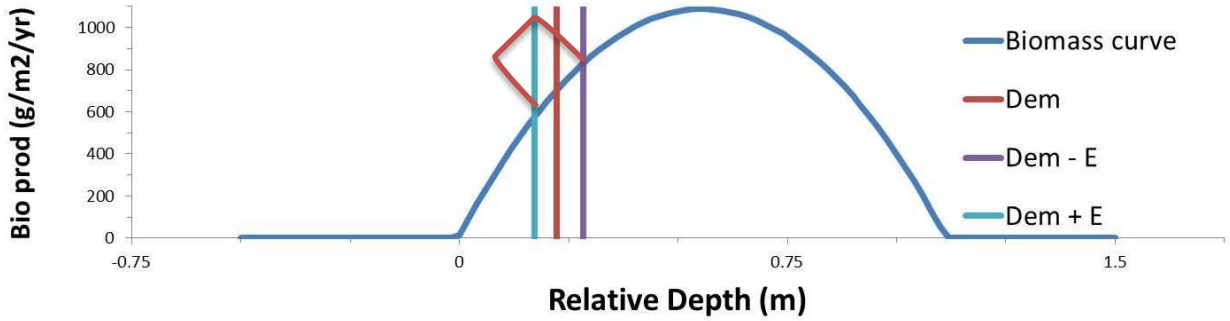

Figure 52. Biomass Curve and Local Predictions for Pellicer Creek (Plot 46) with Error

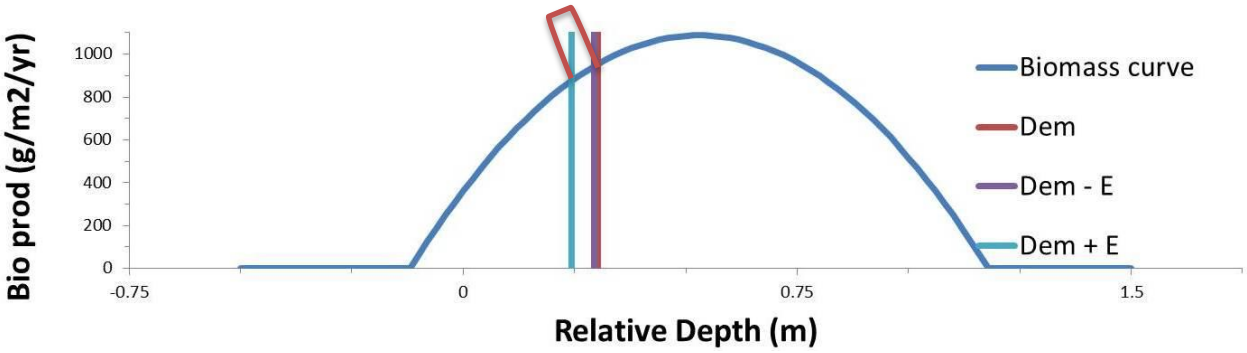

Figure 53. Biomass Curve and Local Predictions for Washington Oaks (Plot 01) with Error

8.2 EFFECTS OF SEA LEVEL RISE ON WATER SURFACE ELEVATION

Possible utility of this model will be in predicting the effects of sea level rise (SLR). In order to better show this, three simulations were adjusted for sea level rise, which was done by creating an initial offset of the sea surface from the geoid. The offset was made at the boundaries of the domain as well, and therefore remained throughout the simulation, which was done by creating a "sea_surface_height_above_geoid_" offset option in the fort.13 file. This means that while flooding of existing landscape was considered in these scenarios, coastal evolution was not.

The well-known standards of mild, moderate and extreme SLR in the north east of Florida were used for these three simulations (Parris et al., 2012). Those values are .13 m, .22 m, and .51m. A run was also made where this value was 0 to check that the simulation would still show the same results as the original. The run where the adjusted offset was 0m produced the exact same results as the run shown in Figures 32 – 39. Figures 54- 61 show the results produced using the three other offsets.

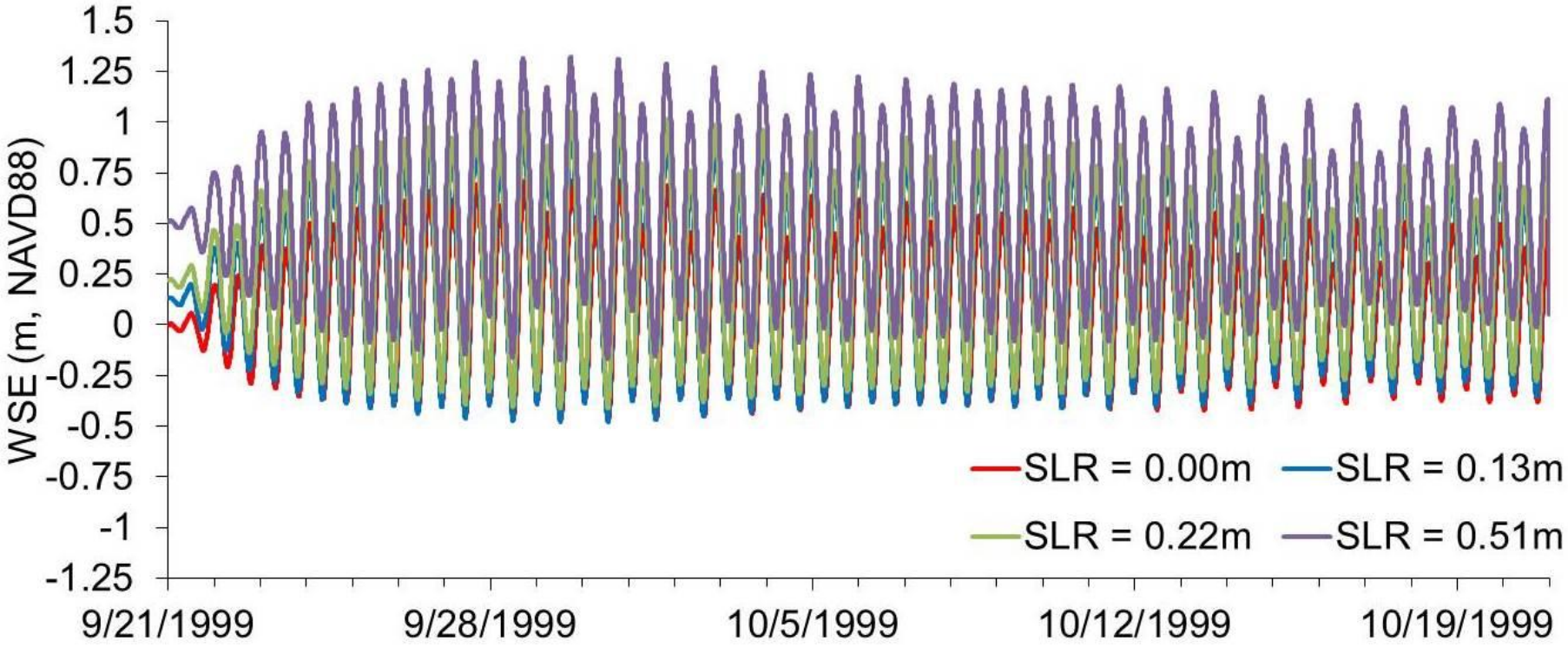

Figure 54. Pablo Creek, FL Model Water Surface Elevation with Possible SLR

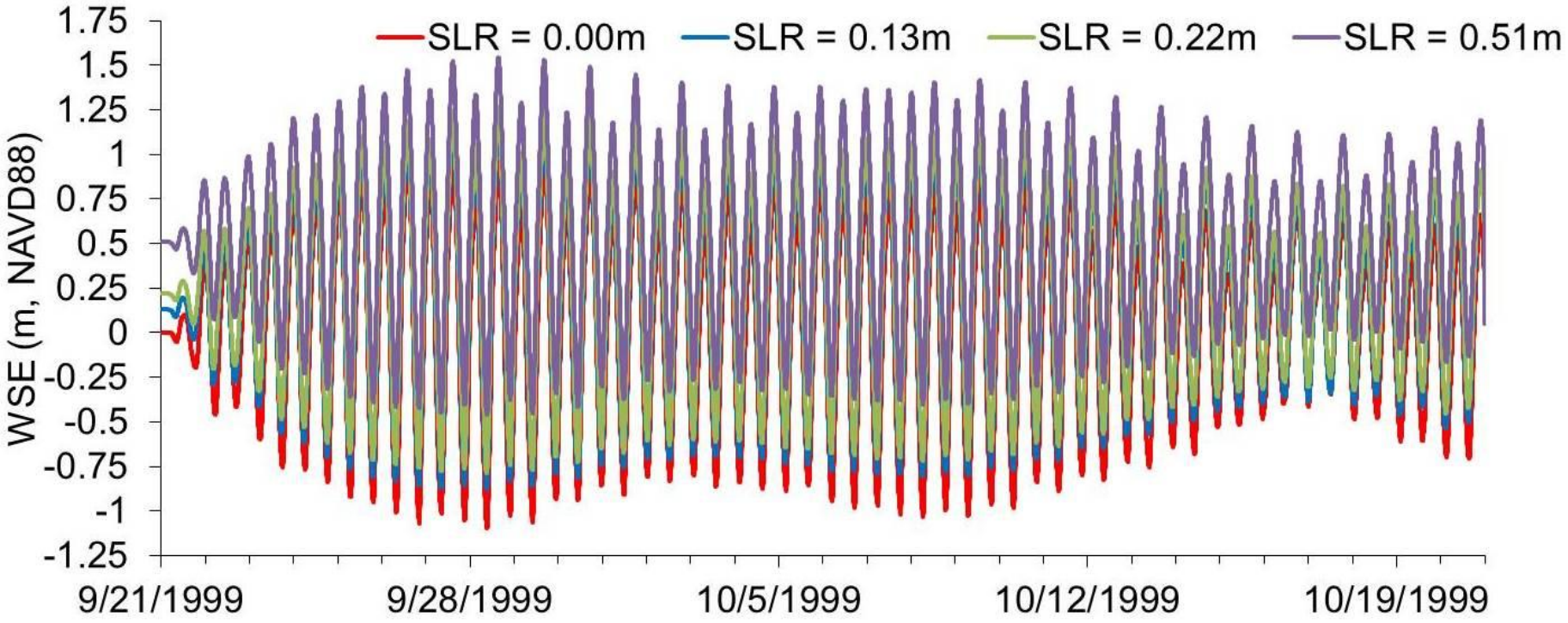

Figure 55. Tolomato River, FL Model Water Surface Elevation with Possible SLR

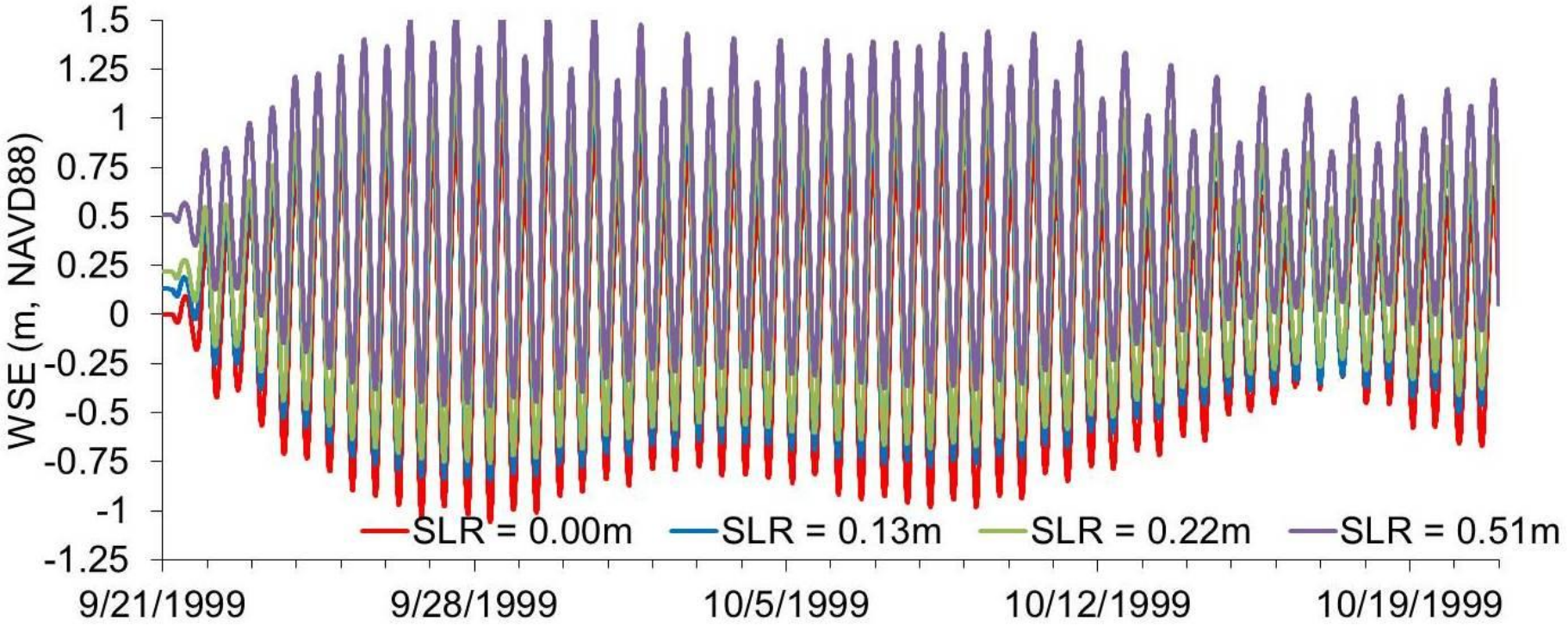

Figure 56. Vilano Bridge, FL Model Water Surface Elevation with Possible SLR

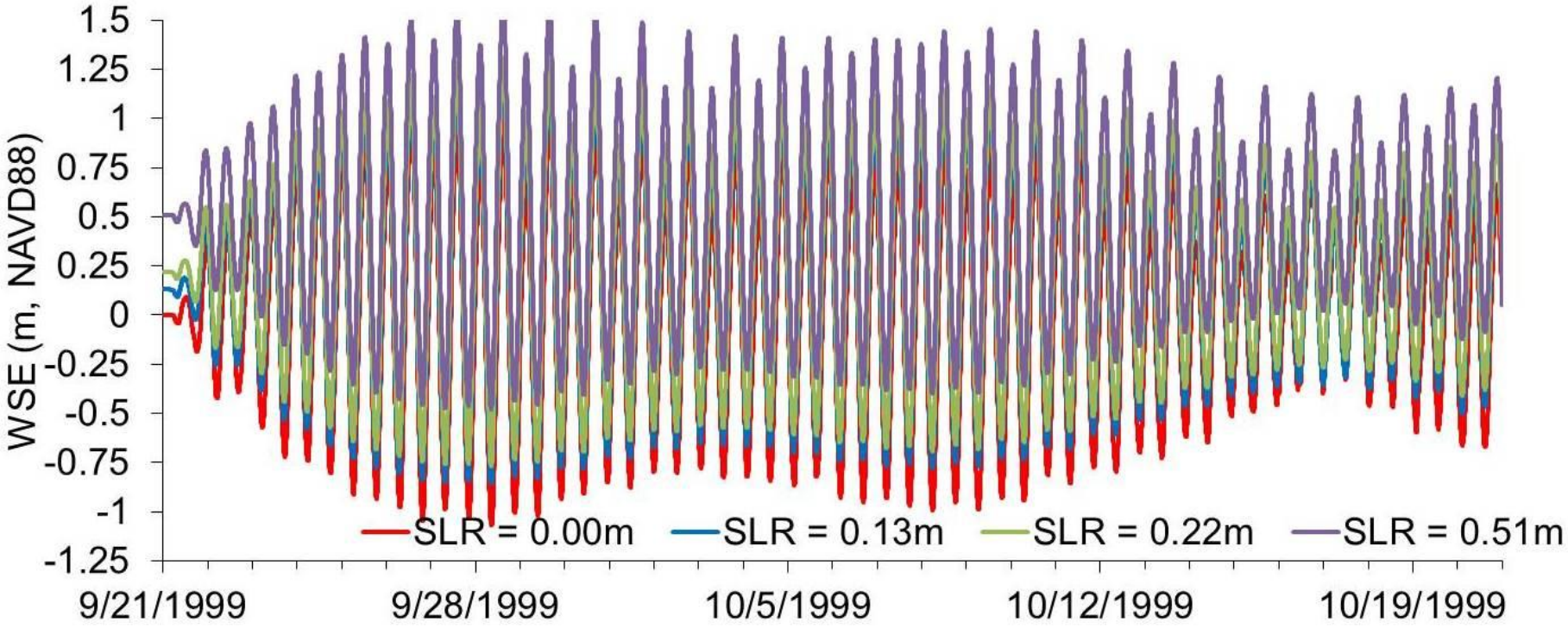

Figure 57. St. Augustine, FL Model Water Surface Elevation with Possible SLR

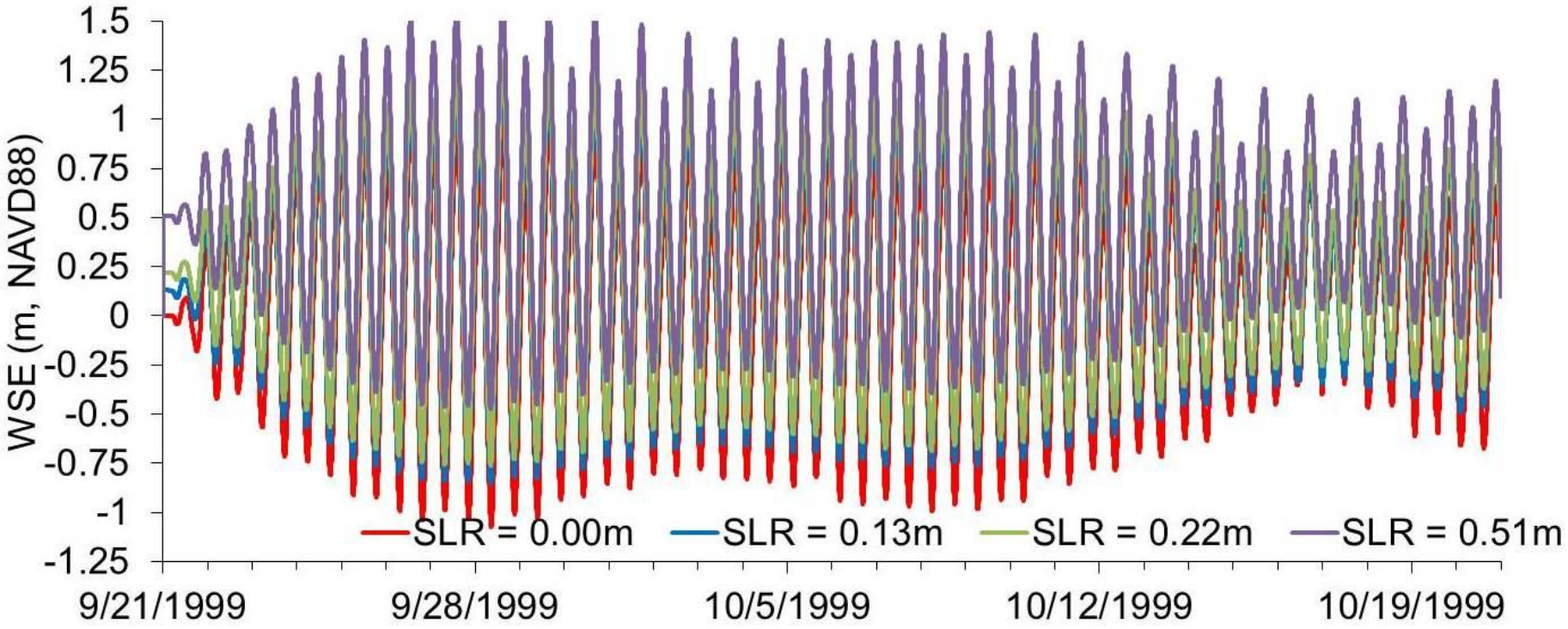

Figure 58. Anastasia Island, FL Model Water Surface Elevation with Possible SLR

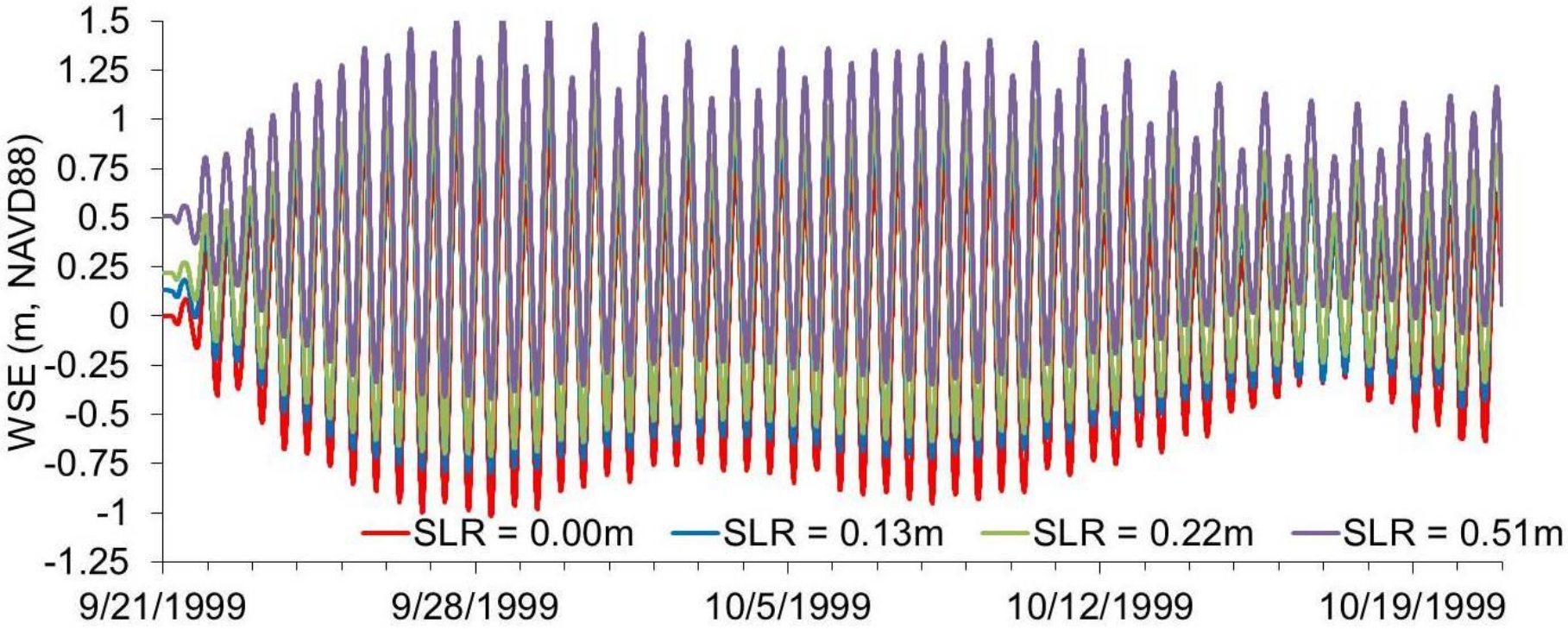

Figure 59. Fort Matanzas, FL Model Water Surface Elevation with Possible SLR

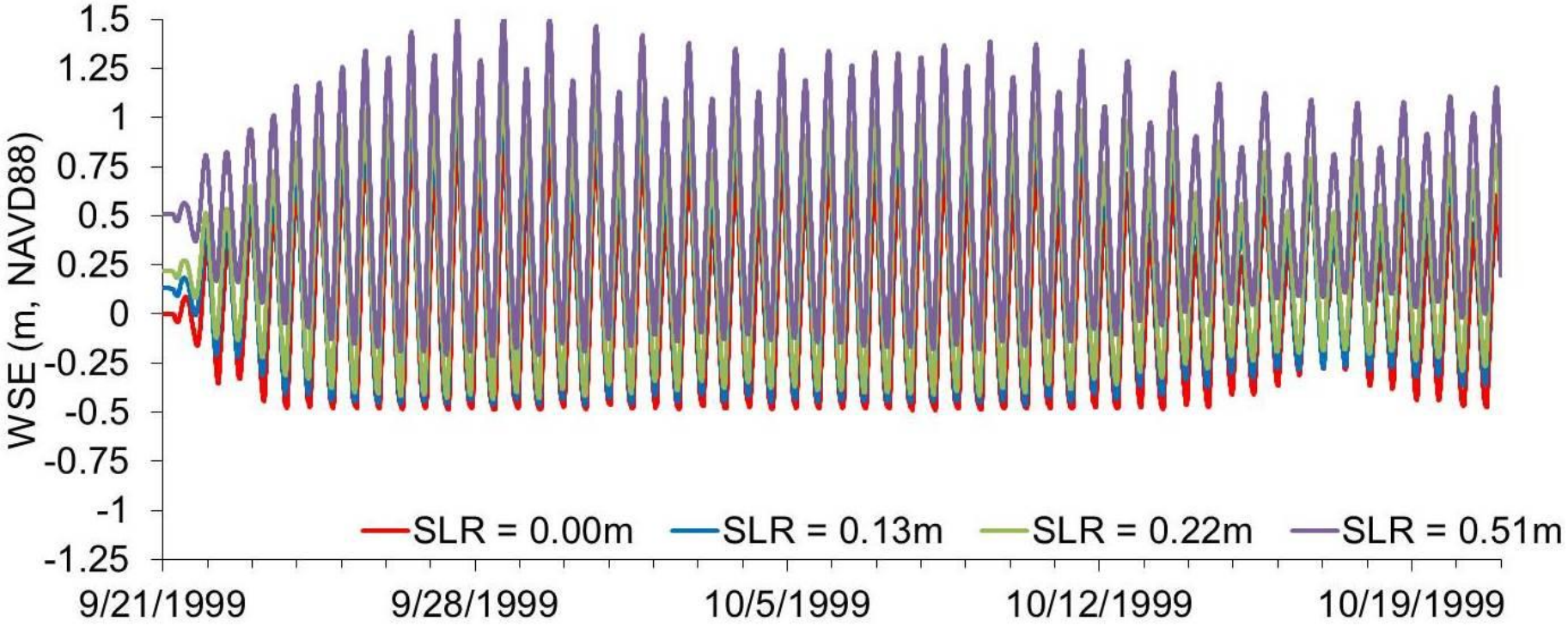

Figure 60. Matanzas River Headwaters, FL Model Water Surface Elevation with Possible SLR

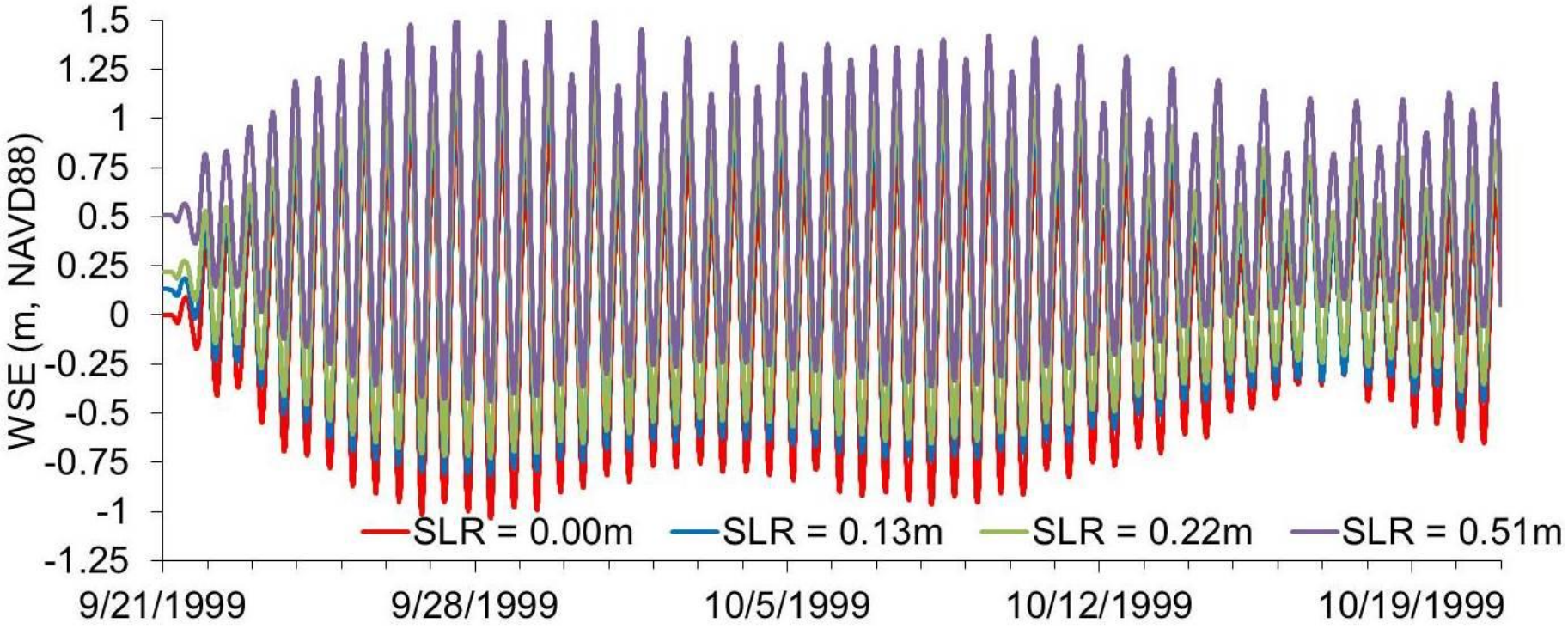

Figure 61. St. Augustine Beach, FL. Model Water Surface Elevation with Possible SLR

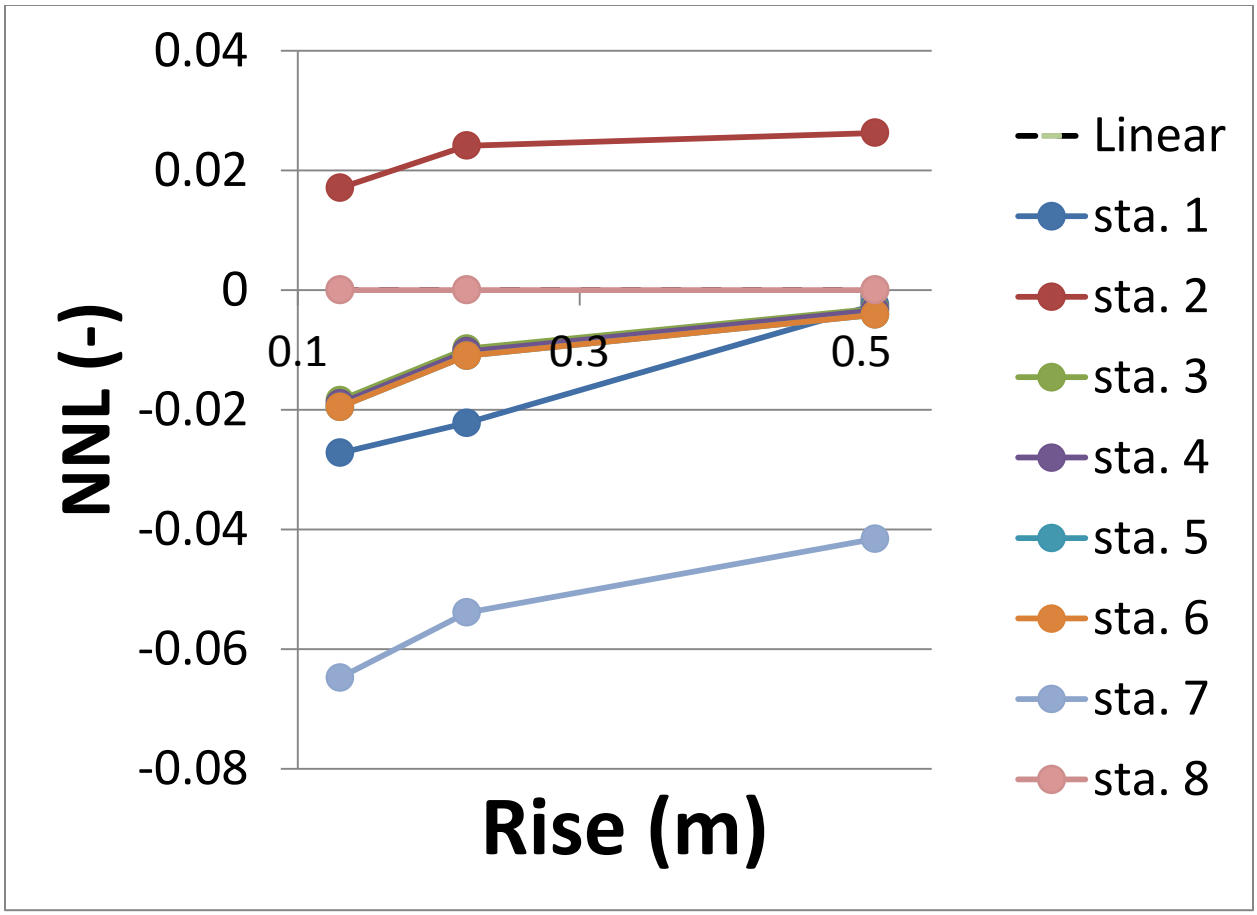

Figure 62. NNL Analysis for Water Surface Elevation at Each Station

Figure 62 shows the Normalized NonLinearity index (NNL) analysis (Bilskie et al., 2014) for water surface elevation at each of the eight stations in the GTMNERR. This index helps compute the amount of nonlinearity (positive or negative) or linearity in a model. In this case this represents the dynamic versus static increase to the water surface elevation with an increase of sea level rise. Equation 27 shows how NNL was calculated for each station for each change in SLR.

$$\textbf{equation 28} \ldots NNL = \frac{\zeta_{SLR} - \zeta_{Control} - \lambda}{\lambda} = \frac{\zeta_{SLR} - \zeta_{Control}}{\lambda} - 1$$

Where ζSLR is the water surface elevation for the given sea level rise scenario, the ζControl is water surface elevation for the present-day condition and λ is the amount of SLR.

Then NNL at every time stamp was calculated, and the averages are shown in Figure 62. The linear line in this figure represents static rise, which occurs when NNL is equal to zero. Static rise is sometimes considered the “bath tub” effect. This occurs when the amount of SLR increase is also the amount of overall water surface elevation increase.

Using the NNL analysis provides a better understanding of the spatial variability of change from SLR from station to station. For instance station 8, the gauge located on St. Augustine beach trends the closest to static change. This is most likely because it is on the coastline, and directly affected by sea level rise. The water surface elevation is not effected by the areas of the GTMNERR that get partially wetted and dried. Basically, the NNL analysis shows how hydrodynamics on the open coast will change linearly with sea-level rise, where sea-level rise does not cause linear changes in hydrodynamics inside the estuary and nonlinear (positive or negative) changes in hydrodynamics will take place.

Station 2 is the only station that had a positive NNL, which means it is the only station that had a larger change in water surface elevation than the change in mean sea level. This is most likely due to its location in relationship to the inlet just to the east of it. The next notable station is seven. This gauge has the lowest NNL value, most likely because, as opposed to gauge 2, is located farther from the inlet. Both of these gauges are located in rivers unlike the other 6 gauges. These gauges are located along creeks, therefore they are more susceptible to the areas that wet and dry. Therefore once the sea level increase pushes the water level above marsh elevation level, the hydrodynamics in these areas are more likely to be affected nonlinearly.

8.3 EFFECTS OF SEA LEVEL RISE ON MHW AND MLW

After running the four simulations for sea level rise scenarios MHW and MLW values were analyzed. Figure 63 shows the MHW and MLW for SLR of 0m, 0.13m, 0.22m, and 0.51m. Table 8 shows the values of each point shown and the average MLW or MHW for that run. It should be noted that the average values increase with the increase in sea level rise. MLW tends to vary at around 0.11 m from present day conditions to 0.8 m in standard deviation for 0.51 m of SLR. MHW varies at around 0.06 m standard deviation. It should be noted that more variability occurs in MLW than MHW. Similar cases have been found in other studies (Bacopoulos et. al, 2014). It is also noted that the variability tends to decrease as sea level rises.

TABLE 8. MHW AND MLW VALUES FOR SLR SCENARIO

	SLR=0m		***SLR=0.13m***		***SLR=0.22m***		***SLR=0.51m***	
Station	*MLW*	*MHW*	*MLW*	*MHW*	*MLW*	*MHW*	*MLW*	*MHW*
1	-0.50	0.61	-0.37	0.78	-0.34	0.84	-0.02	1.09
2	-0.75	0.83	-0.67	0.95	-0.57	0.98	-0.16	1.31
3	-0.77	0.79	-0.62	0.91	-0.52	0.99	-0.25	1.28
4	-0.75	0.76	-0.67	0.91	-0.52	0.94	-0.27	1.27
5	-0.73	0.74	-0.63	0.88	-0.50	0.97	-0.22	1.28
6	-0.72	0.72	-0.56	0.83	-0.50	0.95	-0.21	1.26
7	-0.50	0.69	-0.47	0.76	-0.33	0.92	-0.12	1.21
8	-0.75	0.74	-0.58	0.84	-0.53	0.97	-0.23	1.26
AVG +/- STD	-0.68 ± .11	0.74 ± 0.06	-0.57 ± .1	0.86 ± 0.06	-0.48 ± .08	0.95 ± 0.04 m	-0.19 ± .08	1.25 ± 0.06

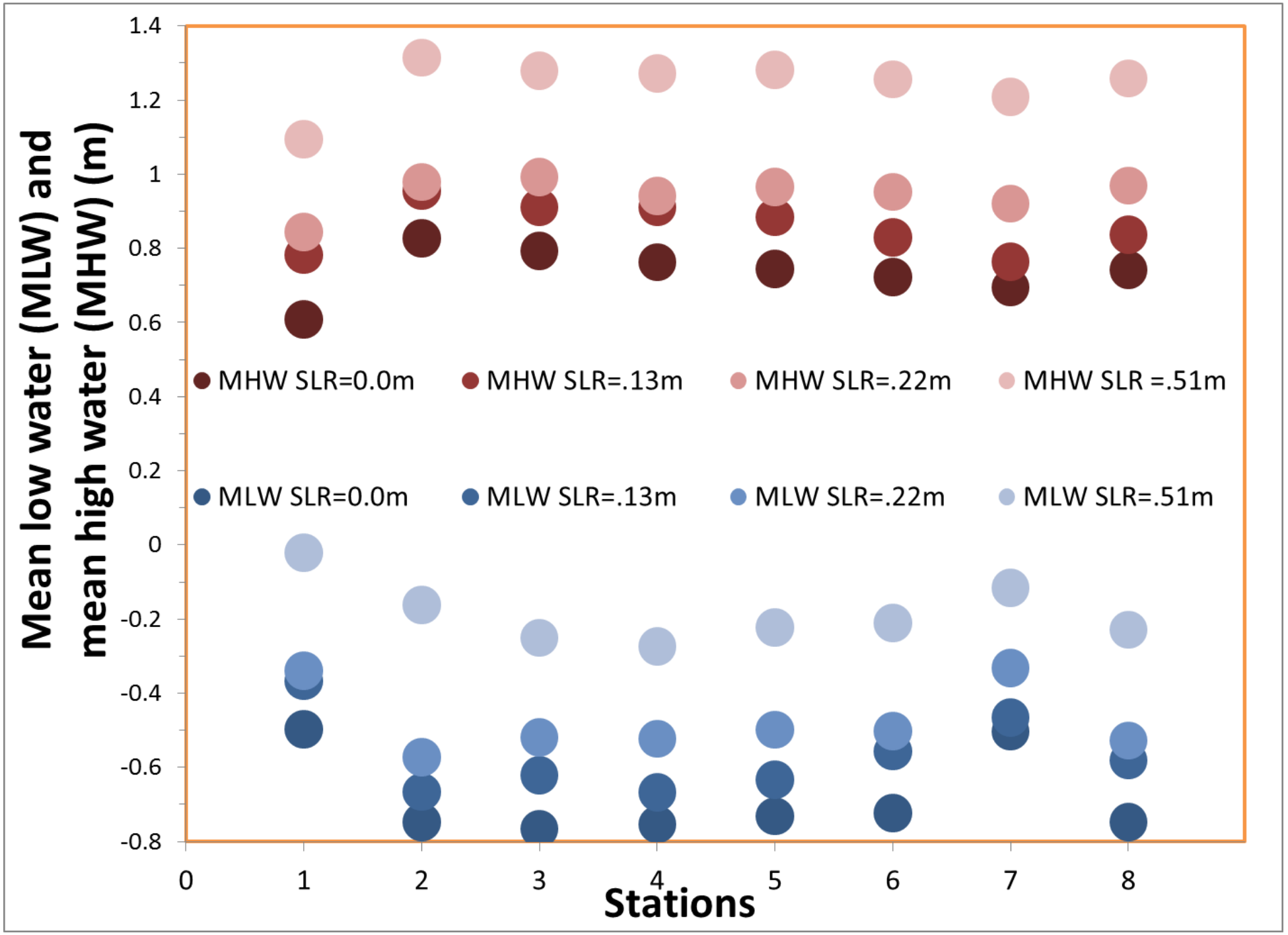

Figure 63. GTMNERR MHW and MLW Model Output for Sea Level Rise Scenarios (none, mild, moderate, and extreme)

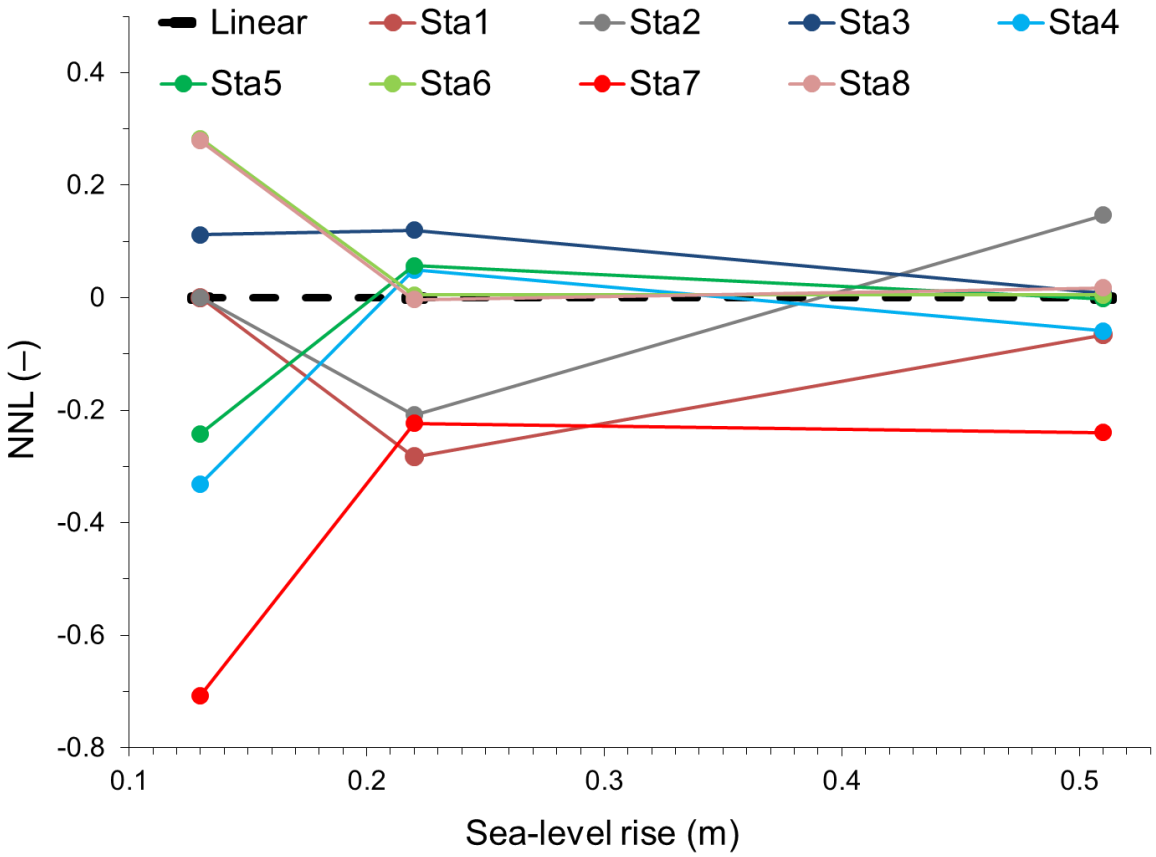

Figure 64. NNL Analysis for MHW at Each Station for Each SLR Scenario

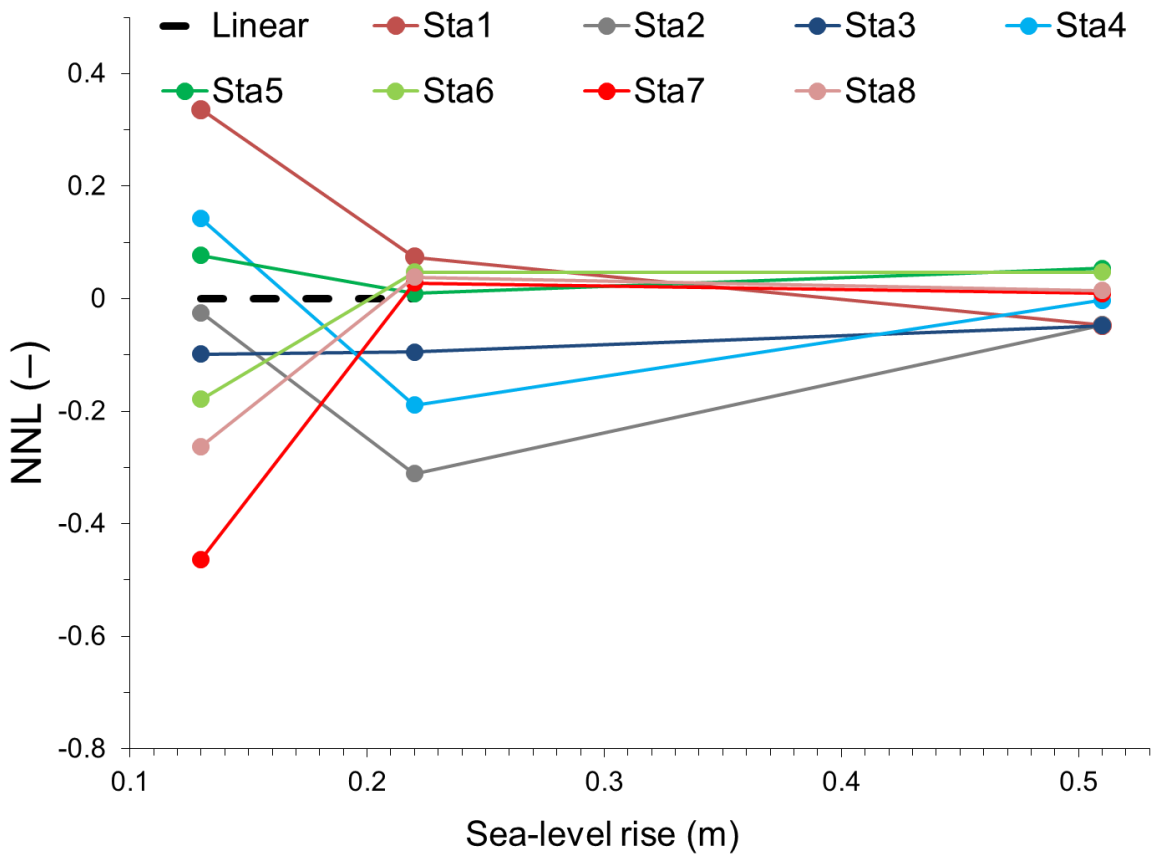

Figure 65. NNL Analysis for MLW at Each Station for Each SLR Scenario

For a better understanding of the nonlinear to linear relationship between an increase in sea level rise and the MHW and MLW another NNL analysis was done for each station for MLW and MHW for the 3 increases in SLR (Figures 64 and 65). Equation 28 shows how these results were calculated.

$$\textbf{equation 29} \ldots NNL = \frac{\eta_{SLR} - \eta_{Control} - \lambda}{\lambda} = \frac{\eta_{SLR} - \eta_{Control}}{\lambda} - 1$$

Where η_{SLR} and $\eta_{control}$ are the MHW or MLW for the sea level rise and control represented the scenario of SLR=0m.

These results represent how vital it is to use multiple points when generating the biomass equation. The linearity differs so extremely for each station's MHW and MLW values from station to station. A result seen in Figures 64 and 65 shows a trend in MLW changing more drastically than MHW. Typically the creeks are showing similar spatial patterns. This is because MLW is dictated more by fully wetted conditions of hydrodynamics, whereas MHW is a function of the fully wetted hydrodynamic conditions but also of the interaction with overland flooding. Thusly, an increase in sea level will cause more variable changes in MHW relative to more consistent changes in MLW, and the NNL analysis follows this understanding.

8.4 EFFECTS OF SEA LEVEL RISE ON BIOMASS DENSITY

The primary utility of this model would be predicting the productivity of the salt marshes in the GTMNERR. Predicted water surface elevations can simply be input into the same biomass equations and new predictions were created for SLR scenarios. It should be noted that the biomass predictions were based on given topography and do not consider natural or engineered accretion of the marsh. This would most likely not be the case, because topography tends to change and adapt as when sea levels change, as the marshes would naturally accrete and/or engineered solutions would assist the marsh accretion. Future work could lead to an adapted model where time steps were taken and the model readjusted for a set of years' worth of SLR (e.g., see Alizad et al., 2015).

Figures 66 through 71 show the biomass curve, updated to show where the biomass density production would be at the three given sea-level rise scenarios. Each scenario is represented by a line. Where the line intercepts the biomass density curve, this is the biomass production for this location for that given scenario. Generally the overall result in a rise in biomass density for the mild condition and moderate condition, however the extreme increase tends to show a start a decrease for the north stations and a consistency in biomass production for the southern stations.

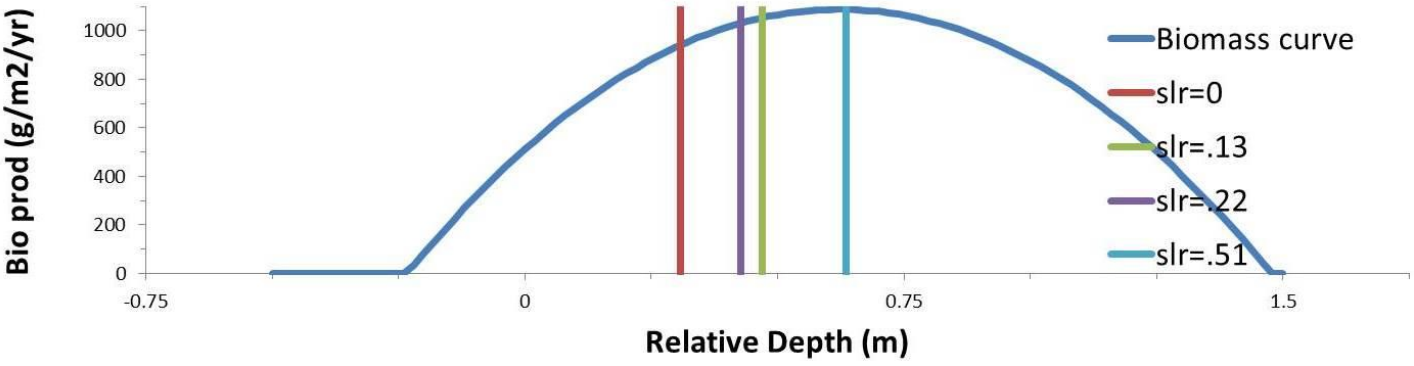

Figure 66. Biomass Curve and Local Predictions for Pine Island (Plot 40) with SLR Scenarios

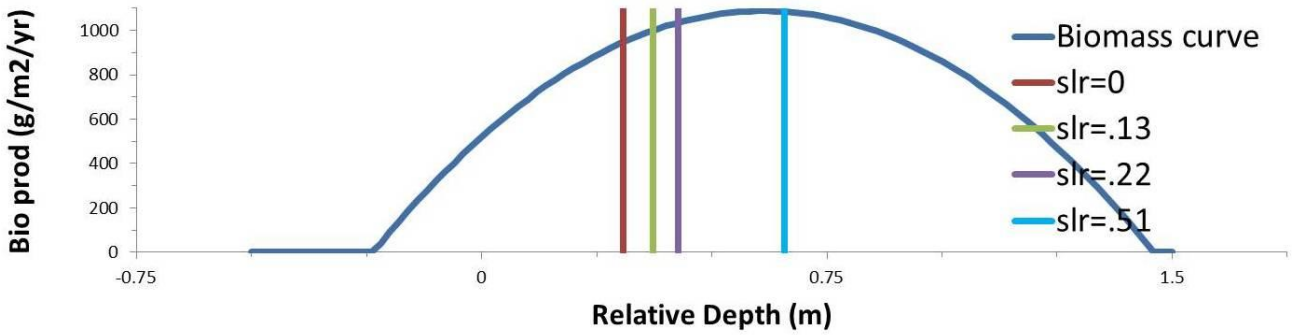

Figure 67. Biomass Curve and Local Predictions for Hat Island (Plot 00) SLR Scenarios

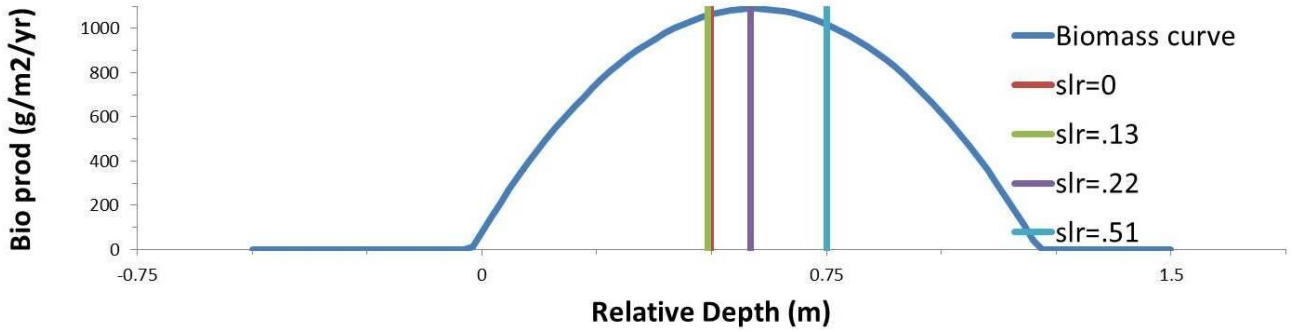

Figure 68. Biomass Curve and Local Predictions for Jason's Creek (Plot 22) SLR Scenarios

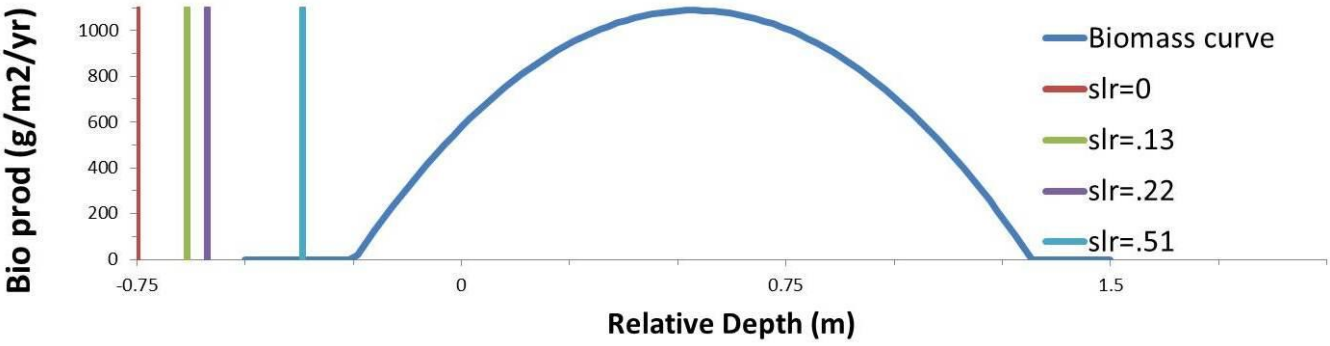

Figure 69. Biomass Curve and Local Predictions for Moses Creek (Plot 06) SLR Scenarios

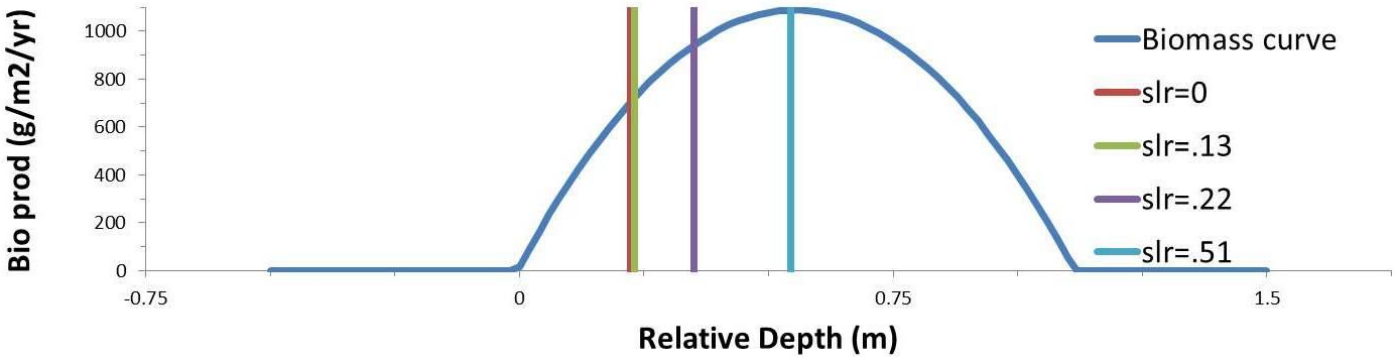

Figure 70. Biomass Curve and Local Predictions for Pellicer Creek (Plot 46) SLR Scenarios

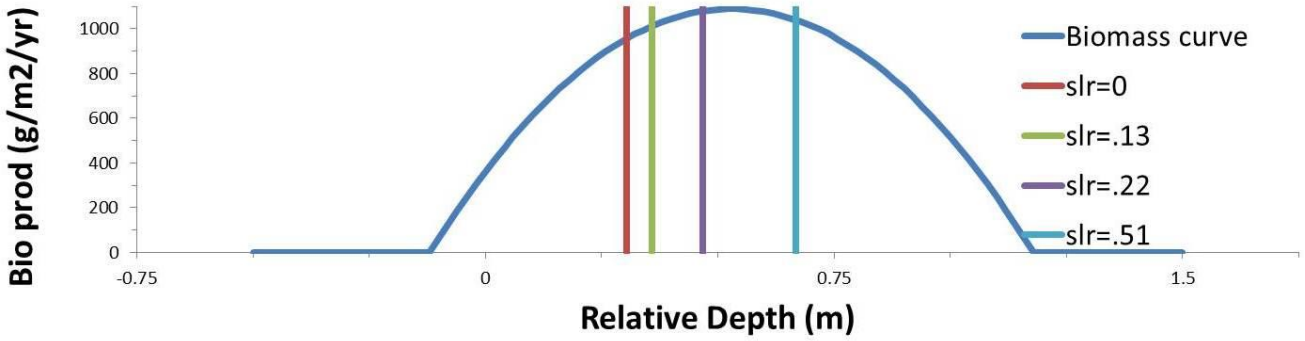

Figure 71. Biomass Curve and Local Predictions for Washington Oaks (Plot 01) SLR Scenarios

Overall this same trend is followed, except in Jason's Creek. Here, the mild sea-level rise increases then decreases for the moderate case. When comparing this to the percent coverage found at Jason's Creek, and it's location along the creek bed, it would seem likely that the change in MHW and MLW, and ultimately relative depth (represented as elevation) would pump the area into higher production. The reduction in biomass production when moving towards the moderate SLR is most likely due to the creek being more variant at this sea level, then most likely experiencing the flooding over that the other stations experience earlier on, at around .51m of SLR.

Hat Island and Washington Oaks both have very similar responses. This is most likely because they are so close to the open channel. While the trends seem to be the same, Hat Island seems to reach the point just after the max biomass density, and Washington Oaks is further into that descending trend. From the vegetation data, it could assumed that because there is more cover in Pine Island, then it is more resilient to the changes in surface water. Washington Oaks is also more centrally located, in that there is water on three sides of it, therefore the effect of SLR on Washington Oaks, though similar in trend, has a more drastic effect.

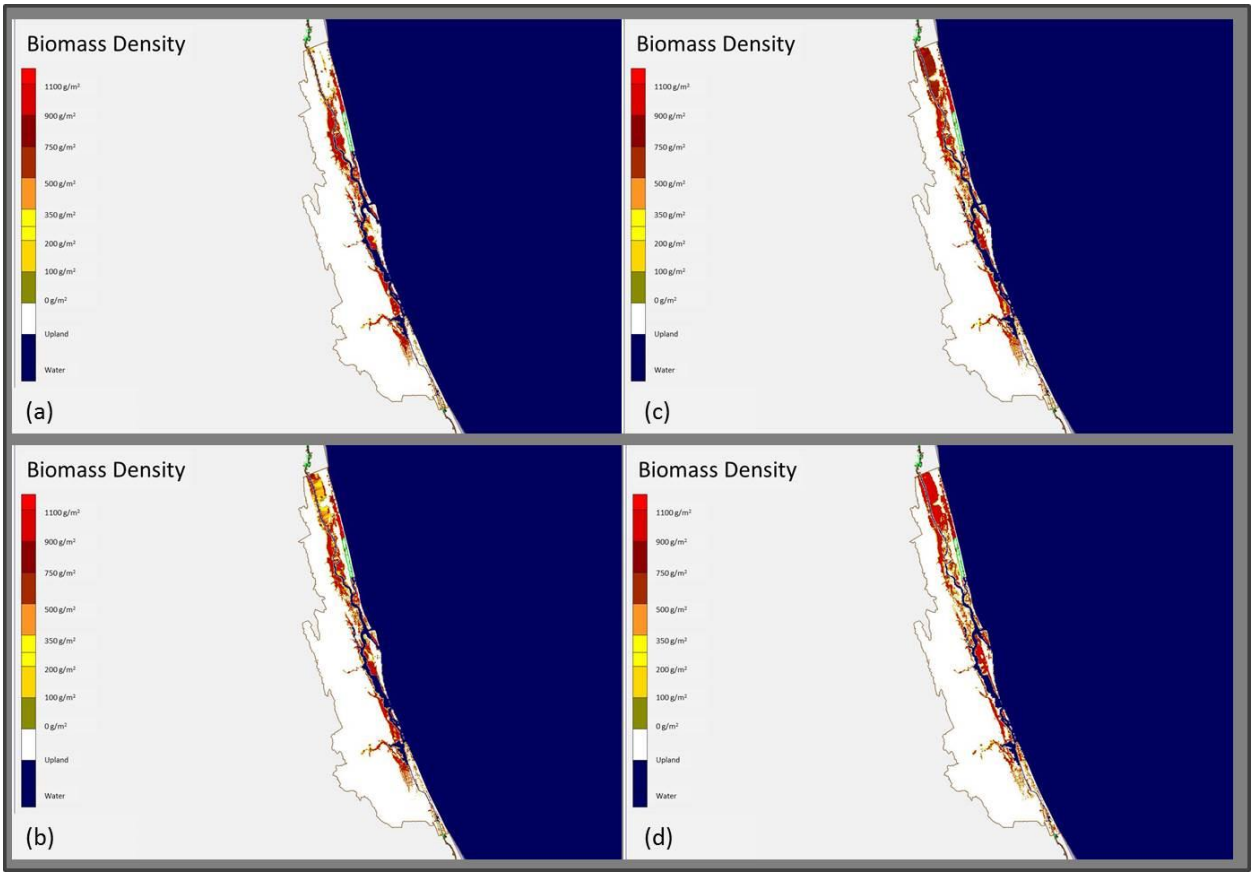

Figure 72. Biomass Density Production in GTMNERR (a) Present Day Conditions (b) SLR of 0.13 m (c) SLR of 0.22 m (d) SLR of 0.51 m

Figure 72 shows the change in biomass production in the GTMNERR (g/m^2 per year) for 50-year simulations of present-day conditions and rise of 0.13, 0.22 and 0.51.

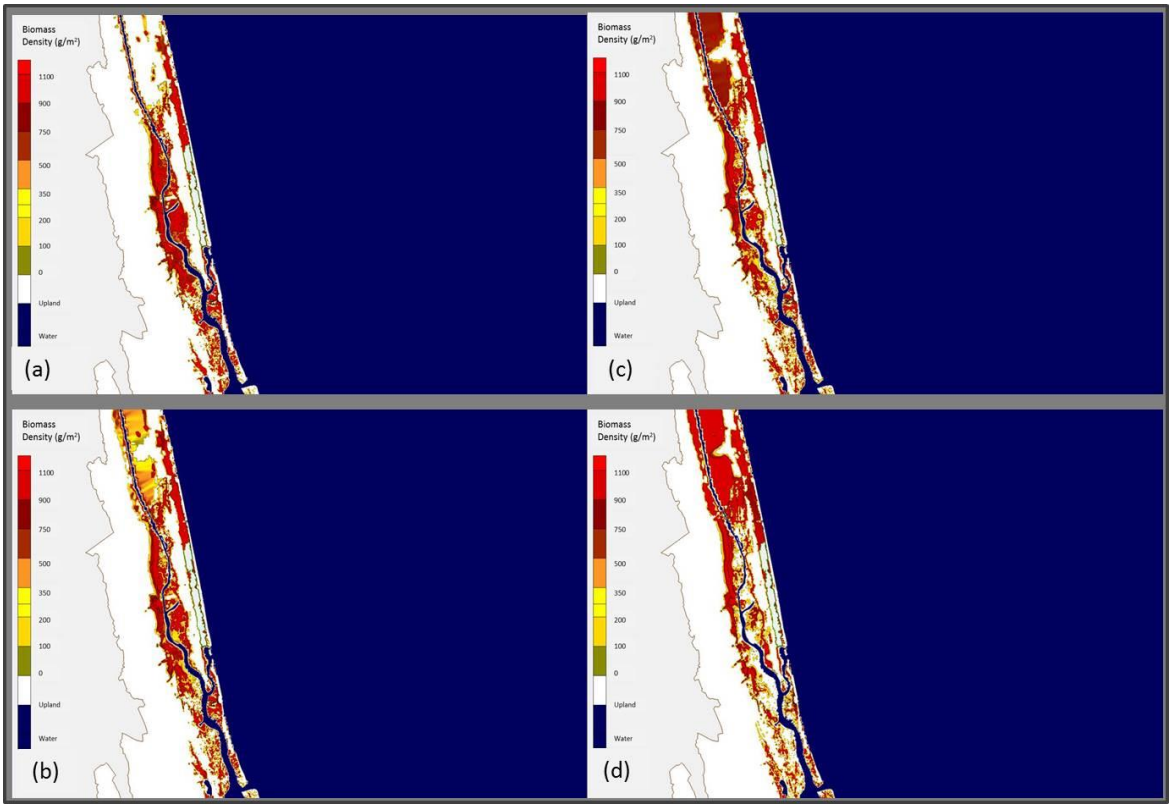

Figure 73. Biomass Density Production in the North Section of the GTMNERR (a) Present Day Conditions (b) SLR of 0.13 m (c) SLR of 0.22 m (d) SLR of 0.51 m

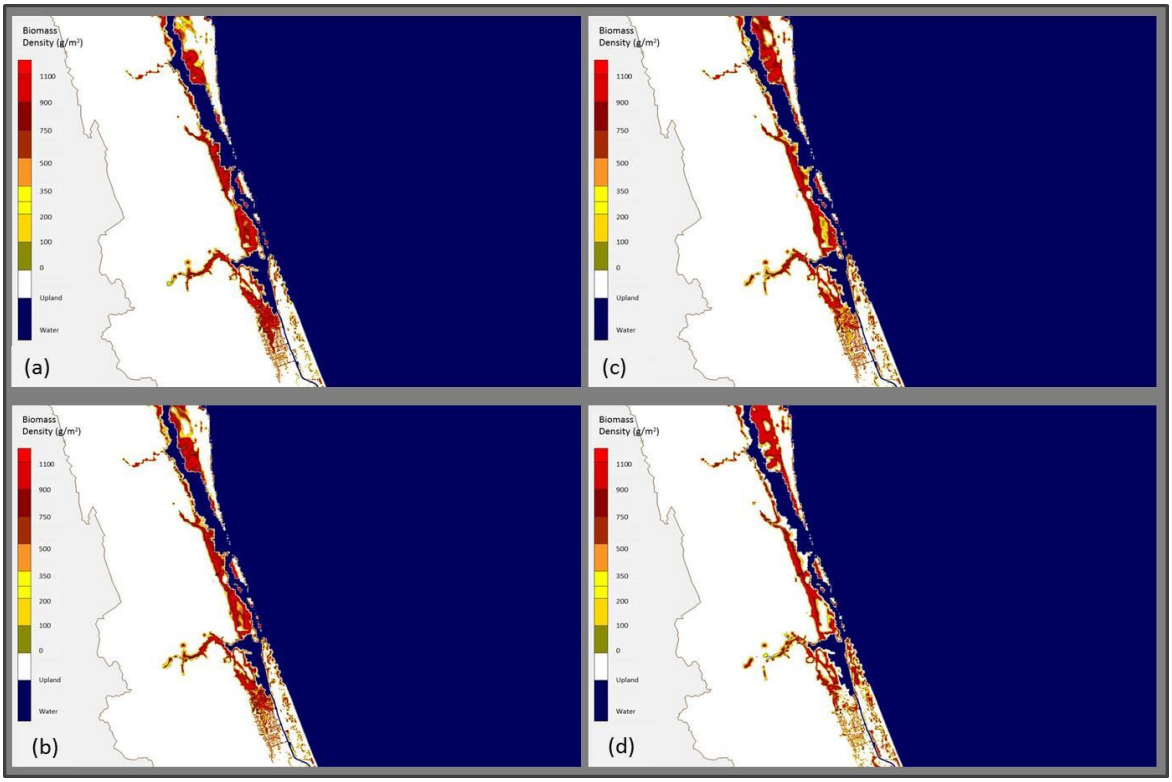

Figure 74. Biomass Density Production in the South Section of the GTMNERR (a) Present Day Conditions (b) SLR of 0.13 m (c) SLR of 0.22 m (d) SLR of 0.51

Figure 73 and 74 show the change in biomass production in the North and the South regions of the GTMNERR (g/m^2 per year) for 50-year simulations of present-day conditions and rise of 0.13, 0.22 and 0.51. These results show that as the sea-level rises, the tides invade further upland. Therefore the lower-topo marshes are submerged in water, converting those areas into water-type class. This then leads to the creation of new marsh in higher-topo areas that were previously of upland-type class.

After applying the output values from the 3 SLR scenarios results in in figures 72, 73, and 74 were found. These results were created by inputting the MHW and MLW outputs from the Tidal Datums code into SMS. Then all but fully wet areas were cut out of the domain and interpolated over the mesh. These results were saved as scatter data and the data calculation tool was used to find biomass density (using equations 20 and 21) all over the domain for each scenario.

Table 9 shows an average of these results over the entire GTMNERR domain. This table shows the Areal coverage by landscape classification for 50-year simulations of present-day conditions and rise of 0.13, 0.22 and 0.51 m. A diminishing areal coverage of upland for greater rise should be noted. There is an increase in areal coverage of water. There is a generally consistent, slightly increasing, areal coverage of marsh as well. Marsh is measured in low B + medium B + high B. This demonstrates the migration of marsh into the upland as more of the overall area becomes affected by water.

A low variation in medium and high B is seen for all four scenarios. This shows how the distribution of low, medium and high B depend on the sea state, as determined by MLW and MHW for present-day conditions as well as for rise of 0.13, 0.22 and 0.51 m. This table demonstrates that as the upland becomes more submerged, more marsh type areal coverage emerges in the GTMNERR. These data prove that geomorphology of the marshes depends on as well as feeds into the hydrodynamics of the basin.

Table 10 shows average and standard deviation of biomass density over the producing marsh landscape for 50-year simulations of present-day conditions and rise of 0.13, 0.22 and 0.51 m. These statistics are on biomass density. These statistics were produced on the producing marsh landscape (not the entire marsh landscape). Typically, marshes with productivity less than 370 g/m^2 are considered low, between 370 and 750 g/m^2 are medium, and more than 750 g/m^2 are categorized as high productivity (Alizad et al., 2013).

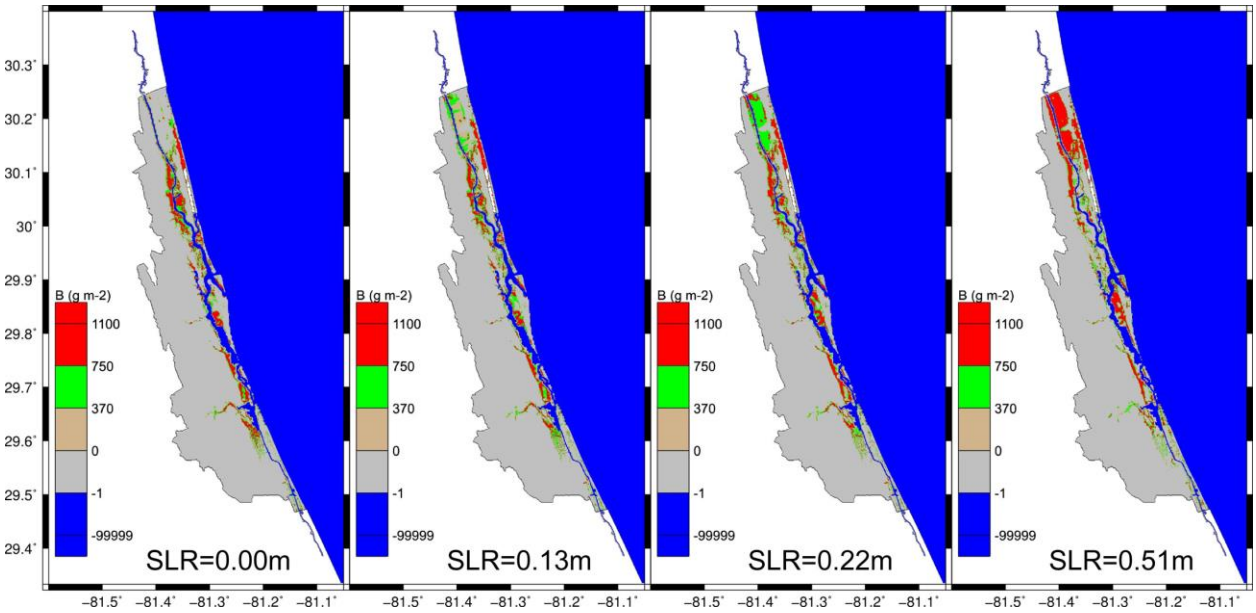

Figure 75. Biomass Density Production Areal Coverage Type Distribution in the GTMNERR for Present Day Conditions, SLR of 0.13 m, SLR of 0.22 m, and SLR of 0.51

TABLE 9. AREAL COVERAGE BY LANDSCAPE CLASSIFICATION

Scenario	Areal coverage of landscape classification (%)					
	Water	Upland	Marsh	Low B	Medium B	High B
Present-day	35.8	56.0	8.2	1.2	2.2	4.8
SLR = 0.13 m	36.0	53.9	10.1	2.3	3.0	4.8
SLR = 0.22 m	36.3	53.2	10.5	1.7	3.5	5.3
SLR = 0.51 m	37.9	51.5	10.5	1.6	2.2	6.7

Table 9 and Figure 75 show an increase in water coverage in the GTMNERR as the sea level rises. This will most likely cause creeks to widen, and friction to decrease. This will also lead to a decrease in upland landscape coverage, as areas in the mesh that were once intermediately wetted and dried become completely wet areas. The marsh will increase, pushing back into the uplands, and levels out. As this occurs, areas that was once of the medium biomass productivity begins to produce high biomass productivity. The tradeoff being that marsh at the edge of the salt marshes will not keep up with seal level rise and will become completely submerged.

TABLE 10. AVERAGE AND STANDARD DEVIATION OF BIOMASS DENSITY OVER THE PRODUCING MARSH LANDSCAPE

Scenario	Average ($g \cdot m^2$)	Standard deviation ($g \cdot m^2$)
Present-day	755	309
SLR = 0.13 m	689	322
SLR = 0.22 m	715	306
SLR = 0.51 m	772	321

These two tables suggest that the marshes in the GTM are resilient in their ability to sustain rising sea level by migrating into the upland. So long as the upland is preserved, the marshes will be able to migrate with rise. However, some existing low-topography marsh will convert to water-type class (e.g., mud flat) after the sea-level rise.

Future consideration to this conclusion would be to investigate the areas where the migration was occurring for land type classification. Though the model shows that the marsh would migrate upland, if that upland is being used, the salt marsh cannot move to that location. These locations of predicted salt marsh migration can be compared to the national land cover maps. It can also be noted that the predictions of similar type SLR of the SLAMM model trend similarly to this model.

9. Conclusion

In this work a finite element mesh was created for the GTMNERR that encompassed both the northern and southern sections of the GTMNERR boundaries. The mesh was generated using the boundary and bathymetry using the spatial discretization method of a three dimensional estuary model. Boundary conditions were applied, and a preliminary run was made of tidal forced hydrodynamics in the GTMNERR. These were then validated by observational data. The model was considered accurate for hydrodynamic predictions.

This preliminary effort produced water surface elevation values that were then applied to the biomass density equations. These equations were then applied to the six locations where vegetation data were being collected by the GTMNERR staff. For each location a biomass productivity curve was generated. These curves predict the biomass density of the six vegetation plots. Future work will be done to validate these curves. The vegetation data collected included percent coverage, canopy height, and dominant species. Therefore the plots with *Spartina alterniflora* as the dominant species can be used to validate the curves.

Ideally samples could be collected of the *Spartina alterniflora* in these plots. They would be dried and then weighed. The weights of several samples could be recorded. Then a ratio would be created between canopy height of the plants weighed and how much they weighed. This would create a relationship between biomass in grams to canopy height (which is recorded). The grams would be calculated from the recorded canopy height then multiplied by the percent coverage. Because each plot is 1m by 1m, this would give a record of biomass density of each plot in grams/m^2. The collected data could then be easily compared to the data predicted by this model.

Four more runs were produced in this study with an included offset in sea level geoid. One increased the sea level by 0m and was compared to the initial run. They produced the same values. The three others increased sea level by .13m, .22m, and .51m. Each run produced different water surface elevations for the different increases in water height. These values were then input into the biomass equations as well.

Limitations were made on this model due to computing power. For example baroclinic forces were ignored. The model is also only two dimensional rather than three dimensional. Coastal models are typically faced with limited computing resources, so this is fairly typical. The model produced results similar to actual observations; therefore it is more efficient to keep these limits. It is also important to pick a model to meet the needs of the coastal community in question.

Geomorphic variation within the marsh platforms and variations in biomass in the marshes, as well as the hydrodynamic tidal flow have an effect on the tidal constants of MHW, and MLW in and across an estuary. Accretion rates and biomass productivity have an effect on areas of the marsh that go through wetting and drying. Furthermore, the result of sea level rise will be an increase in marsh platforms type nodes moving into the category of open water nodes, and thusly resulting in the widening of creeks throughout the GTMNERR. The overall outcome of this would be less bottom friction and less spatial variability in the tides.

The model provides a tool to help protect the GTMNERR. Future work could lead toward making the model adaptable to other national estuary research reserves in the country, as well as coastal communities looking to protect their shorelines. This research could be environmentally and economically beneficial for coastal community planning.

Though the biomass productivity did ultimately increase on average in the marsh, the edges of the marsh were not able to keep up with MHW and were submerged in some places for the more extreme scenarios of SLR. There is a complex dynamic system introduced in the salt marshes, where the bio-geomorphological feedbacks influence hydrodynamic, geomorphological, and biological variables across the marsh. In other words, the change in water surface elevation variance feeds into a change in biomass build up, which feeds into the morphing of the salt marsh, which feeds back into the height of water surface elevation.

The objective of this work was to create a tool that would provide better understanding of the hydrodynamic processes in the GTMNERR, and how they affect the biological processes throughout the marsh landscape. This then would feed into a model that shows how much and where biomass production will be occurring, giving sea-level rise in 50 years. This was accomplished. This tool can now help coastal planners better understand the migration patterns of the salt marsh in the GTMNERR, and make decisions to either designate or reserve uplands or wetlands for future salt marsh locations. This is a valuable tool for coastal managers to have.

BIBLIOGRAPHY

Allen, J. R. L. (1997). Simulation models of salt-marsh morphodynamics: some implications for high-intertidal sediment couplets related to change.*Sedimentary Geology*, *113*(3), 211-223.

Alizad, K., Hagen, S. C., Morris, J. T., & Bacopoulos, P. (2013, December). A Hydro-marsh equilibrium model for marsh system response to Sea Level Rise. In *AGU Fall Meeting Abstracts* (Vol. 1, p. 0572).

Alizad, K., Hagen, S. C., Morris, J. T., Bilskie, M. V., Passeri, D., & Medeiros, S. C. (2015) *Coastal Wetland Response to Sea Level Rise in a Marine and Fluvial Estuarine System.* In Review

Alizad, K., Hagen, S. C., Morris, J. T., Bacopoulos, P., Bilskie, M. V., Weishampel, J. F. (2015) A coupled, Two-Dimensional Hydrodynamic-Marsh Model with Biological Feedback. *In review.*

Apel, J. R. (1987). *Principles of ocean physics* (Vol. 38). Academic Press.

Arcement Jr, G. J., & Schneider, V. R. (1989). Guide for Selecting Manning's Roughness Coefficients for Natural Channels and Flood Plains United States Geological Survey Water-supply Paper 2339. *pubs. usgs. gov/wsp/2339/report. pdf*.

Bacopoulos, P. (2005). *Analysis, modeling, and simulation of the tides in the Loxahatchee River estuary* (*Southeastern Florida)* (Doctoral dissertation, University of Central Florida Orlando, Florida).

Bacopoulos, P., & Hagen, S. C. (2009). Tidal simulations for the Loxahatchee River estuary (southeastern Florida): On the influence of the Atlantic Intracoastal Waterway versus the surrounding tidal flats. *Journal of waterway, port, coastal, and ocean engineering*, *135*(6), 259-268.

Bacopoulos, P., & Hagen, S. C. (2014). Dynamic Considerations of Rise with Respect to Water Levels and Flooding in Apalachicola Bay. *Journal of Coastal Research*, *68*(sp1), 43-48.

Bilskie, M. V., & Hagen, S. C. (2013). Topographic accuracy assessment of bare earth lidar-derived unstructured meshes. *Advances in water resources*, *52*, 165-177.

Bilskie, M. V., Hagen, S. C., Medeiros, S. C., & Passeri, D. L. (2014). Dynamics of sea level rise and coastal flooding on a changing landscape.*Geophysical Research Letters*, *41*(3), 927-934.

Bilskie, M. V., Hagen, S. C., Passeri, D. L., & Alizad, K. Assessment of coastal flood risk in a changing climate along the northern Gulf of Mexico.

Blain, C. A., Westerink, J. J., & Luettich Jr, R. A. (1995). Application of a domain size and gridding strategy for the prediction of hurricane storm surge. *Computational Mechanics Publications, Southhampton, UK. 1995.*

Blanton, B. O., Werner, F. E., Seim, H. E., Luettich, R. A., Lynch, D. R., Smith, K. W., ... & Way, F. (2004). Barotropic tides in the South Atlantic Bight.*Journal of Geophysical Research: Oceans (1978–2012)*, *109*(C12).

Blumberg, A. F., & Mellor, G. L. (1987). A description of a three-dimensional coastal ocean circulation model. *Three-dimensional coastal ocean models*, 1-16.

Brenner, M., Schelske, C. L., & Keenan, L. W. (2001). Historical rates of sediment and nutrient accumulation in marshes of the Upper St. Johns River Basin, Florida, USA. *Journal of Paleolimnology*, *26*(3), 241-257.

Chen, X., Alizad, K., Wang, D., & Hagen, S. C. (2014). Climate Change Impact on Runoff and Sediment Loads to the Apalachicola River at Seasonal and Event Scales. *Journal of Coastal Research*, *68*(sp1), 35-42.

D'Alpaos, A., Lanzoni, S., Mudd, S. M., & Fagherazzi, S. (2006). Modeling the influence of hydroperiod and vegetation on the cross-sectional formation of tidal channels. *Estuarine, Coastal and Shelf Science*, *69*(3), 311-324.

Dame, R., Alber, M., Allen, D., Mallin, M., Montague, C., Lewitus, A., ... & Smith, N. (2000). Estuaries of the south Atlantic coast of North America: their geographical signatures. *Estuaries*, *23*(6), 793-819.

DEP. Map of GTM Research Reserve. (2015, January 15). Retrieved February 6, 2015, from http://www.dep.state.fl.us/coastal/sites/gtm/

Dietrich, J. C., Zijlema, M., Westerink, J. J., Holthuijsen, L. H., Dawson, C., Luettich, R. A., ... & Stone, G. W. (2011). Modeling hurricane waves and storm surge using integrally-coupled, scalable computations. *Coastal Engineering*,*58*(1), 45-65.

Dresser, C. McKee Inc. 2002. *Hydrologic Model Development for MFL Evaluation of Prevatt Lake, Orange County*.

Farber, S., Costanza, R., Childers, D. L., Erickson, J., Gross, K., Grove, M., ... & Wilson, M. (2006). Linking ecology and economics for ecosystem management. *Bioscience*, *56*(2), 121-133.

Egbert, G. D., & Ray, R. D. (2000). Significant dissipation of tidal energy in the deep ocean inferred from satellite altimeter data. *Nature*, *405*(6788), 775-778.

Frazel, D. (2009). Site profile of the Guana Tolomato Matanzas National Estuarine Research Reserve. *Ponte Vedra, FL*, *155*.

Friends of the GTM Reserve., 2014. Guana Tolomato Matanzas National Estuarine Research Reserve. [Available online at: http://www.GTM-NERR.org/.]

Hagen, S. C., Morris, J. T., Bacopoulos, P., & Weishampel, J. F. (2012). rise impact on a salt marsh system of the lower St. Johns River. *Journal of Waterway, Port, Coastal, and Ocean Engineering*, *139*(2), 118-125

Hagen, S. C., Westerink, J. J., & Kolar, R. L. (1998). 2D Finite Element Grids Based on a Localized Truncation Error Analysis. *Int. j. numer. methods fluids*.

Hagen, S.C., Zundel, A.K., Kojima, S., 2006. Automatic, unstructured mesh generation for tidal calculations in a large domain. International Journal of Computational Fluid Dynamics 20, 593–608.

Hladik, C., & Alber, M. (2012). Accuracy assessment and correction of a LIDAR-derived salt marsh digital elevation model. *Remote Sensing of Environment*, *121*, 224-235.

John, C., & Morris, F. (2003). *Northern Coastal Basin bathymetric survey—Oak Landing to Ponce de Leon Inlet*. Technical memorandum. St. Johns River Water Management District, Palatka, Fla.

Kirwan, M. L., Guntenspergen, G. R., & Morris, J. T. (2009). Latitudinal trends in *Spartina alterniflora* productivity and the response of coastal marshes to global change. *Global Change Biology*, *15*(8), 1982-1989.

Kolar, R. L., & Gray, W. G. (1990, June). Shallow water modeling in small water bodies. In *Proc. 8th Int. Conf. Comp. Meth. Water Res* (pp. 39-44).

Kolar, R. L., Westerink, J. J., Cantekin, M. E., & Blain, C. A. (1994). Aspects of nonlinear simulations using shallow-water models based on the wave continuity equation. *Computers & fluids*, *23*(3), 523-538.

Kouwen, N., & Li, R. M. (1980). Biomechanics of vegetative channel linings.*Journal of the Hydraulics Division*, *106*(6), 1085-1103.

Kouwen, N., Unny, T. E., & Hill, H. M. (1969). Flow retardance in vegetated channels.

Kubatko, E. J., Westerink, J. J., & Dawson, C. (2006). < i> hp</i> Discontinuous Galerkin methods for advection dominated problems in shallow water flow. *Computer Methods in Applied Mechanics and Engineering*, *196*(1), 437-451.

Lamb, H. (1945). Hydrodynamics. 1932. *Article*, *257*, 440-442.

Le Provost, C., Lyard, F., Molines, J. M., Genco, M. L., & Rabilloud, F. (1998). A hydrodynamic ocean tide model improved by assimilating a satellite altimeter-derived data set. *Journal of Geophysical Research: Oceans (1978–2012)*, *103*(C3), 5513-5529.

Leendertse, J. J. (1967). *Aspects of a computational model for long-period water-wave propagation* (p. 165). Santa Monica, California: Rand Corporation.

Li, R. M., & Shen, H. W. (1973). Effect of tall vegetations on flow and sediment.*Journal of the Hydraulics Division*, *99*(5), 793-814.

Linhoss, A. C., Kiker, G., Shirley, M., & Frank, K. (2011). Rise, Inundation, and marsh migration: Simulating impacts on developed lands and environmental systems. *Journal of Coastal Research*, *31*(1), 36-46.

Luettich, R. A., & Westerink, J. J. (1995). Implementation and testing of elemental flooding and drying in the ADCIRC hydrodynamic model. *Final report*,*8*, 95.

Luettich Jr, R. A., Westerink, J. J., & Scheffner, N. W. (1992). *ADCIRC: An Advanced Three-Dimensional Circulation Model for Shelves, Coasts, and Estuaries. Report 1. Theory and Methodology of ADCIRC-2DDI and ADCIRC-3DL* (No. CERC-TR-DRP-92-6). COASTAL ENGINEERING RESEARCH CENTER VICKSBURG MS.

MacCready, P., & Geyer, W. R. (2010). Advances in estuarine physics. *Annual Review of Marine Science*, *2*, 35-58.

Medeiros, S., Hagen, S., Weishampel, J., & Angelo, J. (2015). Adjusting Lidar-Derived Digital Terrain Models in Coastal Marshes Based on Estimated Aboveground Biomass Density. *Remote Sensing*, *7*(4), 3507-3525.

Morris, J. T., Sundareshwar, P. V., Nietch, C. T., Kjerfve, B., & Cahoon, D. R. (2002). Responses of coastal wetlands to rising sea level. *Ecology*, *83*(10), 2869-2877.

Nepf, H. M. (1999). Drag, turbulence, and diffusion in flow through emergent vegetation. *Water resources research*, *35*(2), 479-489.

Nyman, J. A., Walters, R. J., Delaune, R. D., & Patrick, W. H. (2006). Marsh vertical accretion via vegetative growth. *Estuarine, Coastal and Shelf Science*,*69*(3), 370-380.

Global sea level rise scenarios for the United States National Climate Assessment. US Department of Commerce, National Oceanic and Atmospheric Administration, Oceanic and Atmospheric Research, Climate Program Office, 2012.

Parker, B. B. (Ed.). (1991). *Tidal hydrodynamics*. John Wiley & Sons.

Pearson, Frederick I. I. (1990). *Map ProjectionsTheory and Applications*. CRC press.

Petryk, S., & Bosmajian, G. (1975). Analysis of flow through vegetation. *Journal of the Hydraulics Division*, *101*(7), 871-884.

Petryk, S. (1969). *Drag on cylinders in open channel flow* (Doctoral dissertation, Colorado State University).

Powell, M. A., Thieke, R. J., & Mehta, A. J. (2006). Morphodynamic relationships for ebb and flood delta volumes at Florida's tidal entrances.*Ocean Dynamics*, *56*(3-4), 295-307.

Raupach, M. R., & Shaw, R. H. (1982). Averaging procedures for flow within vegetation canopies. *Boundary-Layer Meteorology*, *22*(1), 79-90.

Ree, W. O., & Palmer, V. J. (1949). *Flow of water in channels protected by vegetative linings* (No. 967). US Dept. of Agriculture.

Sheng, Y. P., Tutak, B., Davis, J. R., & Paramygin, V. (2008). Circulation and Flushing in the Lagoonal System of the Guana Tolomato Matanzas National Estuarine Research Reserve (GTMNERR), Florida. *Journal of Coastal Research*, 9-25.

Sidén, G. L., & Lynch, D. R. (1988). Wave equation hydrodynamics on deforming elements. *International journal for numerical methods in fluids*, *8*(9), 1071-1093.

Silliman, B. R., & Bertness, M. D. (2002). A trophic cascade regulates salt marsh primary production. *Proceedings of the national Academy of Sciences*,*99*(16), 10500-10505.

Smar, D. (2012). *An Assessment of Ecological Processes in the Apalachicola Estuarine System, Florida* (Doctoral dissertation, University of Central Florida Orlando, Florida).

Tsujimoto, T., Shimizu, Y., and Nakagawa, H. (1991[a]). Concentration distribution of suspended sediment in vegetated sand bed channel. *Int. Symposium on the Transport of Suspended Sediment and its Math. Mod.* Florence, Italy.

Tsujimoto, T., Shimizu, T. and Okada, T. (1991[b]). Turbulent Structure of Flow Over Rigid Vegetation-Covered Bed in Open Channels, *KHL Progressive Report 1 Japan: Hydraulic Laboratory,*

Tsujimoto, T. (1993) Unstable phenomena appearing in open-channel flows with vegetation, *Proc. Intl. Conf. on Hydr-Sci. and Eng.* Washington, DC, 1390.

Tsujimoto, T. and Shimizu, Y. (1994) Flow and Suspended Sediment in a Compound Channel with Vegetation, *KHL Hydraulic Research '94, Hydr. Lab, Kanazawa University, Japan.*

Van de Kreeke, J., & Cotter, D. C. (1974). Tide-induced mass transport in lagoon-inlet systems. *Coastal Engineering Proceedings*, *1*(14).

Wang, D., Hagen, S. C., & Alizad, K. (2013). Climate change impact and uncertainty analysis of extreme rainfall events in the Apalachicola River basin, Florida. *Journal of Hydrology*, *480*, 125-135.

Webb, B. M., King, J. N., Tutak, B., & Valle-Levinson, A. (2007). Flow structure at a trifurcation near a North Florida inlet. *Continental Shelf Research*,*27*(10), 1528-1547.

Westerink, J. J., Luettich, R. A., Blain, C. A., & Hagen, S. C. (1995). Surface elevation and circulation in continental margin waters. *Finite Element Modeling of Environmental Problems*, 39-59.

Westerink, J. J., & Shea, D. (1989). Consistent higher degree Petrov–Galerkin methods for the solution of the transient convection–diffusion equation.*International Journal for Numerical Methods in Engineering*, *28*(5), 1077-1101.

Zomlefer, W. B., Judd, W. S., & Giannasi, D. E. (2006). Northernmost Limit of Rhizophora mangle (Red Mangrove; Rhizophoraceae) in St. Johns County, Florida. *Castanea*, *71*(3), 239-244.

Zundel, A. K. (2006). Surface-water Modeling System reference manual: Version 9.2. *Provo, UT: Brigham Young University Environmental Modeling Research Laboratory*.

VITA - AMANDA TRITINGER

Educational

Masters of Science in Civil Engineering August 2013 - Present
College of Computing, Engineering, and Construction
University of North Florida, Jacksonville, FL
Academic Performance
Anticipated graduation: May, 2015

Bachelor of Science in Environmental Engineering June 2008 – May 2013
College of Engineering and Computer Science
University of Central Florida, Orlando, FL
Academic Performance
Graduated: May, 2013

Professional Licensure

FE
Passed on October 27, 2012

Employment

Graduate Research Assistant August 2013 – Present
Taylor Engineering Research Institute
College of Engineering and Computer Science
University of North Florida, Jacksonville, FL

Undergraduate Research Assistant Spring 2010 – May 2013
Coastal Hydroscience Analysis, Modeling and
Predictive Simulations Laboratory
College of Computing, Engineering, and Construction
University of Central Florida, Orlando, FL

Conference Involvement

ADCIRC Workshop April 2015
Numerical Modeling and Analysis of Tidal Variance,
and Marsh Accretion and Evolution in the Guana Tolomato
Matanzas National Estuarine Research Reserve, Florida
(plan to present)
State of the Reserve (at the GTMNERR) February 2015
Numerical Modeling and Analysis of Tidal Variance,
and Marsh Accretion and Evolution in the Guana Tolomato
Matanzas National Estuarine Research Reserve, Florida (poster)

Conference Involvement

Southeastern Estuarine Research Society (SEERS) November 2014
Numerical Modeling and Analysis of Tidal Variance,
and Marsh Accretion and Evolution in the Guana Tolomato
Matanzas National Estuarine Research Reserve, Florida (presentation)

DEP ArcGIS workshop May 2014
` Certificate of Completion

ADCIRC Workshop April 2013
Attended

Showcase of Undergraduate Research Experience April 2012
Potential Energy of the Florida Current
Honorable Mention

International Conference of Hydro-Science and Engineering November 2012
Volunteered

Showcase of Undergraduate Research Experience April 2011
Potential Energy of the Florida Current

Progress Energy Symposium April 2011
Potential Energy of the Florida Current